

TR 2910

ELECTRONIC STRUCTURE CALCULATIONS ON CERIUM-CONTAINING CRYSTALS

**TOWARDS A BETTER UNDERSTANDING OF
SCINTILLATION IN IONIC CRYSTALS**

07.05.82

21.02.82

17.02.82



The research described in this thesis was done at the section ISO/SST of the faculty of Applied Physics of the Delft University of Technology. This group was hosted at the Interfaculty Reactor Institute of the Delft University of Technology, Mekelweg 15, 2629 JB Delft, The Netherlands.

ELECTRONIC STRUCTURE CALCULATIONS ON CERIUM-CONTAINING CRYSTALS

**TOWARDS A BETTER UNDERSTANDING OF
SCINTILLATION IN IONIC CRYSTALS**

PROEFSCHRIFT

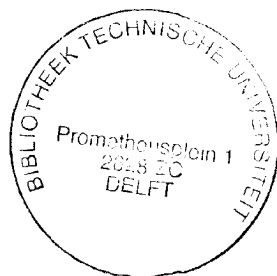
ter verkrijging van de graad van doctor
aan de Technische Universiteit Delft,
op gezag van de Rector Magnificus Prof. dr. ir. J. Blaauwendraad,
in het openbaar te verdedigen ten overstaan van een commissie,
door het College van Dekanen aangewezen,
op dinsdag 11 maart 1997 te 13.30 uur

door

Hirzo MERENGA

doctorandus in de wiskunde en natuurwetenschappen

geboren te Groningen



Dit proefschrift is goedgekeurd door de promotor:
Prof. dr. ir. C. W. E. van Eijk

Samenstelling promotiecommissie:

Rector Magnificus, voorzitter

Prof. dr. ir. C. W. E. van Eijk

Prof. dr. R. A. de Groot

Prof. dr. W. C. Nieuwpoort

Prof. dr. J. Schoonman

Prof. dr. T. van Veen

Dr. J. Andriessen

Dr. P. Dorenbos

TU Delft, promotor

KU Nijmegen

RU Groningen

TU Delft

TU Delft

TU Delft

TU Delft

Published and distributed by:

Delft University Press

Mekelweg 4

2628 CD Delft

The Netherlands

Telephone +31 15 2783254

Fax +31 15 2781661

Cover design:

Leendert Tange

CIP-DATA KONINKLIJKE BIBLIOTHEEK, DEN HAAG

Merenga, Hirzo

Electronic structure calculations on cerium-containing crystals : Towards a better understanding of scintillation in ionic crystals / Hirzo Merenga. - Delft : Delft University Press. - III.

Thesis Delft University of Technology. - With ref. - With summary in Dutch.

ISBN 90-407-1427-4.

NUGI 813

key words: Computational quantum chemistry / Inorganic scintillators / Scintillation crystals / Luminescence

Copyright © 1997 by Hirzo Merenga

All rights reserved.

No part of the material protected by this copyright notice may be reproduced or utilised in any form or by any means, electronic or mechanical, including photocopying, recording or by any information storage and retrieval system, without permission from the publisher.

"Man would of his nature know all; but it is God who decrees what shall or shall not be known; and here must we resign ourselves to accept His great wisdom and mercy in such matters, which is that He deems it often best and kindest to us mortals that we shall not know all."

John Fowles,

A Maggot (1985)

Voorwoord

Nu dit boekje bijna af is, wordt het tijd om iedereen te bedanken, die op de een of andere manier heeft bijgedragen tot het tot stand komen ervan.

Ik wil mijn begeleider Hans Andriessen bedanken voor de vele stimulerende discussies die wij gehad hebben in de afgelopen vier jaar, voor zijn hulp bij lastige problemen en voor het nauwkeurig lezen en corrigeren van dit manuscript. Ook mijn promotor Carel van Eijk wil ik bedanken voor zijn voortdurende interesse in mijn werk en voor het nauwkeurig doorlezen en corrigeren van dit manuscript.

Mijn kamergenoten: Johan de Haas, Martijn Marsman, Eric Schooneveld en Rogier Visser, hebben altijd gezorgd voor een gezellige sfeer op onze kamer; Ook al ging dat wel eens ten koste van het werk.

Alle leden van de sectie ISO wil ik bedanken voor de goede sfeer en onvergetelijke koffiepauzes en uitstapjes.

Luuk Visscher wil ik bedanken voor zijn waardevolle hulp bij het optimaliseren van het MOLFDIR pakket, vooral bij het werk dat in hoofdstuk 4 is beschreven.

Ik wil Leendert Tange bedanken voor het ontwerpen van de omslag van dit boekje. Zonder jou was dit een stuk minder fraai geworden.

Ik wil het management en het personeel van voormalig Hotel De Derde Wereld bedanken voor het verschaffen van onderdak toen ik dakloos was en voor de gezellige tijd die ik daar heb door gebracht.

Ik wil de eetclub: Heleen & Jobert Bijl, Ineke van den Brink, Anneke & Jurrien Drint, Gert Groenewold, Wilma & Albert Haan, Hans Klammer, Leo Roorda, Paola & Rob Smit en Bert Wagenaar, bedanken voor de vele, zeer gezellige, maaltijden die wij samen mochten genieten.

Ik wil de "Van Heinde en Ver" groep bedanken voor alle fantastische kampen en uitstapjes en gezellige avonden die ik met hun mocht beleven. In die dikke drie jaar dat deze club nu draait is het een unieke plaats in mijn leven gaan innemen. Het is niet doenlijk om iedereen die

heeft bijgedragen aan dit succes op te gaan noemen. Maar ik wil voor vier personen toch een uitzondering maken:

Pia Huizinga en Gerda Wubs; Jullie hebben alles opgestart met dat fantastische kamp op Schiermonnikoog en jullie hebben vervolgens ook al die andere augustus-kampen georganiseerd. Gerda, jou wil ik nog bedanken voor al de liften, die je deze autoloze promovendus hebt gegeven.

Aaltje van Dijken; voor vele kleine dingetjes, die je voor mij gedaan hebt en die soms niet zo klein waren.

En last but zeker not least, Betty Hekman; Long may you run.

Janneke Verwoerd, jou wil ik bedanken voor je absolute vertrouwen in mij en voor alle steuntjes in de rug die je mij hebt gegeven.

Verder wil ik iedereen die ik nog niet heb genoemd, maar met wie ik op enigszins reguliere basis te maken heb gehad, bedanken voor het meehelpen opbouwen van een prettige sociale omgeving, waarin het goed toeven was.

Delft, Januari 1997

Acknowledgement

This work was in part supported with grants from the National Computing Facilities Foundation (NCF).

Part of this work was supported by the Netherlands Technology Foundation (STW) with financial aid from the Netherlands Organisation for Scientific Research (NWO).

Contents

Chapter 1

General Introduction	1
1.1 Inorganic Scintillators	1
1.2 Scope of this Thesis	3
References	4

Chapter 2

General Theory	5
2.1 The Material Model	5
Approximations Based on Band Theory	6
The Cluster Approximation	6
2.2 The Non-Relativistic Computational Model	9
The Hartree-Fock Method	11
The Generalised Valence Bond Method	15
The Configuration Interaction Singles Method	18
Reduction of the Basis	19
Effective Core Potentials	20
2.3 The Relativistic Computational Model	21
The Many-Electron Dirac Equation	23
The Basis Set Expansion	24
The Kinetic Balance Principle	25
The Hartree-Fock-Dirac Method	26
References	28

Chapter 3

Improving the Convergence Behaviour of the MOLFDIR Program Package	31
3.1 General Theory	31
3.2 Group 1 Convergence Accelerators	32
Damping	32
Aitken Extrapolation	33
Pople's Extrapolation	33
The DIIS Method	35

3.3	Group 2 Convergence Accelerators	36
	The Quadratic Convergent SCF Method: General Theory	37
	Expressions for the Energy Derivatives	39
	The Direct CI Method	42
	Raleigh-Schrödinger Perturbation Theory	44
	The Algorithm	45
3.4	Results	46
	Details of the Calculations	47
	Discussion of the Results	48
3.5	Conclusions	53
	References	54

Chapter 4

Improving the Overall Efficiency of the MOLFDIR Program Package		57
4.1	Problem Survey	57
4.2	Reduction of the Number of Two-Electron Integrals	58
4.3	The Direct SCF Method	58
4.4	The Use of Spatial Symmetry	59
	Theory	59
	Estimate of the Gain	61
4.5	The Use of Time Reversal Symmetry	62
	General Theory	63
	The Double Group D_2^*	64
	The Other Double Groups	66
4.6	Current Status	68
	References	69

Chapter 5

The Fluorine Compounds		71
5.1	The Model	72
	The Material Model	72
	The Computational Model	73
	The Band Gap	75
	The Position of the Ce Levels in the Gap	75

5.2	CeF ₃ and LaF ₃ :Ce	77
	The Results of the All Electron Hartree-Fock Calculations	79
	The Results of the ECP Calculations	81
	Conclusions	85
5.3	LiLuF ₄ :Ce and LiYF ₄ :Ce	86
	The Results	86
	Conclusions	88
5.4	LiBaF ₃ :Ce	89
	Results	89
	Conclusions	92
	References	92

Chapter 6

The Oxygen Compounds	95
6.1 Computational Details	95
6.2 La ₂ Hf ₂ O ₇ :Ce	97
The Results of the Hartree-Fock Calculations	98
Conclusions	101
6.3 Lu ₂ SiO ₅ :Ce	102
Determination of the Cluster Embedding	104
The Effects of Cluster Size	105
Estimation of Lattice Relaxation	107
The Relativistic calculations	110
Conclusions	111
6.4 CeAlO ₃	113
The Results	113
Conclusions	115
References	115

Chapter 7

The Chlorine Compounds	119
7.1 Computational Details	119

7.2	$\text{SrCl}_2\text{:Ce}$	121
	Results of the Relativistic Calculations	122
	Charge Compensation and Lattice Relaxation	124
	Results of the CIS Calculations	125
	Position of the Ce Levels in the Gap	127
	Conclusions	130
7.3	CeCl_3	131
	Results of the Hartree-Fock Calculations	131
	Results of the ECP Calculations	135
	Conclusions	138
	References	139

Chapter 8

Summary and Concluding Remarks	141
8.1 Summary	141
8.2 Recommendations	145
References	146

Appendix A

Gaussian Basis Sets	149
Lithium	149
Cerium	149
Cobalt	153
Fluorine	154
Hydrogen	155
Lanthanum	156
Oxygen	156
Silicon	157
Strontium	158

Appendix B

Expressions for the Second Derivative of the Total Energy	159
--	-----

Samenvatting

Elektronische Structuurberekeningen aan Cerium-Houdende Kristallen 161

List of Publications..... 167

Curriculum Vitae 169

Chapter 1

General Introduction

Detectors for radiation are becoming more and more widespread in our society. In everyday life infrared light detectors are used for burglar alarms, remote controls and all sorts of wireless appliances. Visible light detectors are used in video cameras and electronic imaging systems. In industry, detectors for γ -rays and X-rays are used for oil well logging and for structural analysis of fabricates and samples. In the medical world detectors for γ -rays and X-rays are used for tracing techniques and for imaging systems. In high energy physics detectors for all kinds of radiation are used to analyse the products of particle beam collider experiments.

1.1 Inorganic Scintillators

There are several ways to detect radiation, depending on the radiation one wants to detect. For hard γ -rays and X-rays the predominant way is based on inorganic scintillators. Scintillators are materials which emit light when hit by ionising radiation. The emitted light can then be detected with the help of a photomultiplier tube or a photodiode.

In the different applications the detector requirements differ considerably and consequently the scintillator requirements differ also. But there are a few basic requirements which are shared by most applications¹:

- A fast response.
- A high light yield.
- A high density.
- A large atomic number.
- The possibility to grow large crystals.
- Low cost.

It seems that in practice these requirements are somewhat contradictory, especially the first two. So depending on the application one has to decide what the most important requirements are and choose the material which best fits these requirements.

It is therefore not surprising that there is an ongoing search for better scintillators. A thorough theoretical understanding of the scintillation process in inorganic compounds would be very beneficial to this search and might eventually lead to the design of scintillators for specific applications.

The scintillation process is very complex, but we can divide the whole process into three major stages². In the first stage the ionising radiation produces very hot so-called primary electrons in the crystal. These primary electrons produce a cloud of hot secondary electrons. These thermalise eventually to electron-hole pairs of low energy. Recently a good phenomenological description of this process has been developed^{3,4}.

In the second stage the electron-hole pairs migrate through the crystal. They can migrate through the crystal as a pair (an exciton) but most of the electrons and holes will migrate separately. Of this stage very little is known on a quantitative basis.

In the third stage an electron and a hole recombine on a luminescence centre, emitting a photon in the process. The luminescence centres are usually lanthanide ions (although there are other classes of inorganic scintillators). By catching an electron and a hole the lanthanide ion is brought into an excited state. Via a 5d - 4f electric dipole transition the ion then falls back to the ground state, while emitting a photon. The lanthanides which are expected to show luminescence according to this scheme are cerium, praseodymium and neodymium¹.

The above leads to the following considerations for an efficient scintillator:

- The number of electron-hole pairs created by the incident radiation should be as large as possible. Since this is mainly a function of the band gap of the material³ we should look for materials with as small a band gap as possible.
- The transfer of the electron-hole pairs to the luminescence centres should be fast and efficient. For an efficient transfer we need pure defect-free crystals. For a fast transfer the cross-section of the luminescence centre for the trapping of a hole or an electron should be large. It is generally believed that this is so if either the lowest lanthanide 4f level is close to the valence band edge or one of the lanthanide 5d levels is close to the conduction band edge⁵. Note that this limits the smallest possible band gap to approximately the smallest 4f - 5d transition energy.
- The luminescence centres should only de-excite radiatively and the life time of the excited state should be short. These conditions are fulfilled in the case of cerium, praseodymium or neodymium as luminescence centres¹.

From the above it follows that there are two important research areas for theoreticians working on scintillation. The first one is the energy transport through the crystal. This process is important for the overall efficiency of the scintillator. Still very little about it is known. The second research area is a good description of the luminescence centres, i.e. the lanthanide ions. This area is somewhat better understood, but up to now mostly on a qualitative basis. Because the positions of the lanthanide 4f and 5d levels (both relative to each other and relative to the bands of the host) are important for the luminescence behaviour of the crystal a more quantitative description would be invaluable.

1.2 Scope of this Thesis

In this thesis we will develop and use a methodology to obtain a reliable quantitative description of lanthanide ions in ionic materials, by the use of *ab initio* quantum chemical methods. We will restrict our research to cerium containing compounds for two reasons. Firstly cerium seems to be the most popular dopant for ionic compounds in scintillation research. Consequently the ability to describe the cerium ion in ionic compounds will already cover a large part of the scintillation research. Secondly, cerium is the easiest lanthanide from a theoretical point of view. In ionic compounds cerium assumes a +3 charge state. The ground state electronic configuration for the +3 charge state consists of a Xenon core and one 4f electron. In such an electronic configuration the correlation effects will be small and calculations on the Hartree-Fock level should suffice to give an adequate description.

Being a lanthanide, cerium is a rather heavy ion. Relativistic effects are therefore expected to be important. Consequently, all the calculations should preferably be done within a relativistic computational model. In the theoretical chemistry group of the university of Groningen a program package called MOLFDIR^{6,7} was developed, which can perform relativistically correct four-component Hartree-Fock-Dirac calculations on arbitrary molecules. For our purposes this program package required prohibitive amounts of computer resources. So it was essential that the program package was optimised before it could be used for our calculations.

To test and adjust our methodology we investigated several cerium containing materials which are relevant for scintillation research and compared our calculated results with the available experimental data.

This thesis is structured as follows:

In chapter 2 we give a brief overview of the theory behind the methods we use for our investigations.

In the chapters 3 and 4 we present our efforts to optimise the MOLFDIR program package so that it can be used for our calculations.

In chapter 5 we present the results of our calculations on cerium containing fluorine compounds.

In chapter 6 we present the results of our calculations on cerium containing oxygen compounds.

In chapter 7 we present the results of our calculations on cerium containing chlorine compounds.

In chapter 8 we give a summary of the main conclusions drawn from the work described in this thesis.

References

- 1) C.W.E. van Eijk, in Proceedings of the Tenth Feofilov Symposium on Spectroscopy of Crystals Activated by Rare-Earth and Transition-Metal Ions, eds. A.I. Ryskin and V.F. Masterov, Proc. SPIE, Vol. 2706, p158, St. Petersburg,, 1996
- 2) J. Andriessen, P. Dorenbos and C.W.E. van Eijk, Mat. Res. Soc. Symp. Proc., **348** 355 (1994)
- 3) P.A. Rodnyi, P. Dorenbos and C.W.E. van Eijk, Phys. Stat. Sol. (b), **187** 15 (1995)
- 4) M. Marsman, P. Dorenbos and C.W.E. van Eijk, in Proceedings of the International Conference on Inorganic Scintillators and their Applications, eds. P. Dorenbos and C.W.E. van Eijk, p156, Delft University Press, Delft, 1996
- 5) C. Pedrini, D. Bouttet and C. Dujardin, in Proceedings of the International Conference on Inorganic Scintillators and their Applications, eds. P. Dorenbos and C.W.E. van Eijk, p103, Delft University Press, Delft, 1996
- 6) Relativistic Quantum Chemistry: The MOLFDIR program package, L. Visscher, O. Visser, P.J.C. Aerts, H. Merenga and W.C. Nieuwpoort, Computer Physics Communications **81** 120 (1994)
- 7) Relativistic Quantum Chemistry: The MOLFDIR program package, L. Visscher, W.A. de Jong, O. Visser, P.J.C. Aerts, H. Merenga and W.C. Nieuwpoort, in METECC-95, E. Clementi and G. Corongiu, (STEF, Cagliari, 1995)

Chapter 2

General Theory

The theoretical study of the electron distribution and the energy levels of impurities in inorganic solids starts with the determination of the simulation model. We can identify two different aspects of the simulation model: the material model and the computational model. The material model is concerned with the material representation we choose for the physical system of interest. The computational model is concerned with the level of theory we use to determine the wave function of our representation of the physical system.

In the first section of this chapter we will briefly discuss the material model we use. The following sections of this chapter are dedicated to the computational model we use. In those sections we will give a brief overview of all the computational methods employed in this thesis.

2.1 The Material Model

The natural starting point for describing inorganic crystalline solids is band structure theory¹. This theory makes full use of the translational symmetry of the material.

In band theory it is assumed that the adiabatic (Born-Oppenheimer) approximation is valid. The Hamiltonian is written as a part referring only to the electrons and a part referring only to the nuclei. The cross terms in the Hamiltonian are neglected. The Schrödinger equation can now be separated in an electronic and a nuclear equation. These equations can be solved separately. Normally the nuclei are assumed to be frozen at their equilibrium positions. The electronic Hamiltonian shows the small group² symmetry of the frozen lattice. The small group symmetry is a combination of the point group symmetry and the translational symmetry of the lattice, where the symmetry operations which do not leave \mathbf{k} invariant have been deleted. Because of this translational symmetry the eigenstates of the electronic Schrödinger equation can be labelled with a continuous quantum number \mathbf{k} . The

eigenfunctions transform according to the irreducible representations of the space group of the Hamiltonian.

Usually in band theory one assumes that the many electron Schrödinger equation can be reduced to a system of one electron equations. The resulting one electron Hamiltonian is assumed to have the same space group symmetry as the many electron Hamiltonian. So the eigenfunctions (Bloch functions) can be labelled with a continuous quantum number \mathbf{k} .

If impurities are present in the material the translational symmetry is broken. Instead of an orderly array of a repetitive unit, the crystal has become one huge molecule with little or no symmetry. A quantum mechanical calculation on such a system is clearly impossible, without using some sort of approximation.

Approximations Based on Band Theory

One of the simplest approximations we can make, which remains in the spirit of band theory, is the so-called supercell method³. This method is essentially a band theory method in which the repetitive unit (the unit cell) can be freely chosen. By choosing the unit cell very large and by having only one impurity atom per unit cell we approximate the case of one isolated impurity in a host crystal. Because of the need to choose a very large unit cell the computational resources needed to perform a calculation also become very large. This makes the method less suited to our purposes.

The second well known method to describe impurities and defects in crystals consists of performing a band theory calculation on the pure host and then describing the impurity or defect in terms of the pure host Bloch functions, by perturbation theory. The resulting equations are usually solved using a Green's function approach. For shallow impurities it can be shown that, with some approximations and the use of perturbation theory, this method is equivalent to the effective mass theory. The effective mass theory has successfully been applied to several shallow level impurities⁴. For localised deep level impurities however very large expansions to very high \mathbf{k} values are needed to give an accurate description of the impurity. In these cases these methods become impractical.

The Cluster Approximation

When one wants to describe localised defects or impurities in solids a band structure calculation is not very suitable. In these cases it is more natural to use a local approach. The entire crystal with the impurity is considered to be one large molecule and we want to study this molecule. Because of its huge size and the lack of translational symmetry it is impossible

to study this system with standard quantum chemical methods. We need additional approximations. Because we are primarily interested in the characterisation of the impurity atom, we will concentrate on that and treat the host as a perturbation on the impurity. Within this approach there are two starting points possible. The first is a band structure calculation on the pure host.

Zunger and co-workers⁵ developed such a Green's function method. It is based on the fact that the total potential of the system $V(\mathbf{r})$ can be written as a sum of the periodic potential of the pure host $V_H(\mathbf{r})$ and the perturbation due to the impurity $\Delta V(\mathbf{r})$. The same holds for the total density of the system $\rho(\mathbf{r})$. They first compute $V_H(\mathbf{r})$ and $\rho_H(\mathbf{r})$ from a self-consistent band structure calculation on the host crystal. The impurity wave function is expanded in the host crystal quasi bands and a set of orbitals centred on the impurity. The Green's function for the resulting problem is then solved using local density techniques. This is essentially a one-electron description of the system. For many properties of impurities the many electron effects may be very important. Zunger et al account for this by calculating the many electron effects for each state of the impurity from the *atomic* Racah parameters B_0 and C_0 . This method seems to work reasonably well. Nevertheless it does have some problems. These problems can be divided in problems due to the computational scheme used and problems due to the way in which the entire system is represented.

- (i) Because of the use of the local density approach this method is effectively a local one electron approach. The many electron and non-local effects which may be important can only be estimated from their values in the free impurity atom. These estimates may significantly deviate from the crystal values. The non-local exchange correlation can only be approximated by a local potential. So the Pauli principle is not strictly enforced. Furthermore local density methods yield only the electronic density of the system under study with good accuracy. The wave function is much less accurate. So properties which depend explicitly on the wave function cannot be computed accurately.

Of course the Green's function can also be solved by using methods which do not have the above mentioned deficiencies. However the required computational resources for such a computation could easily become prohibitive.

- (ii) The perturbation of the potential $\Delta V(\mathbf{r})$ and the charge density $\Delta \rho(\mathbf{r})$ describe only a small piece of the crystal, typically the impurity or defect surrounded by a few shells of host atoms. This region must be large enough to contain the defect specific effects of the impurity. The change in $V(\mathbf{r})$ and $\rho(\mathbf{r})$ due to the impurity is only described in that region. The polarisation of the charge density of the crystal, induced by charged states of the impurity is not confined to this region. Therefore calculations which pertain to charged states of the impurity will lack some important polarisation effects.

The other starting point is the cluster calculation. A cluster consists of the defect or impurity surrounded by at most a few layers of the host material. These clusters can then be studied with standard quantum chemical methods. So in principle the wave function of the cluster can be determined to any desired level of approximation. The cluster should be large enough to contain the defect specific effects of the impurity or defect.

The cluster approach still poses some problems⁶. The cluster can be regarded as a piece of material which is cut out of the crystal. So the interactions between the cluster and the rest of the crystal are missing. We will give here a short resume of the different aspects of this deficiency.

- (i) In cutting the cluster out of the crystal we may have broken some bonds. The resulting dangling bonds may produce levels in the gap which may have a large unphysical interaction with the gap levels of the impurity. To counteract this the dangling bonds are normally saturated with hydrogen atoms or some sort of pseudo atoms. This procedure pushes the bonding levels deep into the valence band and the anti-bonding levels high into the conduction band. In the case of highly ionic materials the dangling bonds do not seem to be a real problem.
- (ii) In the cluster approach we study a small piece of the crystal. The interaction of the cluster atoms with crystal atoms not included in the cluster is missing. This interaction can be divided into two contributions: a static contribution and a dynamic contribution. The static contribution pertains to the interaction of the cluster atoms with the unperturbed charge density of the rest of the crystal. This interaction is mainly coulombic in nature. For the short range however there may be significant exchange contributions. The dynamic contribution pertains to the response of the charge density of the rest of the crystal to alterations in the charge state of the impurity or defect.

In this thesis we will be dealing with highly ionic compounds. Therefore the problems enumerated under point (i) will not concern us. The problems mentioned under point (ii) do need our attention.

The static part of the interaction can be modelled by surrounding the cluster with a set of point charges, which are fitted to reproduce the Madelung potential due to the rest of the crystal at the cluster sites⁷. The exchange repulsion of the cluster atoms with the rest of the crystal is still missing. This will mainly effect the atoms at the edge of the cluster. For highly ionic compounds we expect this effect to be small as far as the calculation of the electronic charge distribution is concerned. For geometry optimisations on the clusters the effects will probably be significant. In those cases we can, in some cases, remedy the problems by enlarging the cluster and freezing the positions of the atoms on the cluster edge.

To take into account the dynamic part of the interaction is more complicated. We need to represent the rest of the cluster with some sort of (semi)classical response function. This

response function can be based on a continuous dielectricum or on a discrete set of dipole polarisabilities⁸. The effect of the environment on the cluster can then be calculated with perturbation theory or in some methods self consistently by putting the appropriate terms in the Hamiltonian. For highly ionic compounds the dynamic part of the interaction is expected to be small, as long as the charge of the impurity does not change. We will not attempt to describe this part of the interaction.

The material model we will be using in this thesis will be a cluster surrounded by point charges, which reproduce the Madelung potential due to the rest of the crystal. The cluster will consist of the impurity (Ce) atom and one or more shells of atoms from the host.

2.2 The Non-Relativistic Computational Model

Our non-relativistic computational model is based on the time-independent Schrödinger equation⁹:

$$\left(-\frac{1}{2} \sum_i^{n_e} \frac{\partial^2}{\partial \mathbf{r}_i^2} - \sum_i^{n_e} \sum_a^{n_n} \frac{Z_a}{\mathbf{R}_a - \mathbf{r}_i} + \frac{1}{2} \sum_{a,b}^{n_n} \frac{Z_a Z_b}{\mathbf{R}_{ab}} + \frac{1}{2} \sum_{i,j}^{n_e} \frac{1}{\mathbf{r}_{ij}} \right) \Psi = E \Psi, \quad 2.2.1$$

where n_e is the number of electrons in the system and n_n is the number of nuclei in the system. The \mathbf{r}_i give the coordinates of the electrons and the \mathbf{R}_a give the coordinates of the nuclei. The notation \mathbf{r}_{ij} is shorthand for $\mathbf{r}_i - \mathbf{r}_j$ and \mathbf{R}_{ab} is shorthand for $\mathbf{R}_a - \mathbf{R}_b$. A prime after the sum symbol denotes that the sum indices cannot be equal. The whole equation is given in atomic units. It can easily be seen from equation 2.2.1 that we can write the many-electron Schrödinger equation as a sum of one-electron Schrödinger equations and an interaction term⁹:

$$\left(\sum_i^{n_e} h_i + \frac{1}{2} \sum_{i,j}^{n_e} g_{ij} + V_{nn} \right) \Psi = E \Psi, \quad 2.2.2$$

$$\text{with } h_i = -\frac{1}{2} \frac{\partial^2}{\partial \mathbf{r}_i^2} - \sum_a^{n_n} \frac{Z_a}{\mathbf{R}_a - \mathbf{r}_i} \quad 2.2.3$$

$$\text{and } g_{ij} = \frac{1}{r_{ij}}, \quad 2.2.4$$

$$\text{and } V_{nm} = \frac{1}{2} \sum_{a,b}^{n_n} \frac{Z_a Z_b}{R_{ab}}. \quad 2.2.5$$

The many particle wave function $\Psi(\mathbf{r}_1 \dots \mathbf{r}_n)$ can be written in terms of the one-electron functions $\{\psi_r(\mathbf{r})\}$ ⁹:

$$\Psi = N \left(c_0 \Phi_0 + \sum_r^{n_e} \sum_{v=n_e+1}^{n_d} c_r^v \Phi_r^v + \sum_{r,s}^{n_e} \sum_{v,w=n_e+1}^{n_d} c_{rs}^{vw} \Phi_{rs}^{vw} + \dots \right). \quad 2.2.6$$

The factor N is the normalisation constant; the term Φ_0 is the Slater determinant:

$$\Phi_0 = \frac{1}{\sqrt{n_e!}} |\psi_1 \psi_2 \dots \psi_r \dots \psi_{n_e}| \quad 2.2.7$$

and the terms $\Phi_{rs}^{vw} \dots$, etc. are constructed from Φ_0 by replacing ψ_r with ψ_v , ψ_s with ψ_w , etc. in the determinant. The reason that Φ_0 is given by a Slater determinant and not by a simple product of one-electron functions stems from the fact that the wave function must be an eigenfunction of the parity operator \mathcal{P} with eigenvalue -1.

The expansion of equation 2.2.6 is slowly converging, given that Φ_0 is a reasonable approximation for Ψ . One has to keep in mind however that the determinants with an even number of substitutions have a larger effect on the energy of the wave function than the determinants which have an odd number of substitutions¹⁶.

The number n_d gives the dimension of the set $\{\psi_r(\mathbf{r})\}$. This number is at best extremely large and can even be infinite. This means that in almost all cases the wave function of equation 2.2.6 cannot be determined to full precision. To get an estimate for the wave function Ψ we will have to make some approximations.

There are two basic strategies we can follow: We can reduce the dimension of the set $\{\psi_r(\mathbf{r})\}$ and we can limit the expansion of Ψ in equation 2.2.6. In the following subsections we will elucidate these possibilities. We will start with limiting the expansion of Ψ in equation 2.2.6.

The Hartree-Fock Method

If we restrict the expansion for Ψ in equation 2.2.6 to only the first term, we obtain the simplest form for Ψ which is still consistent with the Pauli exclusion principle:

$$\Psi = N\Phi_0. \quad 2.2.8$$

This is a reasonable ansatz for the wave function in the case of groundstates with high lying excited states. The method which results from this choice of wave function is called the Hartree-Fock method¹⁰.

The expectation value for the energy E for a normalised wave function Ψ is given by:

$$E = \langle \Psi | \mathbf{H} | \Psi \rangle. \quad 2.2.9$$

If we substitute equations 2.2.8 and 2.2.7 in equation 2.2.9 and use the Hamiltonian of equation 2.2.2, we find:

$$E = N^2 \left(\sum_r^{n_e} \langle r | \mathbf{h} | r \rangle + \frac{1}{2} \sum_{r,s}^{n_e} [\langle rs | \mathbf{g} | rs \rangle - \langle rs | \mathbf{g} | sr \rangle] + V_{nn} \right), \quad 2.2.10$$

$$\text{where } \mathbf{h} = \sum_i^{n_e} \mathbf{h}_i \quad 2.2.11$$

$$\text{and } \mathbf{g} = \sum_{i,j}^{n_e} \mathbf{g}_{ij}. \quad 2.2.12$$

Up to now we have ignored spin. Assume that the one-electron functions $\{\psi_r(\mathbf{r})\}$ can be written as a product of a spatial function $\{\phi_r(\mathbf{r})\}$ and a spin function $\{\sigma=\alpha,\beta\}$:

$$\psi_r(\mathbf{r}) = \phi_r(\mathbf{r})\sigma_r. \quad 2.2.13$$

For a "closed shell" system, in which every orbital is doubly occupied (once for α spin and once for β spin) equation 2.2.10 becomes:

$$E = N^2 \left(2 \sum_r^{n_e} \langle r | \mathbf{h} | r \rangle + \sum_{r,s}^{n_e} [2 \langle rs | \mathbf{g} | rs \rangle - \langle rs | \mathbf{g} | sr \rangle] + V_{nn} \right). \quad 2.2.14$$

The first term of equation 2.2.14 are the so-called one-electron integrals. This term describes the kinetic energy of the electrons and the potential energy of the electrons relative to the nuclear skeleton. The third term just gives the potential energy of the nuclei. This is a constant; so we will ignore this term in the rest of this section. The second term is the most interesting. It consists of the so-called coulomb repulsion and exchange integrals. They describe the interaction of the electrons with each other.

We now express the one-electron functions $\{\phi_r(\mathbf{r})\}$ in terms of a set of gaussian basis functions $\{\chi_i\}$:

$$\phi_r = \sum_i^{n_b} c_i^r \chi_i, \quad 2.2.15$$

with:

$$\chi_i(\mathbf{r}) = r^{l_i+1} e^{-\alpha_i r^2} \quad 2.2.16$$

We can now define the projection operator \mathcal{R} with matrix elements:

$$R_{kl} = \sum_{i,j,r} \langle \chi_k | c_i^r \chi_i \rangle \langle c_j^r \chi_j | \chi_l \rangle = \mathbf{c}_k \mathbf{c}_l^\dagger \quad 2.2.17$$

where \mathbf{c} is the coefficient matrix. If we assume that the set basis functions $\{\chi_i\}$ is orthonormal we can write equation 2.2.14 as:

$$E = 2\text{tr}(\mathbf{R}\mathbf{h}) + \text{tr}(\mathbf{R}\mathbf{G}), \quad 2.2.18$$

where the matrix \mathbf{h} is the one-electron matrix with the elements:

$$h_{ij} = \langle \chi_i | \hat{h} | \chi_j \rangle, \quad 2.2.19$$

and \mathbf{G} is the two-electron interaction matrix with the elements:

$$G_{ij} = \sum_{kl} R_{lk} \left(2\langle \chi_i \chi_k | \hat{g} | \chi_j \chi_l \rangle - \langle \chi_i \chi_k | \hat{g} | \chi_l \chi_j \rangle \right) = 2J_{ij} - K_{ij}. \quad 2.2.20$$

For any change $\delta\mathbf{R}$, the first-order energy change will be:

$$\delta E^{(1)} = 2\text{tr}(\delta \mathbf{R} \mathbf{h}) + 2\text{tr}(\delta \mathbf{R} \mathbf{G}) = 2\text{tr}(\delta \mathbf{R} \mathbf{h}^{\mathbf{F}}), \quad 2.2.21$$

$$\text{where } \mathbf{h}^{\mathbf{F}} = \mathbf{h} + \mathbf{G} \quad 2.2.22$$

is the matrix of the Hartree-Fock Hamiltonian.

The eigenvalues ε_r of the operator $\mathbf{h}^{\mathbf{F}}$ can be expressed as:

$$\varepsilon_r = \mathbf{c}_r^\dagger \mathbf{h}^{\mathbf{F}} \mathbf{c}_r. \quad 2.2.23$$

We now define:

$$E^{\mathbf{F}} = \text{tr}(\mathbf{R} \mathbf{h}^{\mathbf{F}}) = \sum_r \varepsilon_r. \quad 2.2.24$$

To find a solution for the wave function Ψ we have to minimise the energy (2.2.18). So:

$$\delta E^{(1)} = 2\text{tr}(\delta \mathbf{R} \mathbf{h}^{\mathbf{F}}) = 0. \quad 2.2.25$$

Obviously the eigenvalues ε_r of the operator $\mathbf{h}^{\mathbf{F}}$ are stationary against any change $\delta \mathbf{R}$. Therefore the sum of all eigenvalues is also stationary. To satisfy the requirements of equation 2.2.25 it is enough to solve:

$$\mathbf{h}^{\mathbf{F}} \mathbf{c} = \varepsilon \mathbf{c}. \quad 2.2.26$$

Note that this equation needs to be solved iteratively. Because of the definition of \mathbf{G} (2.2.20) the matrix $\mathbf{h}^{\mathbf{F}}$ depends on the solution \mathbf{c} .

The above explained version of the Hartree-Fock method is called the Restricted Hartree-Fock method because the spatial functions of the α and β electron in the same orbital are forced to be equal. We can lift this restriction and obtain the Unrestricted Hartree-Fock equations:

$$\mathbf{h}_\alpha^{\mathbf{F}} \mathbf{c}^\alpha = \varepsilon^\alpha \mathbf{c}^\alpha, \quad 2.2.27$$

$$\mathbf{h}_\beta^{\mathbf{F}} \mathbf{c}^\beta = \varepsilon^\beta \mathbf{c}^\beta, \quad 2.2.28$$

where the Hamilton matrices are defined by:

$$\mathbf{h}_\alpha^F = \mathbf{h} + \mathbf{G}_\alpha = \mathbf{h} + \mathbf{J}(\mathbf{R}^\alpha) - \mathbf{K}(\mathbf{R}^\alpha) + \mathbf{J}(\mathbf{R}^\beta), \quad 2.2.29$$

$$\mathbf{h}_\beta^F = \mathbf{h} + \mathbf{G}_\beta = \mathbf{h} + \mathbf{J}(\mathbf{R}^\beta) - \mathbf{K}(\mathbf{R}^\beta) + \mathbf{J}(\mathbf{R}^\alpha). \quad 2.2.30$$

These equations have the advantage that they can also be used to describe non closed-shell systems. The disadvantage of this method is that the obtained wave function is not necessarily an eigenfunction of \hat{S}^2 anymore. To remedy this Roothaan¹¹ developed a version of the restricted Hartree-Fock method, that can handle open shells.

The expression for the total energy becomes:

$$E = v_1 \text{tr}(\mathbf{R}_1(\mathbf{h} + \frac{1}{2} \mathbf{G}_1)) + v_2 \text{tr}(\mathbf{R}_2(\mathbf{h} + \frac{1}{2} \mathbf{G}_2)), \quad 2.2.31$$

where v_1 is the occupation number of the closed shell orbitals, v_2 the occupation number of the open shell orbitals, and:

$$\mathbf{G}_1 = (\mathbf{G}(v_1 \mathbf{R}_1) + \mathbf{G}(v_2 \mathbf{R}_2)), \quad 2.2.32$$

$$\mathbf{G}_2 = \mathbf{G}(v_1 \mathbf{R}_1) + (\mathbf{J}(v_2 \mathbf{R}_2) - \mathbf{K}(v_2 \mathbf{R}_2)). \quad 2.2.33$$

We have factorised the total function space into three parts: the closed shell space \mathbf{R}_1 , the open shell space \mathbf{R}_2 and the virtual (empty) space \mathbf{R}_3 .

Energy minimisation leads to two Fock matrices:

$$\mathbf{h}_1 = \mathbf{h} + \mathbf{G}_1, \quad \mathbf{h}_2 = \mathbf{h} + \mathbf{G}_2. \quad 2.2.34$$

These two matrices have to be diagonalised simultaneously. This can be written in the form of one effective eigenvalue equation with the Hamiltonian⁹:

$$\begin{aligned} \bar{\mathbf{h}} = & (\mathbf{1} - \mathbf{R}_2) \mathbf{h}_1 (\mathbf{1} - \mathbf{R}_2) + (\mathbf{1} - \mathbf{R}_1) \mathbf{h}_2 (\mathbf{1} - \mathbf{R}_1) + \\ & (\mathbf{1} - \mathbf{R}_3) (v_1 \mathbf{h}_1 - v_2 \mathbf{h}_2) (\mathbf{1} - \mathbf{R}_3) \end{aligned} \quad 2.2.35$$

This equation also has to be solved iteratively because the matrices \mathbf{J} and \mathbf{K} depend on the solution \mathbf{c} .

The Generalised Valence Bond Method

The non-relativistic calculations described in this thesis were mainly performed with Gaussian 92¹². The implementation of the open-shell Hartree-Fock method in this program is severely limited. For the calculations on more complicated open-shell configurations we have had to use the implementation of the Generalised Valence Bond (GVB) method of that program. In this sub-section we will explain briefly the for us relevant parts of the GVB method as implemented in the Gaussian 92 program. A complete description can be found in reference 13.

In the GVB method we use a wave function of the form:

$$\Psi = \mathcal{A}[\{\text{core}\}\phi_{11}\phi_{21}(\alpha\beta - \beta\alpha)\cdots\phi_{1m}\phi_{2m}(\alpha\beta - \beta\alpha)\phi_{m+1}\alpha\cdots\phi_n\alpha]. \quad 2.2.36$$

In this equation \mathcal{A} is the antisymmetriser operator; $\{\text{core}\}$ is just a product of one-electron orthonormal spin functions (leading to a Hartree-Fock type wave function); the $\{\phi_n\}$ are spatial orthonormal one-electron functions and the $\{\phi_{1m}, \phi_{2m}\}$ are pairs of one-electron functions (with their spins coupled to a singlet), which need not be orthogonal to each other:

$$\langle \phi_{1m} | \phi_{2m} \rangle = S_m \neq 0. \quad 2.2.37$$

The wave function of 2.2.36 is normally referred to as the GVB-PP (Perfect Pairing) function. In principle we can also allow for other spin-couplings in 2.2.36, but we will not dwell on this possibility here.

The expression for the total energy of the wave function of equation 2.2.36 becomes quite complicated. We can simplify the expression by transforming the orbital pair part of the wave function to natural orbitals¹⁴:

$$\begin{aligned} \phi_{1m} &= \frac{\sqrt{\sigma_{1m}}\phi_{1m}^{\text{NO}} + \sqrt{\sigma_{2m}}\phi_{2m}^{\text{NO}}}{\sqrt{\sigma_{1m} + \sigma_{2m}}} \\ \phi_{2m} &= \frac{\sqrt{\sigma_{1m}}\phi_{1m}^{\text{NO}} - \sqrt{\sigma_{2m}}\phi_{2m}^{\text{NO}}}{\sqrt{\sigma_{1m} + \sigma_{2m}}} \end{aligned} \quad 2.2.38$$

$$\sigma_{1m} > 0, \quad \sigma_{2m} > 0, \quad \langle \phi_{1m}^{\text{NO}} | \phi_{2m}^{\text{NO}} \rangle = 0$$

The energy expression now reduces to the form:

$$E = 2 \sum_i f_i h_{ii} + \sum_{i,j} (a_{ij} J_{ij} + b_{ij} K_{ij}), \quad 2.2.39$$

where:

$$\begin{aligned} f_i &= 1 && \text{if } \phi_i \text{ is a core orbital} \\ f_i &= \sigma_i^2 && \text{if } \phi_i \text{ is a pair orbital} \\ f_i &= \frac{1}{2} && \text{if } \phi_i \text{ is an open orbital} \end{aligned} \quad 2.2.40$$

and:

$$\begin{aligned} \left. \begin{aligned} a_{ij} &= 2f_i f_j \\ b_{ij} &= -\frac{1}{2} \end{aligned} \right\} && \text{if } \phi_i \text{ and } \phi_j \text{ are both open orbitals} \\ \left. \begin{aligned} a_{ii} &= f_i \\ b_{ii} &= 0 \end{aligned} \right\} && \text{if } \phi_i \text{ is a pair orbital} \\ \left. \begin{aligned} a_{ij} &= 0 \\ b_{ij} &= -\sigma_i \sigma_j \end{aligned} \right\} && \text{if } \phi_i \text{ and } \phi_j \text{ are in the same pair} \\ \left. \begin{aligned} a_{ij} &= 2f_i f_j \\ b_{ij} &= -f_i f_j \end{aligned} \right\} && \text{otherwise.} \end{aligned} \quad 2.2.41$$

The form of the energy expression 2.2.39 is equal to the form of the energy expression for the Hartree-Fock method, except for the meaning of the coefficients f_i , a_{ij} and b_{ij} .

Just as in the Hartree-Fock case (equation 2.2.15) we expand the one-electron orbitals $\{\phi_r\}$ in linear combinations of gaussian type functions $\{\chi_i\}$. When optimising the orbitals $\{\phi_r\}$ we have to recognise that there are two different types of variations possible. The first type mixes the occupied orbitals with the virtual orbitals. These variations (when performed on an orbital by orbital basis) keep the occupied orbitals orthogonal. The second type of variation lets the occupied orbitals mix among each other. In this case a change in an orbital has to be accompanied by an equal but opposite change in the other occupied orbital with which it is mixing, else the orthogonality of the orbitals is destroyed.

The total optimisation of the orbitals $\{\phi_r\}$ is accomplished in two steps. In the first step we allow only the first type of variation. In the second step we also allow the second type of variation.

The variational equations for the first step are given by:

$$\mathbf{H}_r \mathbf{c}_r = \epsilon_r \mathbf{c}_r \quad 2.2.42$$

where:

$$\mathbf{H}_r = f_r \mathbf{h} + \sum_{i \neq r} (a_{ri} \mathbf{J}_i + b_{ri} \mathbf{K}_i) + (a_{rr} + b_{rr}) \mathbf{J}_r + \mathbf{X}_r. \quad 2.2.43$$

and:

$$(\mathbf{X}_r)_{ij} = 2(a_{rr} + b_{rr})(1 - \delta_{ir})(1 - \delta_{jr})(\mathbf{K}_r)_{ij} \quad 2.2.44$$

There is a different equation 2.2.42 for each orbital ϕ_r . If we ignore the matrix \mathbf{X}_r then the operator \mathbf{H}_r of equation 2.2.42 will be equal for all orbitals in a shell; i.e. all the orbitals in the closed-shell core, all the orbitals in one pair, or all the open-shell orbitals coupled to one spin-state. This can give significant savings in computation time.

Assuming that our starting guess for $\{\phi_r\}$ is reasonable we can suffice in the second step by optimising the orbitals pairwise. So:

$$\begin{aligned} \phi_i &= \frac{(\phi_i^0 + \lambda_{ij} \phi_j^0)}{\sqrt{1 + \lambda_{ij}^2}} \\ \phi_j &= \frac{(\phi_j^0 + \lambda_{ji} \phi_i^0)}{\sqrt{1 + \lambda_{ji}^2}} \end{aligned} \quad 2.2.45$$

To preserve orthogonality we require:

$$\lambda_{ij} = -\lambda_{ji}. \quad 2.2.46$$

In second order the λ_{ij} 's can be found by:

$$\lambda_{ij} = \frac{-1}{2\lambda_{ij}^0} \pm \left[\left(\frac{1}{2\lambda_{ij}^0} \right)^2 + 1 \right]^{\frac{1}{2}} \quad 2.2.47$$

where:

$$\lambda_{ij}^0 = \frac{\langle i_0 | \mathbf{H}_{j_0} - \mathbf{H}_{i_0} | j_0 \rangle}{\langle i_0 | \mathbf{H}_{j_0} - \mathbf{H}_{i_0} | i_0 \rangle - \langle j_0 | \mathbf{H}_{j_0} - \mathbf{H}_{i_0} | j_0 \rangle + \gamma_{ij}} \quad 2.2.48$$

and:

$$\gamma_{ij} = 2(a_{ii} + a_{jj} - 2a_{ij})K_{i_0j_0} + (b_{ii} + b_{jj} - 2b_{ij})(J_{i_0j_0} + K_{i_0j_0}) \quad 2.2.49$$

Usually equation 2.2.47 is sequentially solved for all orbital pairs without redefining the initial orbitals in between. After all the λ_{ij} 's are found the orbitals are updated and the process is repeated till self consistency is reached.

The Configuration Interaction Singles Method

The CI-singles method¹⁵ is a method developed to obtain wave functions and observables for excited states of molecules. It is assumed that the groundstate of the molecule (the reference state) can be written as a one-determinantal (Hartree-Fock) wave function. The singly excited determinants Φ_r^v can be viewed as zeroth order approximations to the excited states of the molecule. Of course these determinants do not provide a good description of the excited states because the orbitals they contain are optimised for the groundstate of the molecule. We can partially improve the description of the excited states by allowing linear combinations of the Φ_r^v . The wave function for an excited state will then become:

$$\Psi_{\text{CIS}} = \sum_r \sum_{v=n_g+1}^{n_d} c_r^v \Phi_r^v. \quad 2.2.50$$

The Φ_r^v are defined by the Hartree-Fock calculation on the groundstate of the molecule. The CI-singles calculation consists of finding the correct coefficients c_r^v . To find these coefficients it is sufficient to solve the eigenvalue equation:

$$\mathbf{H}\mathbf{c} = \mathbf{E}\mathbf{c}, \quad 2.2.51$$

where the matrix \mathbf{H} consists of the matrix elements:

$$H_{rv,sw} = \langle \Phi_r^v | \mathbf{H} | \Phi_s^w \rangle. \quad 2.2.52$$

The wave functions Ψ_{CIS} for the excited states obtained this way are orthogonal to the groundstate Ψ_{HF} by virtue of Brillouin's theorem:

$$\langle \Phi_r^v | \mathbf{H} | \Phi_0 \rangle = 0 \quad 2.2.53$$

Because the CI-singles coefficients are determined variationally the overall wave function should be able to relax and give a better description of the excited states than the singly substituted Hartree-Fock determinants alone. The CI-singles method leads to a well-defined wave function and differentiable energy, thus analytical gradient techniques to determine properties and optimised excited-state geometries are straightforward to apply. Finally the CI-singles method is size-consistent, meaning that it scales in the proper way with the number of electrons in the system.

Reduction of the Basis

Reducing the dimension of the set $\{\psi_r(\mathbf{r})\}$ is potentially very dangerous. If we delete functions from the set, which will occur with a significant coefficient in the final wave function Ψ , our estimate for the wave function becomes very inaccurate.

On the other hand, it is clear that if we choose the set $\{\psi_r(\mathbf{r})\}$ well, we can get an accurate estimate for Ψ with a relatively small number of one-electron functions.

Consider a Hartree-Fock calculation on an arbitrary system. Such a calculation would yield a Φ_0 and a set of one-electron molecular orbitals $\{\psi_r(\mathbf{r})\}$. We can use these molecular orbitals as the one-electron functions in the expansion 2.2.6 for Ψ . It is clear that we can limit the expansion of 2.2.6 for the groundstate, without too much loss of accuracy, to the occupied and the lowest virtual molecular orbitals. The molecular orbitals with very high orbital energies will not have a significant contribution to Ψ .

Because of this, molecular quantum mechanical methods that go beyond the Hartree-Fock method usually start with a Hartree-Fock calculation to obtain a set of one-electron functions, from which one can easily select an reasonable subset for the further calculations¹⁶.

To reduce the dimension of $\{\psi_r(\mathbf{r})\}$ for a Hartree-Fock calculation we can do something similar. Consider a molecule consisting of several atoms. The electrons in the molecule can be described with functions which resemble but are not identical to the atomic functions. If we would perform a Hartree-Fock calculation on each atom separately and use the thus found sets of orbitals $\{\psi_r^{\text{At}}(\mathbf{r})\}$ or parts of those orbitals as the basis for the expansion of the molecular functions, we can restrict the sizes of the basis sets to the occupied orbitals plus a few extra, and still obtain a fairly accurate result¹⁷.

Effective Core Potentials

Chemical properties of molecules or solids are mainly determined by the valence electrons of the constituent atoms. Furthermore, the core orbitals of atoms will hardly change when the atoms will form chemical bonds. It is therefore convenient to describe the core-electrons with an effective potential and not explicitly in molecular calculations.

The ECP calculations described in this thesis were performed with the ECP's developed by Stevens et al^{18,19}. In this section we will describe their method.

The method starts with performing a numerical Hartree-Fock²⁰ or numerical Hartree-Fock-Dirac²¹ calculation on the atom in the charge state for which the ECP is needed. The (large component of the) orbitals are then transformed to nodeless pseudo-orbitals by the procedure developed by Christiansen et al.²²:

$$\chi_{li}(r) = \sum_{k=0}^4 c_{ki} r^{l+k+1} \quad r \leq R_l$$

$$\chi_{li}(r) = \phi_{li}(r) \quad r \geq R_l$$
2.2.54

where R_l is usually chosen to be the position where the radial part of the orbital reaches its outermost maximum. Beyond R_l the pseudo-orbital has exactly the same shape as the original orbital. For radial distances smaller than R_l the pseudo-orbital is defined by a polynomial expansion that goes to zero smoothly. The coefficients of the polynomial are defined by matching the value and first three derivatives of the orbital at R_l and by requiring that χ_{li} is normalised.

The effective potential has the form:

$$V^{\text{eff}} = V_{l_{\text{max}}}^{\text{eff}} + \sum_{l=0}^{l_{\text{max}}-1} (V_l^{\text{eff}} - V_{l_{\text{max}}}^{\text{eff}}) |lm\rangle \langle lm|$$
2.2.55

where:

$$r^2 V_l^{\text{eff}} = \sum_k A_{l,k} r^{n_{l,k}} e^{-B_{l,k} r^2}$$
2.2.56

The coefficients A_{lk} and B_{lk} are found by minimising the functional $\|O\|$ ²³:

$$\|O\| = \langle \chi_{li} | O^2 | \chi_{li} \rangle^{\frac{1}{2}}$$

2.2.57

$$O = \tilde{\epsilon}_{li} |\tilde{\chi}_{li}\rangle \langle \tilde{\chi}_{li}| - \epsilon_{li} |\chi_{li}\rangle \langle \chi_{li}|$$

where the quantities capped with a tilde are obtained by solving the Hartree-Fock(-Dirac) equation with the trial potential. In the case the effective potential is derived from a relativistic Hartree-Fock-Dirac calculation the final potential is obtained as a weighted average of the potentials for the two different j -values.

After the effective potential has been found a small basis set is made by varying the exponents and coefficients of a trial basis and thus minimising the total energy.

The expansion 2.2.55 for the effective potential can be very short, while still obtaining fairly accurate results. Errors in the orbital energies ϵ_{li} , due to the effective potential rarely exceed 0.03 eV for an expansion of only three terms. Because the orbitals are nodeless, the valence basis set can also remain small. So this method leads to very compact ECP's and basis sets. Atomic calculations of Stevens et al. on several atomic states show that the ECP's are able to reproduce all-electron results within an error of 0.2 eV.

2.3 The Relativistic Computational Model

In the previous section we used the Schrödinger equation as the basic equation of motion. This equation is found by using the correspondence principle of the Hamiltonian formalism of non-relativistic classical mechanics. It has all the invariance properties of the Hamiltonian from which it derives. It can also be shown that the Schrödinger equation is invariant under the Galilean transformation, but not under the Lorentz transformation²⁴. Therefore the Schrödinger equation does not provide a proper description of systems for which relativistic effects are important.

In 1928 Dirac^{25,26} proposed an equation for a single electron moving in a potential ϕ , which is invariant under the Lorentz transformation:

$$i\hbar \frac{\partial}{\partial t} \Psi = [\alpha \cdot \mathbf{p} + \beta mc^2 - e\phi] \Psi. \quad 2.3.1$$

In this equation \mathbf{p} is the impulse and $\alpha \cdot \mathbf{p}$ is a shorthand notation for:

$$\alpha \cdot \mathbf{p} = \alpha_x \cdot p_x + \alpha_y \cdot p_y + \alpha_z \cdot p_z. \quad 2.3.2$$

The α 's and β are 4x4 matrices:

$$\alpha_x = \begin{pmatrix} \mathbf{0} & \sigma_x \\ \sigma_x & \mathbf{0} \end{pmatrix}; \alpha_y = \begin{pmatrix} \mathbf{0} & \sigma_y \\ \sigma_y & \mathbf{0} \end{pmatrix}; \alpha_z = \begin{pmatrix} \mathbf{0} & \sigma_z \\ \sigma_z & \mathbf{0} \end{pmatrix}; \beta = \begin{pmatrix} \mathbf{1} & \mathbf{0} \\ \mathbf{0} & -\mathbf{1} \end{pmatrix}, \quad 2.3.3$$

where the σ 's are the usual Pauli matrices:

$$\sigma_x = \begin{pmatrix} 0 & 1 \\ 1 & 0 \end{pmatrix}; \sigma_y = \begin{pmatrix} 0 & -i \\ i & 0 \end{pmatrix}; \sigma_z = \begin{pmatrix} 1 & 0 \\ 0 & -1 \end{pmatrix}. \quad 2.3.4$$

Just as in the case of the Schrödinger equation, the Dirac equation can be separated into an equation dependent on time only and an equation dependent on the spatial coordinates only. The time-independent Dirac equation is usually written as:

$$[c\alpha \cdot \mathbf{p} + \beta mc^2 - e\phi]\Psi = E\Psi. \quad 2.3.5$$

From the dimension of the matrices α and β it is clear that the solution of this equation must be a four-component spinor:

$$\Psi = \begin{pmatrix} \Psi_1^L \\ \Psi_2^L \\ \Psi_1^S \\ \Psi_2^S \end{pmatrix}. \quad 2.3.6$$

The upper half of the spinor is referred to as the large component and the lower half of the spinor is referred to as the small component. These names derive from the fact that the amplitude of the energy of the large component is of order c larger than that of the small component.

The eigenvalue spectrum of the Dirac equation ranges from $-\infty$ to ∞ , with a forbidden gap between $-mc^2$ and mc^2 . A possible physical interpretation of this spectrum and its drawbacks can be found in standard textbooks^{24,27}, and will not be dealt with here.

The Many-Electron Dirac Equation

To describe a system with more than one electron we need a generalisation of the Dirac equation. We will do this in analogy with the many-electron Schrödinger equation. We then get the Hamiltonian:

$$\mathbf{H}_D = \sum_{i=1}^n \mathbf{h}_i^D + \frac{1}{2} \sum_{i=1}^n \sum_{j=1}^n \mathbf{g}_{ij}, \quad 2.3.7$$

where \mathbf{h}_i^D is the Dirac-Hamiltonian of the i^{th} electron and \mathbf{g}_{ij} is the interaction between electrons i and j . In the Schrödinger equation \mathbf{g}_{ij} has the form:

$$\mathbf{g}_{ij} = \frac{1}{r_{ij}}, \quad 2.3.8$$

i.e. the Coulomb operator. It can be shown however that the Coulomb operator is not Lorentz invariant; so it can never be a correct relativistic operator. With the use of Quantum Electrodynamics it can be shown that the Coulomb term is the first term in an expansion of the true electron-electron interaction. This interaction cannot be written down in closed form. In practice only the first two terms of the expansion are retained²⁸. In the so-called low frequency limit this leads to an operator first derived by Breit²⁹:

$$\mathbf{g}_{ij}^{\text{Coulomb+Breit}} = \frac{1}{r_{ij}} - \frac{1}{2} \left(\frac{\boldsymbol{\alpha}_i \cdot \boldsymbol{\alpha}_j}{r_{ij}} + \frac{(\boldsymbol{\alpha}_i \cdot \mathbf{r}_{ij})(\boldsymbol{\alpha}_j \cdot \mathbf{r}_{ij})}{r_{ij}^3} \right). \quad 2.3.9$$

The first part of this operator is the usual Coulomb interaction, the second part is the magnetic interaction between the two electrons and the third part describes the retardation effects due to the finite velocity of the interaction. The magnetic term is also called the Gaunt interaction³⁰.

The many-electron time-independent Dirac equation can now be written as:

$$\mathbf{H}_D \Psi(\mathbf{r}_1 \cdots \mathbf{r}_n) = E \Psi(\mathbf{r}_1 \cdots \mathbf{r}_n), \quad 2.3.10$$

with \mathbf{H}_D given by equation 2.3.7 and \mathbf{g}_{ij} by equation 2.3.8 or 2.3.9. All relativistic calculations described in this thesis were performed with the \mathbf{g}_{ij} of equation 2.3.8. This was done because inclusion of the Gaunt interaction increases the resource demands of the

calculations considerably and only has a marginal effect on the results of Hartree-Fock-Dirac calculations^{31,32}.

The wave function $\Psi(\mathbf{r}_1 \dots \mathbf{r}_n)$ can be written in the form of equations 2.2.6 and 2.2.7, with the only difference that the set of one-electron functions $\{\psi_r(\mathbf{r})\}$ now consists of four-component spinors and not of scalar functions.

To solve equation 2.3.10 we can use in principle the same methodology as for the time-independent Schrödinger equation. There are two factors which make a small adjustment of the methods necessary. The first one is the different form of the one-electron functions. The second is the fact that the Dirac Hamiltonian is not bounded from below. As a consequence the variation theorem does not apply. However most variational methods only determine stationary states. By selecting only the lowest positive energy solutions we are able to determine the lowest positive energy state. The so-called variational collapse does not occur^{33,34,35}.

The Basis Set Expansion

The time-independent many-electron Dirac equation as written down in equation 2.3.10 looks at first glance very similar to the time-independent many-electron Schrödinger equation. To solve equation 2.3.10 we can use the same methodology as for solving the Schrödinger equation.

We write the wave function $\Psi(\mathbf{r}_1 \dots \mathbf{r}_n)$ again in the form of equations 2.2.6 and 2.2.7. There is one significant difference: The set one-electron functions $\{\psi_r(\mathbf{r})\}$ now consists of four-component spinors instead of scalar functions. To be able to use the basis set expansion in gaussian type functions we define two scalar gaussian type basis sets^{34,36,37}: one for the large component $\{\chi_r^L(\mathbf{r})\}$ and one for the small component $\{\chi_r^S(\mathbf{r})\}$ of the one-electron functions. We can then express the one-electron functions in the two basis sets:

$$\psi_r^{\alpha L} = \begin{pmatrix} \sum_i c_{iL}^r \chi_i^L \\ 0 \\ 0 \\ 0 \end{pmatrix}; \quad \psi_r^{\beta L} = \begin{pmatrix} 0 \\ \sum_i c_{iL}^r \chi_i^L \\ 0 \\ 0 \end{pmatrix}; \quad \psi_r^{\alpha S} = \begin{pmatrix} 0 \\ 0 \\ \sum_i c_{iS}^r \chi_i^S \\ 0 \end{pmatrix}; \quad \psi_r^{\beta S} = \begin{pmatrix} 0 \\ 0 \\ 0 \\ \sum_i c_{iS}^r \chi_i^S \end{pmatrix}. \quad 2.3.11$$

Just as in the non-relativistic case we can make more compact basis sets by optimising the exponents of the gaussians for the free atom and by determining the optimal coefficients c_{iX}^r and keep some of them fixed relative to each other in the subsequent molecular calculations.

The Kinetic Balance Principle

We can write the time-independent Dirac equation from equation 2.3.5 in the following way:

$$\begin{pmatrix} -e\phi & c\boldsymbol{\sigma} \cdot \mathbf{p} \\ c\boldsymbol{\sigma} \cdot \mathbf{p} & -e\phi - 2mc^2 \end{pmatrix} \begin{pmatrix} \psi^L \\ \psi^S \end{pmatrix} = \epsilon \begin{pmatrix} \psi^L \\ \psi^S \end{pmatrix}. \quad 2.3.12$$

From this notation it is immediately clear that we can formally express the small component of the spinor in terms of the large component:

$$\psi^S = \frac{1}{e\phi + \epsilon + 2mc^2} c\boldsymbol{\sigma} \cdot \mathbf{p} \psi^L \quad 2.3.13$$

Equation 2.3.13 can only be used if equation 2.3.12 has been solved and ϕ and ϵ are known. If we assume that ϕ and ϵ are small compared to $2mc^2$ (which is approximately true for valence electrons, but not for core electrons in heavy atoms) equation 2.3.13 reduces to:

$$\psi^S = \frac{1}{2mc} \boldsymbol{\sigma} \cdot \mathbf{p} \psi^L \quad 2.3.14$$

This relation is known as the kinetic balance³⁸ relation.

If the basis sets used for the expansion of the one-electron functions $\{\psi_i(\mathbf{r})\}$ are such that the relation 2.3.14 cannot be fulfilled the solution of equation 2.3.12 will not converge to the correct non-relativistic result in the limit of very large c . Furthermore there will occur spurious positive energy solutions, which have not enough kinetic energy. These spurious solutions may lead to a variational collapse³⁹.

To make sure that relation 2.3.14 can be fulfilled, the primitive small-component basis set is obtained by operating with the spatial part of $\boldsymbol{\sigma} \cdot \mathbf{p}$ on the primitive large-component basis set:

$$\{\chi_r^S\} \leftarrow \frac{\partial}{\partial \mathbf{r}} \{\chi_r^L\}. \quad 2.3.15$$

A basis set constructed in this way is said to be kinetically balanced. The primitive large-component basis set is determined in the same way as in the non-relativistic case.

In the case the large-component basis set is contracted a straightforward application of relation 2.3.15 may give erroneous results^{40,41}. We prefer to use the so-called atomic balance⁴². An atomic balanced basis set is constructed by performing a four-component relativistic calculation on the relevant atom, using a non-contracted kinetically balanced basis

set. The large and small-component functions are then separately contracted using the coefficients from this calculation.

The Hartree-Fock-Dirac Method

In this section we will briefly explain the relativistic analogue of the Hartree-Fock method: the Hartree-Fock-Dirac method.

We write the wave function $\Psi(\mathbf{r}_1 \dots \mathbf{r}_n)$ as a Slater determinant of one-electron four-component spinors:

$$\Psi(\mathbf{r}_1 \dots \mathbf{r}_n) = \Phi_0(\mathbf{r}_1 \dots \mathbf{r}_n) = \frac{1}{\sqrt{n!}} |\psi_1(\mathbf{r}_1) \psi_2(\mathbf{r}_2) \dots \psi_n(\mathbf{r}_n)|. \quad 2.3.16$$

The energy expression for an average of configurations⁴³ becomes:

$$\begin{aligned} E = & \sum_r \langle r | \mathbf{h} | r \rangle + \frac{1}{2} \sum_{r,s} [\langle rs | \mathbf{g} | rs \rangle - \langle rs | \mathbf{g} | sr \rangle] + \\ & f \sum_t \langle t | \mathbf{h} | t \rangle + \frac{1}{2} a f^2 \sum_{t,u} [\langle tu | \mathbf{g} | tu \rangle - \langle tu | \mathbf{g} | ut \rangle] + \\ & f \sum_{r,t} [\langle rt | \mathbf{g} | rt \rangle - \langle rt | \mathbf{g} | tr \rangle] \end{aligned} \quad 2.3.17$$

where r and s run over the closed-shell orbitals and t and u run over the open-shell orbitals. The operators \mathbf{h} and \mathbf{g} have the same meaning as in section 2.2. The factor f is the occupation number of the open shells:

$$f = \frac{n}{m}, \quad 2.3.18$$

where n is the number of open-shell electrons and m is the number of open-shell spinors. The constant a is the coupling constant:

$$a = \frac{m(n-1)}{n(m-1)}. \quad 2.3.19$$

If we now introduce the basis set expansion of equation 2.3.11 we can derive the Hartree-Fock-Dirac-Roothaan pseudo eigenvalue equations:

$$\mathbf{h}_{\text{HFD}}^c \mathbf{c}^c = \epsilon^c \mathbf{c}^c \quad 2.3.20$$

$$\mathbf{h}_{\text{HFD}}^o \mathbf{c}^o = \epsilon^o \mathbf{c}^o, \quad 2.3.21$$

where the superscript c refers to the closed shells and the superscript o to the open shells. The Hamiltonians are given by:

$$\mathbf{h}_{\text{HFD}}^c = \mathbf{h} + \mathbf{G}(\mathbf{R}^c) + \mathbf{G}(\mathbf{fR}^o) + \alpha \mathbf{L}^o \quad 2.3.22$$

$$\mathbf{h}_{\text{HFD}}^o = \mathbf{h} + \mathbf{G}(\mathbf{R}^c) + \mathbf{aG}(\mathbf{fR}^o) + \alpha \mathbf{L}^c \quad 2.3.23$$

where, in contrast to the non-relativistic case \mathbf{G} is now given by:

$$\mathbf{G}(\mathbf{R}) = \mathbf{J}(\mathbf{R}) - \mathbf{K}(\mathbf{R}). \quad 2.3.24$$

The coupling matrices \mathbf{L} take care of the orthogonality between the closed and open shell spaces and are given by:

$$\mathbf{L}^c = \mathbf{SR}^c \mathbf{G}(\mathbf{fR}^o) + \mathbf{G}(\mathbf{fR}^o) \mathbf{R}^c \mathbf{S} \quad 2.3.25$$

$$\mathbf{L}^o = \mathbf{SR}^o \mathbf{G}(\mathbf{fR}^o) + \mathbf{G}(\mathbf{fR}^o) \mathbf{R}^o \mathbf{S},$$

where the matrix \mathbf{S} is the overlap matrix of the basis. The coefficient α is given by:

$$\alpha = \frac{1-a}{1-f}. \quad 2.3.26$$

This method is basically the same as the open-shell restricted Hartree-Fock method outlined in the equations 2.2.31 through 2.2.35, although the problem of simultaneously diagonalising two Fock matrices is handled here differently. In contrast with 2.2.35 in this formalism Koopmans' theorem⁴⁴ is still valid⁴³; i.e. the orbital energies can be interpreted as zeroth order ionisation energies.

References

- 1) F. Bloch, *Z. Phys.*, **57** 545 (1929)
- 2) L.P. Bouckaert, R. Smoluchowski and E. Wigner, *Phys. Rev.*, **50** 58 (1936)
- 3) M. Jaros, in *Deep Levels in Semiconductors*, Chapter 6, Bristol, Adam Hilger Ltd. (1982)
- 4) S.T. Pantelides, *Rev. Mod. Phys.*, **50** 797 (1978) and references therein.
- 5) A. Zunger, *Solid State Phys.*, **39** 276 (1986)
- 6) J. Sauer, *Chem. Rev.*, **89** 199 (1989)
- 7) J. Almlöf and U. Wahlgren, *Theoret. Chim. Acta*, **28** 161 (1973)
- 8) B.T. Thole and P.Th. van Duijnen, *Theor. Chim. Acta*, **55** 307 (1980)
- 9) R. McWeeny and B.T. Sutcliffe, *Methods of Molecular Quantum Mechanics*, Academic Press Inc., London (1976)
- 10) C.C.J. Roothaan, *Rev. Mod. Phys.*, **23** 69 (1951)
- 11) C.C.J. Roothaan, *Rev. Mod. Phys.*, **32** 179 (1960)
- 12) Gaussian 92, Revision G.2, M. J. Frisch, G. W. Trucks, M. Head-Gordon, P. M. W. Gill, M. W. Wong, J. B. Foresman, B. G. Johnson, H. B. Schlegel, M. A. Robb, E. S. Replogle, R. Gomperts, J. L. Andres, K. Raghavachari, J. S. Binkley, C. Gonzalez, R. L. Martin, D. J. Fox, D. J. Defrees, J. Baker, J. J. P Stewart and J. A. Pople, Gaussian, Inc., Pittsburgh PA, 1992.
- 13) Bobrowicz and Goddard, Chapter 2 of *Modern Theoretical Chemistry*, Volume 3, H.F. Schaefer III, ed. (1977)
- 14) P.O. Löwdin, *Phys. Rev.*, **97** 1474 (1955)
- 15) J.B. Foresman, M. Head-Gordon, J.A. Pople and M.J. Frisch, *J. Phys. Chem.*, **96** 135 (1992)
- 16) A. Szabo and N.S. Ostlund, *Modern Quantum Chemistry*, McGraw-Hill Publishing Company, New York (1982)
- 17) R.C. Raffanetti, *J. Chem. Phys.*, **58** 4452 (1973)
- 18) W.J. Stevens, H. Basch and M. Krauss, *J. Chem. Phys.*, **81** 6026 (1984)
- 19) T.R. Cundari and W.J. Stevens, *J. Chem. Phys.*, **98** 5555 (1993)
- 20) C.F. Fischer, *Comp. Phys. Commun.*, **1** 151 (1969)
- 21) J.P. Desclaux, *Comp. Phys. Commun.*, **9** 31 (1975)
- 22) P. Christiansen, Y.S. Lee and K.S. Pitzer, *J. Chem. Phys.*, **71** 4445 (1979)
- 23) J.C. Barthelat, Ph. Durand and A. Serafini, *Mol. Phys.*, **33** 159 (1977)
- 24) A. Messiah, *Quantum Mechanics*, Volume II, North Holland Publishing Company, Amsterdam (1986)
- 25) P.A.M. Dirac, *Proc. Roy. Soc. A*, **117** 610 (1928)
- 26) P.A.M. Dirac, *Proc. Roy. Soc. A*, **118** 351 (1928)
- 27) P.A.M. Dirac, *The Principles of Quantum Mechanics*, Clarendon Press, Oxford (1984)
- 28) L.P. Grant and H.M. Quiney, *Advances in Atomic and Molecular Physics*, **23** 37 (1988)

-
- 29) G. Breit, *Phys. Rev.*, **34** 553 (1929)
 - 30) J.A. Gaunt, *Proc. Roy. Soc. A*, **122** 513 (1929)
 - 31) O. Visser, *Relativity in Quantum Chemistry*, PhD Thesis, University of Groningen, (1992)
 - 32) L. Visscher, *Relativity and Electron Correlation in Chemistry*, PhD Thesis, University of Groningen (1993)
 - 33) W. Kutzelnigg, *Int. J. Quant. Chem.*, **25** 107 (1984)
 - 34) P.J.C. Aerts, *Towards Relativistic Quantum Chemistry*, PhD Thesis, University of Groningen, (1986)
 - 35) D. Hegarty, *Theor. Chim. Acta*, **70** 351 (1986)
 - 36) *Relativistic Quantum Chemistry: The MOLFDIR program package*, L. Visscher, O. Visser, P.J.C. Aerts, H. Merenga and W.C. Nieuwpoort, *Computer Physics Communications* **81** 120 (1994)
 - 37) *Relativistic Quantum Chemistry: The MOLFDIR program package*, L. Visscher, W.A. de Jong, O. Visser, P.J.C. Aerts, H. Merenga and W.C. Nieuwpoort, in *METECC-95*, E. Clementi and G. Corongiu, (STEF, Cagliari, 1995)
 - 38) A.D. McLean and Y.S. Lee, in *Current Aspects of Quantum Chemistry 1981*, ed. R. Carbó, Elsevier, Amsterdam (1982)
 - 39) R.E. Stanton and S. Havriliak, *J. Chem. Phys.*, **81** 1910 (1984)
 - 40) Y. Ishikawa, H. Sekino and R.C. Binning Jr., *Chem. Phys. Lett.*, **165** 237 (1990)
 - 41) O. Matsuoka, *Chem. Phys. Lett.*, **195** 184 (1992)
 - 42) L. Visscher, P.J.C. Aerts, O. Visser and W.C. Nieuwpoort, *Int. J. Quant. Chem.: Quant. Chem. Symp.*, **25** 131 (1991)
 - 43) O. Visser, L. Visscher and P.J.C. Aerts, in *The effects of relativity in atoms, molecules and the solid state*, eds. I.P. Grant, B. Gyorffy and S. Wilson, Plenum, New York (1991)
 - 44) T. Koopmans, *Physica, 's Grav.*, **1** 104, (1933)

Chapter 3

Improving the Convergence Behaviour of the MOLFDIR Program Package

In this chapter we describe our work to optimise the convergence behaviour of the SCF part of the MOLFDIR^{1,2} package. We will review some convergence accelerator methods commonly used in traditional Hartree-Fock calculations and we will ascertain the applicability of these methods to the Hartree-Fock-Dirac case. The similarity of the SCF procedure in both the traditional and the relativistic Hartree-Fock calculations suggests that accelerator methods should show similar performances in both cases. After the review we will discuss the gains in performance realised by the implementation of the methods to enhance the convergence.

3.1 General Theory

There are basically two ways to reduce the number of SCF cycles needed to obtain the wave function to a certain degree of convergence:

- i) provide a good starting guess.
- ii) enhance the convergence gain per SCF cycle.

With the advent of generalised contracted basis sets³ a so-called core guess (i.e. the starting vectors for the SCF procedure are obtained by diagonalising the one-electron part of the Fock matrix) is approximately equal to a guess based on non-interacting atomic orbitals of the constituent atoms. Making better starting vectors is quite difficult and in our experience does not reduce the number of SCF cycles significantly. So we will not investigate this option any further. For the remainder of this chapter we will focus our attention on option ii).

Convergence enhancers can roughly be subdivided into two groups. Group 1 contains the methods that leave the traditional iterative scheme intact. These methods make use of interpolation or extrapolation schemes on the density or Fock matrix or on the vectors to enhance the convergence gain per SCF cycle. The second group of methods (Group 2) uses an alternative to the normal iterative scheme. These methods usually try to minimise the energy directly, without repeated diagonalisation of the Fock matrix.

3.2 Group 1 Convergence Accelerators

We will review a number of well-known extrapolation methods and explain the principles on which they work. For each method we will try to assess if it is worthwhile to implement it in MFDSCF, the SCF program of the MOLFDIR program package.

Damping

The simplest interpolation/extrapolation method that can be applied is damping. Damping is usually applied either to the vectors or to the density matrix. The new set of extrapolated vectors \mathbf{V}_f can be found by:

$$\mathbf{V}_f = \eta \mathbf{V}_{n-1} + (1 - \eta) \mathbf{V}_n, \quad 3.2.1$$

where \mathbf{V}_{n-1} are the vectors of the previous iteration, \mathbf{V}_n are the vectors of the current iteration and η is the damping constant.

The normal iterative procedure has a tendency to overestimate the needed changes in the vectors and density. This can lead to oscillations that sometimes even prevent the process from converging. With damping we can counteract these oscillations and force the process to convergence. When oscillations do not occur damping will only slow down the convergence. For the damping constant η we have two options: We can use a fixed damping constant or we can make the damping constant dependent on the achieved convergence. In practice methods with a variable damping constant work somewhat better than methods with a fixed damping constant.

The old MFDSCF program contains two damping methods that work on the vectors. The first method uses a fixed damping constant and the second method uses a variable damping

constant⁴. The variable damping constant is determined for each orbital separately, according to the formula:

$$\eta = \frac{\epsilon_i - \epsilon_{i-1}}{\epsilon_i - \epsilon_{i-1} - \epsilon'_{i-1} + \epsilon'_{i-2}}, \quad 3.2.2$$

where $\{\epsilon_i\}$ are the eigenvalues of the orbitals generated by the diagonalisation of the Fock matrix and $\{\epsilon'_i\}$ are the corrected eigenvalues of the orbitals after the damping procedure.

Both methods worked very poorly. The reason is that the extrapolated vectors were orthonormalised with the Schmidt orthogonalisation method. If the changes in the vectors in consecutive iterations are considerable the orthogonalisation will result in large corrections to especially the last vectors. The effect of the extrapolation is thus largely undone resulting in poor convergence. Therefore we have chosen to apply the damping to the density matrix.

Aitken Extrapolation

A somewhat more sophisticated extrapolation method is Aitken⁵. Aitken is a three point quadratic extrapolation method, where the change in a vector is considered as a function of that vector only and is extrapolated to zero. Let us call the vector of the last diagonalisation **c**, the vector of the previous iteration **b** and the vector of the iteration before that **a**. Each component of the extrapolated vector **e** is then found by the formula:

$$e_i = \frac{a_i c_i - b_i^2}{a_i + c_i - 2b_i}. \quad 3.2.3$$

Aitken is a reasonably efficient convergence accelerator as long as the not corrected iterative process is not wildly oscillating. Aitken has already been built into the MFDSCF program and the results are rather poor because of the reasons noted earlier.

Pople's Extrapolation

A very popular extrapolation method is the method due to Pople. It is implemented in many current quantum chemical program packages like Gaussian⁶, HONDO⁷ and GAMESS⁸. This method can be applied on the density matrix, the Fock matrix or the eigenvectors. In our discussion of the method we will assume it will be used on the density matrix. We first have to calculate the differences between four consecutive density matrices:

$$\mathbf{d}_1 = \mathbf{D}_n - \mathbf{D}_{n-1}, \quad 3.2.4$$

$$\mathbf{d}_2 = \mathbf{D}_{n-1} - \mathbf{D}_{n-2}, \quad 3.2.5$$

$$\mathbf{d}_3 = \mathbf{D}_{n-2} - \mathbf{D}_{n-3}. \quad 3.2.6$$

If the three \mathbf{d}_n vectors are nearly coplanar we extrapolate. To that end we write \mathbf{d}_1 in terms of \mathbf{d}_2 and \mathbf{d}_3 :

$$\mathbf{d}_1 = x\mathbf{d}_3 + y\mathbf{d}_2. \quad 3.2.7$$

We can write this alternatively as:

$$\begin{pmatrix} \mathbf{d}_1 \\ \mathbf{d}_2 \end{pmatrix} = \begin{pmatrix} y & x \\ 1 & 0 \end{pmatrix} \begin{pmatrix} \mathbf{d}_2 \\ \mathbf{d}_3 \end{pmatrix}. \quad 3.2.8$$

If the eigenvalues of the 2x2 matrix lie on the interval $[-0.95, 0.95]$ we can do the four point extrapolation:

$$\mathbf{D}_{\text{new}} = \mathbf{D}_n + \alpha\mathbf{d}_2 + \beta\mathbf{d}_3, \quad 3.2.9$$

with:

$$\alpha = \frac{x}{1-x-y} \text{ and } \beta = \frac{x+y}{1-x-y}. \quad 3.2.10$$

If the four point extrapolation is not possible we try the three point extrapolation. The three point extrapolation is only attempted if the vectors \mathbf{d}_1 and \mathbf{d}_2 are nearly parallel. The new density matrix is calculated according to:

$$\mathbf{D}_{\text{new}} = \mathbf{D}_n + \alpha\mathbf{d}_3, \quad 3.2.11$$

with

$$\alpha = \frac{|\mathbf{d}_1|}{|\mathbf{d}_2|\cos\phi - |\mathbf{d}_1|}, \quad 3.2.12$$

where ϕ is the angle between \mathbf{d}_1 and \mathbf{d}_2 .

Pople's extrapolation method was implemented in the MOLFDIR package. The extrapolation was done on the density matrix for the same reasons as stated in the discussion on the damping methods.

The DIIS Method

The most successful and best extrapolation method to date is Pulay's Direct Inversion in the Iterative Subspace^{9,10,11} method. This method can be used to extrapolate the density matrix and the Fock matrix.

Consider the error vector \mathbf{e}_i :

$$\mathbf{e}_i = [\mathbf{F}_i, \mathbf{D}_i], \quad 3.2.13$$

where in the commutator \mathbf{F}_i is the Fock matrix of the current iteration and \mathbf{D}_i is the density matrix of the current iteration. At convergence $\mathbf{e}_i = \mathbf{0}$. We now define a total error vector \mathbf{e} :

$$\mathbf{e} = \sum_{i=1}^n c_i \mathbf{e}_i, \quad 3.2.14$$

where n is the number of the current iteration. We will now minimise \mathbf{e} in a least squares sense:

$$\frac{\partial}{\partial c_i} \langle \mathbf{e} | \mathbf{e} \rangle = 0, \quad 3.2.15$$

under the constraint:

$$\sum_{i=1}^n |c_i|^2 = 1. \quad 3.2.16$$

The sets of equations 3.2.15 and 3.2.16 lead to a small set of linear equations:

$$\begin{pmatrix} 0 & -1 & -1 & \cdots & -1 \\ -1 & B_{11} & B_{12} & \cdots & \\ \cdots & & & & \\ -1 & \cdots & & B_{ij} & \\ \vdots & & & & \end{pmatrix} \begin{pmatrix} -\lambda \\ c_i \\ \vdots \\ c_i \\ \vdots \end{pmatrix} = \begin{pmatrix} -1 \\ 0 \\ \vdots \\ 0 \\ \vdots \end{pmatrix}, \quad 3.2.17$$

where

$$B_{ij} = \langle \mathbf{e}_i | \mathbf{e}_j \rangle \quad 3.2.18$$

and λ is a lagrangian multiplier. Equation 3.2.17 can be solved for \mathbf{c} with standard techniques. In the relativistic case the error vectors \mathbf{e}_i are complex. If we use the entire commutator matrix $[\mathbf{F}_i, \mathbf{D}_i]$ and not only the upper or lower triangle for the error supervectors \mathbf{e}_i , then the dot products $\langle \mathbf{e}_i | \mathbf{e}_j \rangle$ will be real and the remainder of the DIIS procedure can be standard. In practice we do not solve equation 3.2.17 as it stands. Firstly we multiply the diagonal elements of \mathbf{B} with a factor 1.02. This procedure is recommended by Pulay and serves to stabilise the process. Secondly we subtract row i from row $i+1$ in the \mathbf{B} matrix. This eliminates the lagrangian multiplier.

The new extrapolated Fock matrix can be calculated by:

$$\mathbf{F}_{\text{new}} = \sum_{i=1}^n c_i \mathbf{F}_i. \quad 3.2.19$$

We have applied the DIIS extrapolation on the Fock matrix. This is the least CPU intensive solution and it has the added advantage that at every cycle of the SCF process we have a correct idempotent density matrix.

3.3 Group 2 Convergence Accelerators

Group 2 methods usually try to minimise the energy expression directly. To do this one usually needs the first and the second derivatives of the energy with respect to the orbital coefficients. This is not a real problem for MCSCF calculations for which these methods were originally developed. For Hartree-Fock SCF calculations however the computation of the derivatives of the total energy cause such a high CPU overhead that these methods are not

of any practical value. Fortunately some methods were recently developed which avoid the direct computation of the energy derivatives.

In this section we will review the Quadratic Convergent SCF method, originally developed by Bacskey^{12,13}.

The Quadratic Convergent SCF Method: General Theory

The total orbital space for a molecule can be divided in three subspaces: The closed shell orbital space (D), the open shell orbital space (P) and the virtual orbital space (V). The wave function representing the ground state $|0\rangle$ must be invariant for any unitary V/D, V/P and P/D orbital mixing. This means that the first derivative of the total energy corresponding to such rotations must vanish, while the second derivative must be positive definite. The basic strategy of the QC-SCF method is to approximate the energy hypersurface with respect to a set of such orbital rotations by a quadratic surface whose minimum is then located, yielding an improved set of orbitals.

Let us consider a unitary orbital transformation:

$$\Phi = \Phi^0 U, \quad 3.3.1$$

$$U = e^{\mathbf{X}} = \mathbf{1} + \mathbf{X} + 1/2 \mathbf{X}^2 + \dots, \quad 3.3.2$$

where \mathbf{X} is an anti-hermitian matrix, i.e.:

$$X_{u,t} = -X_{t,u}^*, \quad 3.3.3$$

with the added constraint:

$$X_{i,j} = X_{p,q} = X_{a,b} = 0, \quad 3.3.4$$

where i and j run over the closed shell orbitals, p and q run over the open shell orbitals and a and b run over the virtual orbitals. So we will not bother with rotations within a subspace. The transformed orbitals can now be written as:

$$\Phi_s = \Phi_s^0 + \sum_t X_{t,s} \Phi_t^0 + \frac{1}{2} \sum_{t,u} X_{t,u} X_{u,s} \Phi_t^0 + \dots. \quad 3.3.5$$

The total energy as a function of \mathbf{X} up to second order can be written as:

$$E^{(2)} = E^{(0)} + \mathbf{X}^\dagger \mathbf{E}' + 1/2 \mathbf{X}^\dagger \mathbf{E}'' \mathbf{X}, \quad 3.3.6$$

where \mathbf{E}' is the first derivative and \mathbf{E}'' is the second derivative of the total energy with respect to the matrix elements $X_{t,u}$ at $\mathbf{X} = \mathbf{0}$. Expressions for the derivatives will be given later. The equations 3.3.5 and 3.3.6 are only valid for the real \mathbf{X} . For complex \mathbf{X} the equations become much more elaborate. We will for the remainder of this subsection assume that \mathbf{X} is real and discuss the results for complex \mathbf{X} in the next subsection.

In order to get a secular equation for \mathbf{X} we now define an energy functional $\epsilon[\mathbf{X}]$ that is quadratic in \mathbf{X} :

$$\epsilon[\mathbf{X}] = \frac{\mathbf{E}^{(2)} + \mathbf{E}^{(0)} \mathbf{D}^{(2)}}{1 + \mathbf{D}^{(2)}}. \quad 3.3.7$$

For an orthonormal orbital set the term $\mathbf{D}^{(2)}$ is defined by:

$$\mathbf{D}^{(2)} = \sum_{s < t} S_{ts,ts} |X_{t,s}|^2. \quad 3.3.8$$

The matrix \mathbf{S} is a diagonal matrix containing the terms:

$$\begin{aligned} S_{ia,ia} &= \text{closed shell occupation number,} \\ S_{pa,pa} &= \text{open shell occupation number,} \\ S_{pi,pi} &= (\text{closed} - \text{open}) \text{ shell occupation number.} \end{aligned} \quad 3.3.9$$

Minimising the functional $\epsilon[\mathbf{X}]$ yields the following two secular equations:

$$\mathbf{E}' + (\mathbf{E}'' + 2(\mathbf{E}^{(0)} - \epsilon)\mathbf{S})\mathbf{X} = \mathbf{0}, \quad 3.3.10$$

$$2(\mathbf{E}^{(0)} - \epsilon) = -\mathbf{X}^\dagger \mathbf{E}'. \quad 3.3.11$$

Making use of the hermiticity of $\mathbf{X}^\dagger \mathbf{E}'$ these two equations can be written as one eigenvalue equation:

$$\begin{pmatrix} E^{(0)} - \epsilon & \frac{1}{2} E'^{\dagger} \\ \frac{1}{2} E' & \frac{1}{2} E'' + (E^{(0)} - \epsilon) S \end{pmatrix} \begin{pmatrix} 1 \\ X \end{pmatrix} = 0. \quad 3.3.12$$

The matrix of equation 3.3.12 shows a resemblance with a Configuration Interaction (CI) matrix and will therefore be called the CI matrix for the remainder of this chapter.

Expressions for the Energy Derivatives

The definitions of E' and E'' differ in the relativistic case from the ones Bacskay uses. In the relativistic case the matrix X is complex. So the total energy now has to be differentiated with respect to the real and imaginary components of X separately. Thus we obtain two expressions for E' :

$$E'_{t,s}^R = \left[\left(\frac{\partial}{\partial X_{t,s}} - \frac{\partial}{\partial X_{s,t}} \right) E(X) \right]_{X=0}, \quad 3.3.13$$

$$E'_{t,s}^I = \left[\left(\frac{\partial}{\partial X_{t,s}} + \frac{\partial}{\partial X_{s,t}} \right) E(X) \right]_{X=0}, \quad 3.3.14$$

where the superscripts R and I denote the real and imaginary parts respectively. We get four expressions for E'' :

$$E''_{ts,vu}^{RR} = \left[\left(\frac{\partial}{\partial X_{t,s}} - \frac{\partial}{\partial X_{s,t}} \right) \left(\frac{\partial}{\partial X_{v,u}} - \frac{\partial}{\partial X_{u,v}} \right) E(X) \right]_{X=0} \text{ etc.} \quad 3.3.15$$

The term $E'^{\dagger} X$ in equation 3.3.12 now becomes:

$$\text{Re}(E' X) = E'^R X^R - E'^I X^I, \quad 3.3.16$$

$$\text{Im}(E' X) = 0. \quad 3.3.17$$

The term $E'' X$ in equation 3.3.12 now becomes:

$$\text{Re}(E'' X) = E''^{RR} X^R - E''^{RI} X^I, \quad 3.3.18$$

$$\text{Im}(E'' X) = E''^{IR} X^R - E''^{II} X^I. \quad 3.3.19$$

The two components of the first derivative and the four components of the second derivative can be calculated in the way outlined in the paper of Douady et al¹⁴ for the case of real \mathbf{X} . For complex \mathbf{X} the formalism becomes much more complicated.

Assuming the total energy can be written as¹⁵:

$$\begin{aligned}
 E = & \sum_i \langle i|h|i \rangle + \frac{1}{2} \sum_{i,j} \left[(ii||jj) - (ij||ji) \right] + \\
 & f \sum_p \langle p|h|p \rangle + \frac{1}{2} af^2 \sum_{p,q} \left[(pp||qq) - (pq||qp) \right] +, \\
 & f \sum_{i,p} \left[(ii||pp) - (ip||pi) \right]
 \end{aligned} \tag{3.3.20}$$

(where the two-electron integrals are written in the charge cloud notation) the components of the first derivatives of the energy are:

$$E'_{ai}{}^R = 2 \operatorname{Re}(F_{ai}^C), \tag{3.3.21}$$

$$E'_{ai}{}^I = -2 \operatorname{Im}(F_{ai}^C), \tag{3.3.22}$$

$$E'_{ap}{}^R = 2f \cdot \operatorname{Re}(F_{ap}^O), \tag{3.3.23}$$

$$E'_{ap}{}^I = -2f \cdot \operatorname{Im}(F_{ap}^O), \tag{3.3.24}$$

$$E'_{pi}{}^R = 2(1-f) \cdot \operatorname{Re}(F_{pi}^W), \tag{3.3.25}$$

$$E'_{pi}{}^I = -2(1-f) \cdot \operatorname{Im}(F_{pi}^W), \tag{3.3.26}$$

and the real components of the second derivative of the total energy are:

$$\begin{aligned}
 E''_{ai,bj}{}^{R,R} = & 2 \operatorname{Re}(F_{ab}^C) \delta_{ij} - 2 \operatorname{Re}(F_{ij}^C) \delta_{ab} + \\
 & 2 \left\{ 2(\operatorname{Re}(ai) \parallel \operatorname{Re}(bj)) - \operatorname{Re}((ib \parallel ja) + (ij \parallel ba)) \right\},
 \end{aligned} \tag{3.3.27}$$

$$\begin{aligned}
 E''_{ai,bp}{}^{R,R} = & \left\{ (1-f) \cdot \operatorname{Re}(F_{ip}^W) + 2f \cdot \operatorname{Re}(F_{ip}^O) \right\} \delta_{ab} + \\
 & 2f \cdot \left\{ 2(\operatorname{Re}(ai) \parallel \operatorname{Re}(bp)) - \operatorname{Re}((ib \parallel pa) + (ip \parallel ba)) \right\},
 \end{aligned} \tag{3.3.28}$$

$$\begin{aligned}
 E''_{ai,pj}{}^{R,R} = & \left\{ 2(1-f) \cdot \operatorname{Re}(F_{ap}^W) + f \cdot \operatorname{Re}(F_{ap}^O) \right\} \delta_{ij} + \\
 & 2(1-f) \cdot \left\{ 2(\operatorname{Re}(ai) \parallel \operatorname{Re}(pj)) - \operatorname{Re}((ip \parallel ja) + (ij \parallel pa)) \right\},
 \end{aligned} \tag{3.3.29}$$

$$E''_{ap,bq}{}^{R,R} = 2f \cdot \text{Re}(F_{ab}^O) \delta_{pq} - 2f \cdot \text{Re}(F_{pq}^O) \delta_{ab} + 2af^2 \cdot \left\{ 2(\text{Re}(ap) \parallel \text{Re}(bq)) - \text{Re}((pb \parallel qa) + (pq \parallel ba)) \right\}, \quad 3.3.30$$

$$E''_{ap,qi}{}^{R,R} = \left\{ (1-f) \cdot \text{Re}(F_{ai}^W) - f \cdot \text{Re}(F_{ai}^O) \right\} \delta_{pq} + 2f(1-af) \cdot \left\{ 2(\text{Re}(ap) \parallel \text{Re}(qi)) - \text{Re}((pq \parallel ia) + (pi \parallel qa)) \right\}, \quad 3.3.31$$

$$E''_{pi,qj}{}^{R,R} = 2(1-f) \cdot \text{Re}(F_{pq}^W) \delta_{ij} - 2(1-f) \cdot \text{Re}(F_{ij}^W) \delta_{pq} + 2(1-2f+af^2) \cdot \left\{ 2(\text{Re}(pi) \parallel \text{Re}(qj)) - \text{Re}((iq \parallel jp) + (ij \parallel qp)) \right\}. \quad 3.3.32$$

The imaginary and mixed components of the second derivative of the energy are listed in appendix B. In the equations 3.3.21 - 3.3.32 we made use of the following definitions:

$$\mathbf{F}^C = \mathbf{h} + \mathbf{Q}^C + \mathbf{Q}^O,$$

$$\mathbf{F}^O = \mathbf{h} + \mathbf{Q}^C + a\mathbf{Q}^O,$$

$$\mathbf{F}^W = \mathbf{h} + \mathbf{Q}^C + \frac{1-af}{1-f} \mathbf{Q}^O,$$

where \mathbf{h} : one-electron part of the Fock matrix,,

$$\mathbf{Q}^C = \sum_i (\mathbf{J}_i - \mathbf{K}_i) \text{ and } \mathbf{Q}^O = \sum_p (\mathbf{J}_p - \mathbf{K}_p)$$

$f = \frac{n}{d}$: occupation of open spin orbitals and

$$a = \frac{d(n-1)}{n(d-1)}: \text{coupling coefficient},$$

with n : number of electrons and

d : number of available spin orbitals.

3.3.33

\mathbf{J} and \mathbf{K} are the matrix representations of the coulomb and exchange operators respectively.

The components of the first derivative (equations 3.3.21 to 3.3.26) and the one-electron part (i.e. the Fock matrix part) of the components of the second derivative (equations 3.3.27 to 3.3.32) of the total energy are easily calculated, requiring only the construction of three Fock matrices and their transformation to the molecular orbital basis. The two-electron part of the components of the second derivative of the energy is much more involved.

The Direct CI Method

To compute the two-electron parts of the second derivative of the total energy we need to evaluate two-electron integrals over the molecular orbitals. This is usually done with the help of a four-index transformation on the two-electron integrals in the atomic orbital basis. Four-index transformations are very time consuming, so we would like to avoid this step. This is possible because we do not need E'' explicitly. We only need the quantity Q :

$$Q = E''X. \quad 3.3.34$$

We can calculate $Q(2 \text{ el.})$ relatively easy by first transforming the matrix X to the atomic orbital basis (i.e. the basis over which the two-electron integrals are calculated), then contracting this matrix with the two-electron integrals and finally transforming the resulting matrix back to the molecular orbital basis.

We write the matrix X as:

$$X = \begin{pmatrix} 0 & X_{co} & X_{cv} \\ X_{oc} & 0 & X_{ov} \\ X_{vc} & X_{vo} & 0 \end{pmatrix} \quad 3.3.35$$

and we write the matrix of the molecular orbital coefficients as:

$$C = \begin{pmatrix} C_c \\ C_o \\ C_v \end{pmatrix}. \quad 3.3.36$$

Transform X to the atomic orbital basis and call the new matrix D :

$$D = CXC^\dagger. \quad 3.3.37$$

When we write this out in the non-redundant components we get:

$$\begin{aligned} \mathbf{D}_{oc} &= \mathbf{C}_o \mathbf{X}_{oc} \mathbf{C}_c^\dagger \\ \mathbf{D}_{vc} &= \mathbf{C}_v \mathbf{X}_{vc} \mathbf{C}_c^\dagger \\ \mathbf{D}_{vo} &= \mathbf{C}_v \mathbf{X}_{vo} \mathbf{C}_o^\dagger \end{aligned} \quad 3.3.38$$

When we write the contraction of the density matrices \mathbf{D} with the two-electron integrals of the equations 3.3.27 to 3.3.32 as \mathbf{PD} (i.e. as the multiplication of the supermatrix \mathbf{P} with the supervector \mathbf{D}), the matrices \mathbf{Q}_{xy} (2 el.) can be written as:

$$\begin{aligned} \mathbf{Q}_{oc}(2 \text{ el.}) &= \mathbf{C}_o^\dagger \left[\mathbf{P} \left\{ 2(1-2f+af^2)\mathbf{D}_{oc} + 2(1-f)\mathbf{D}_{vc} + 2f(1-af)\mathbf{D}_{vo} \right\} \right] \mathbf{C}_c \\ &= \mathbf{C}_o^\dagger \left[\mathbf{PD}_\Sigma^{oc} \right] \mathbf{C}_c \end{aligned} \quad 3.3.39$$

$$\begin{aligned} \mathbf{Q}_{vc}(2 \text{ el.}) &= \mathbf{C}_v^\dagger \left[\mathbf{P} \left\{ 2(1-f)\mathbf{D}_{oc} + 2\mathbf{D}_{vc} + 2f\mathbf{D}_{vo} \right\} \right] \mathbf{C}_c \\ &= \mathbf{C}_v^\dagger \left[\mathbf{PD}_\Sigma^{vc} \right] \mathbf{C}_c \end{aligned} \quad 3.3.40$$

$$\begin{aligned} \mathbf{Q}_{vo}(2 \text{ el.}) &= \mathbf{C}_v^\dagger \left[\mathbf{P} \left\{ 2f(1-af)\mathbf{D}_{oc} + 2f\mathbf{D}_{vc} + 2af^2\mathbf{D}_{vo} \right\} \right] \mathbf{C}_o \\ &= \mathbf{C}_v^\dagger \left[\mathbf{PD}_\Sigma^{vo} \right] \mathbf{C}_o \end{aligned} \quad 3.3.41$$

Inspection of the equations 3.3.39 to 3.3.41 shows that:

$$\mathbf{D}_\Sigma^{oc} = \mathbf{D}_\Sigma^{vc} - \mathbf{D}_\Sigma^{vo} \quad 3.3.42$$

So we only have to compute two density matrices:

$$\mathbf{D}_\Sigma^{vc} = 2(1-f)\mathbf{D}_{oc} + 2\mathbf{D}_{vc} + 2f\mathbf{D}_{vo} \quad 3.3.43$$

$$\mathbf{D}_\Sigma^{vo} = 2f(1-af)\mathbf{D}_{oc} + 2f\mathbf{D}_{vc} + 2af^2\mathbf{D}_{vo} \quad 3.3.44$$

The density matrix \mathbf{D}_Σ^{oc} can then be found by applying equation 3.3.42. The three matrices \mathbf{Q}_{xy} are then easily obtained by applying the equations 3.3.39 to 3.3.41.

The equations 3.3.39 to 3.3.41 are only valid for the real component of the second derivative of the energy. The other components cannot be written in exactly the same form. The

supermatrix \mathbf{P} would be different for all the components of E'' . They can easily be derived from the equations in appendix B and will not be given here.

Raleigh-Schrödinger Perturbation Theory

The CI matrix will be diagonalised with the help of Raleigh-Schrödinger perturbation theory. We divide the CI matrix into two parts:

$$\text{CI matrix} = \mathbf{H}_0 + \mathbf{V} \quad 3.3.45$$

The matrix \mathbf{H}_0 is a diagonal matrix containing the term $E^{(0)}$ in the upper left corner and the term $E^{(0)}\mathbf{S}$ and the diagonal part of the one-electron (Fock) part of the second derivative of the total energy, in the lower right corner. The matrix \mathbf{V} contains the rest of the CI matrix. The zeroth order vector corresponding to the solution we seek is:

$$|0\rangle = (1 \ 0 \ 0 \ \dots). \quad 3.3.46$$

The i^{th} order correction to $|0\rangle$ is¹⁶:

$$|i\rangle = \frac{Y(0)}{A} \left\{ (\mathbf{V} - \epsilon_1)|i-1\rangle - \sum_{k=2}^i \epsilon_k |i-k\rangle \mathbf{S} \right\}, \quad 3.3.47$$

where:

$$\frac{Y(0)}{A} = \sum_{j \neq 0}^{\text{basis}} \frac{|j\rangle\langle j|}{S_{jj,jj}(E_0 - E_j)}, \quad 3.3.48$$

and ϵ_i is the i^{th} order correction to E_0 and E_j is the zeroth order energy belonging to the function $|j\rangle$. The RS perturbation theory is used to generate a small set of basis vectors on which the CI matrix is computed and diagonalised. The basis is extended until the changes in the lowest eigenvector of the CI matrix remain below a certain threshold.

The Algorithm

To summarise all the preceding theory we will present here a schematical overview of the algorithm of the QCSCF method. At the highest level we have the so-called macro iterations:

- i) Calculate \mathbf{F}^C , \mathbf{F}^O and \mathbf{F}^W . (equation 3.3.33)
- ii) Transform the Fock matrices to the molecular orbital basis.
- iii) Construct \mathbf{H}_0 .
- iv) Solve the CI equation for \mathbf{X} . (equation 3.3.12)
- v) Evaluate $e^{\mathbf{X}}$ and transform the molecular orbitals. (equation 3.3.5)
- vi) Check for convergence.
- vii) If the calculation has converged build the "normal" Fock matrix and diagonalise it to obtain the canonical molecular orbitals and stop.
Else go back to i)

In step iv) the CI matrix is diagonalised with the help of an iterative method. These iterations are called the micro iterations:

- i) Construct the zeroth order approximation to \mathbf{X} (i.e. equation 3.3.46).
- ii) Compute $\sigma_1 = \mathbf{V}|0\rangle$.
- iii) Construct the next (i^{th}) order correction \mathbf{X} with RSPT. (equation 3.3.47)
- iv) Compute $\sigma_{i+1} = \mathbf{V}|i\rangle$.
- v) Compute the $(i+1)^{\text{th}}$ row and column of the CI matrix in the basis of the perturbation correction functions, i.e. the matrix elements:

$$\langle j|\mathbf{H}|i\rangle = \langle j|\mathbf{H}_0|i\rangle + \langle j|\sigma_{i+1}\rangle$$
- vi) Diagonalise the CI matrix.
- vii) Check for convergence.
- viii) If the calculation has converged transform \mathbf{X} back to the MO basis,
Else go back to iii)

Step ii) and iv) can be subdivided as follows:

- i) Transform the matrices \mathbf{X}_{oc} , \mathbf{X}_{vc} and \mathbf{X}_{vo} to the non-symmetry basis and combine them with the proper coefficients to \mathbf{D}_{Σ}^{vc} and \mathbf{D}_{Σ}^{vo} . (equations 3.3.43 and 3.3.44)
- ii) Contract the \mathbf{D}_{Σ} matrices with the two-electron supermatrices to form the \mathbf{Q}' matrices.
- iii) Construct $\mathbf{Q}'_{oc} = \mathbf{Q}'_{vc} + \mathbf{Q}'_{vo}$.

- iv) Transform the \mathbf{Q}' matrices back to the MO basis. We now have the two-electron part of the vector σ .
- v) Add the first derivative part $\begin{pmatrix} \mathbf{0} & \mathbf{E}'^\dagger \\ \mathbf{E}' & \mathbf{0} \end{pmatrix} \begin{pmatrix} 1 \\ |i\rangle \end{pmatrix}$ to the vector σ .
- vi) Add the one-electron (Fock) part of the second derivative to the vector σ .

Because of the enormous complexity of this method we decided not to implement the imaginary components of the two-electron part of \mathbf{E}'' . This has simplified the programming considerably. The current implementation will still work properly when the eigenvectors of the Fock-Dirac matrix can be expressed with real valued coefficients in the basis set. In all other cases the current implementation may not work optimally.

In the next section we will, among other things, assess how bad this omission is and if it is worthwhile to implement the method fully.

3.4 Results

In this section we will present calculations we have done on some small systems to assess the performance of all the methods we have discussed in sections 3.2 and 3.3. We will present the systems in order of increasing complexity and show the results of non-relativistic and full four component relativistic calculations. For each system we will compare the performances of all relevant extrapolation methods and discuss the differences.

All the Group 1 methods are directly comparable because the CPU overhead they cause is small compared to the CPU requirements of a pure SCF cycle. The QCSCF method uses a very different scheme to obtain the wave function. Comparison with the other methods is therefore more difficult. We have chosen to compare the number of micro iterations needed by the QCSCF method to obtain a certain convergence to the number of traditional SCF cycles needed by the other methods to obtain the same convergence. This is a fair comparison because the amount of work needed for one QCSCF micro iteration is comparable to the amount of work needed for one traditional SCF cycle.

The test calculations are done in the same manner as they would be done in normal practice. The damping and Pople procedures are started at the first iteration and are not combined. The DIIS and QCSCF procedures are started when the convergence on the density is better than 10^{-2} . This is the minimal initial convergence these methods need to be able to converge to a proper state. The initial convergence of 10^{-2} is obtained by using the damping procedure because in this way it is guaranteed that one can reach this initial convergence.

Details of the Calculations

We have performed calculations on four different test systems. The first system is the boric atom. This is the simplest not trivial system we can test. It is small, containing only five electrons. It is only one atom, so it can be treated with the highest symmetry the MOLFDIR package can handle: O_h . The orbitals can be expressed with real valued coefficients in the basis set. So the current implementation of the QCSCF method should work correctly for this system. The system is not trivial because it does contain two fully occupied s orbitals and a partial occupied p orbital.

We used an uncontracted basis set, with the exponents taken from the STO-3G¹⁷ basis set. For the relativistic calculations we added a small component to the basis according to the strict kinetic balance principle.

The second system we have tested is the Co^{4+} ion. Just like the boric atom it has very high symmetry and its orbitals can be expressed with real valued coefficients in the basis set. However it is more complex than the boric atom. It is substantially bigger and it contains a half-filled 3d shell.

We used a (10/9/4) uncontracted basis set with the four d-exponents equal to the last four s-exponents. The small component basis set was derived from the large component basis set through the extended kinetic balance principle. The basis set is listed in appendix A.

We will now look at a more complex system: the SiH_4 molecule. This is a small, high symmetry (T_d) closed shell system. The molecular orbitals of this system cannot be expressed with real valued coefficients in the basis set. Even for the non-relativistic calculation the basis functions are chosen such that the molecular orbital coefficients are complex. So our implementation of the QCSCF method will not be able to handle this system correctly. The calculations on this system will give us a chance to assess the implications of the current implementation limits on the convergence behaviour of the QCSCF method.

The large component of the basis sets consisted of a (12/8) primitive basis contracted to (9/6) for Si, and a (6) primitive basis contracted to (3) for H. The small component of the basis set was derived from the large component through the extended kinetic balance recipe. The basis sets are listed in appendix A.

The final test system we look at is the CoF_6^{2-} molecular ion. This is a very difficult system. With the old version of the MFDSCF code we could not obtain a converged result. So this is an almost perfect test system for our new convergence accelerators. The symmetry of the ion is high: O_h . The large component basis set of Co consists of a (16/9/6) primitive basis generalised contracted to a (5/5/3) basis. The generalised contraction was based on a full four-component relativistic SCF calculation on the Co^{4+} ion. The small component basis set for Co was derived from the large component basis set through the extended kinetic balance principle. The large component basis set for F consists of the (10/6) primitive basis developed by Wachters¹⁸ generalised contracted to a (4/3) basis. The generalised contraction was based

on a full four-component relativistic SCF calculation on the F^- ion. The small component basis was derived from the large component basis through the extended kinetic balance principle. Both basis sets are listed in appendix A.

Discussion of the Results

The convergence behaviour of our test calculations is shown in the figures 3.4.1 to 3.4.8. For each system we have done a non-relativistic and a full four component relativistic calculation. For each system we only show the results of those methods that lead to some sort of converged result.

For the calculations on the two atoms we see that the normal non-extrapolated SCF procedure already shows a smooth convergence. Damping would slow the convergence down, so for these systems we did not try that, except in the preparatory cycles for the DIIS and QCSCF method. We can see that the convergence gain in those cycles is indeed smaller than in the non-extrapolated cycles. In the other cases the non-extrapolated SCF procedure will start to oscillate. For the non-relativistic calculation on the SiH_4 molecule the oscillations will damp out after 45 iterations and the subsequent convergence is smooth. For the remaining three calculations the SCF procedure will keep oscillating and a converged result cannot be reached. The suppression of oscillations is the main reason we implemented the fixed damping scheme. From figure 3.4.5 we can see that this is indeed what the damping procedure does. The convergence is smooth, but still very slow. This is partly due to the high damping constant ($\eta = 0.5$) we used. This high damping constant was needed to successfully suppress the oscillations in the early stages of the calculation. In the later stages of the calculation such a high damping constant obviously slows the convergence down. So the overall convergence is poor. The same holds for the relativistic calculation on SiH_4 . For the calculations on CoF_6^{2-} the situation is even worse. To successfully suppress the oscillations we needed a damping constant $\eta \geq 0.7$. As a result we needed more than 800 iterations to achieve a convergence of 10^{-10} on the density. These results are not shown in the figures.

The Pople extrapolation procedure only shows good results for the calculations on SiH_4 . For both the relativistic and the non-relativistic calculation the Pople procedure performs one three-point extrapolation, which brings the system out of oscillation. The subsequent convergence is fast and smooth. In all the other cases we were either not able to achieve a converged result or the Pople procedure performed approximately equal to the non-extrapolated SCF procedure.

The DIIS procedure performed very well in all cases. For the first three test systems we started the DIIS procedure after we had reached an initial convergence of 10^{-2} on the density. After the DIIS procedure was started convergence was smooth and very fast in all cases.

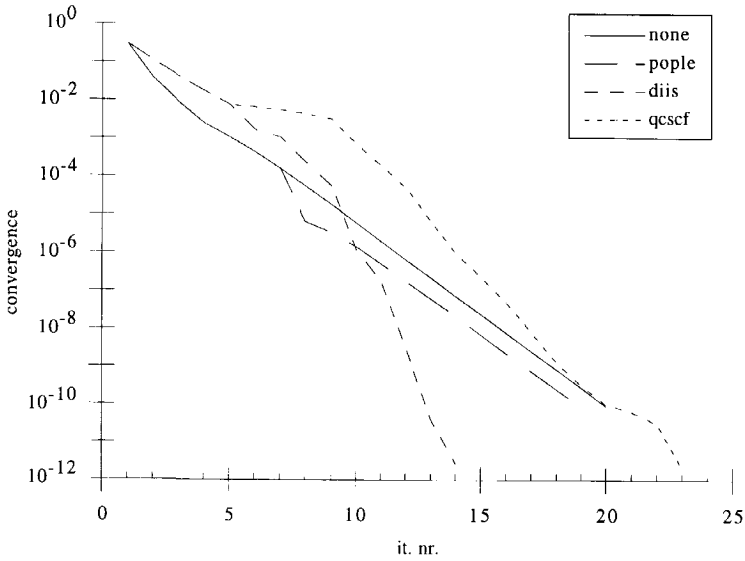


Figure 3.4.1 The convergence behaviour of the non-relativistic calculations on B.

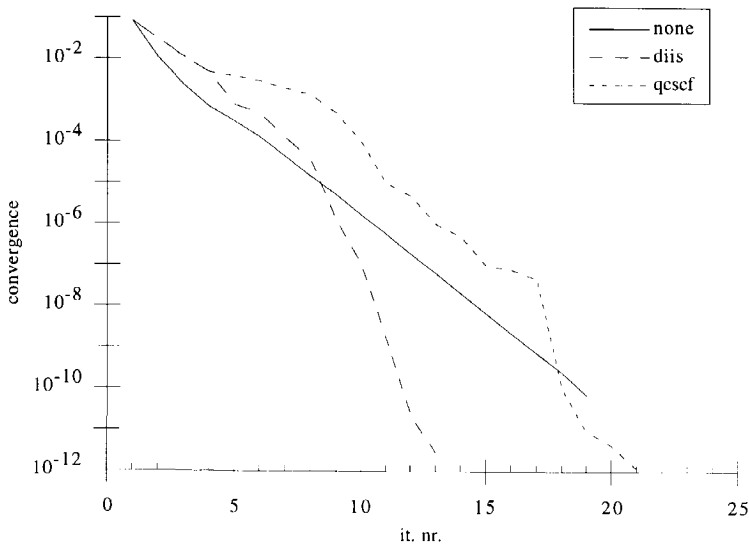


Figure 3.4.2 The convergence behaviour of the relativistic calculations on B.

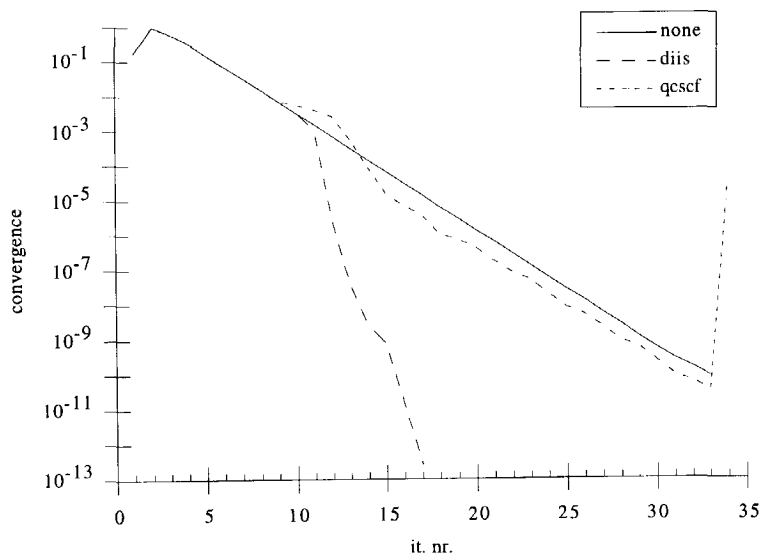


Figure 3.4.3 The results of the non-relativistic calculations on the Co^{4+} ion.

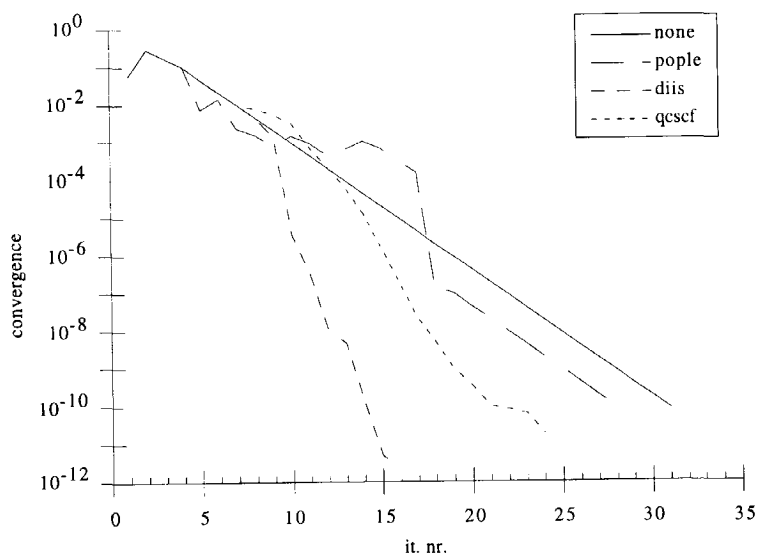


Figure 3.4.4 The results of the relativistic calculations on the Co^{4+} ion.

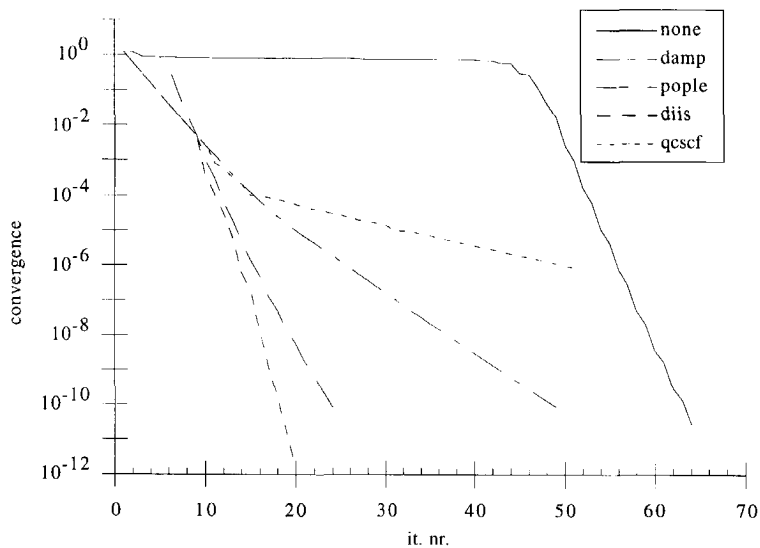


Figure 3.4.5 The results of the non-relativistic calculations on SiH_4 .

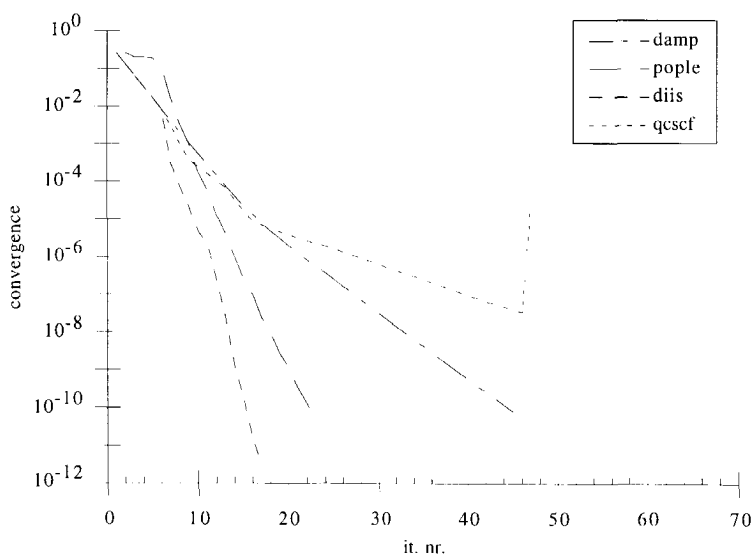


Figure 3.4.6 The results of the relativistic calculations on SiH_4 .

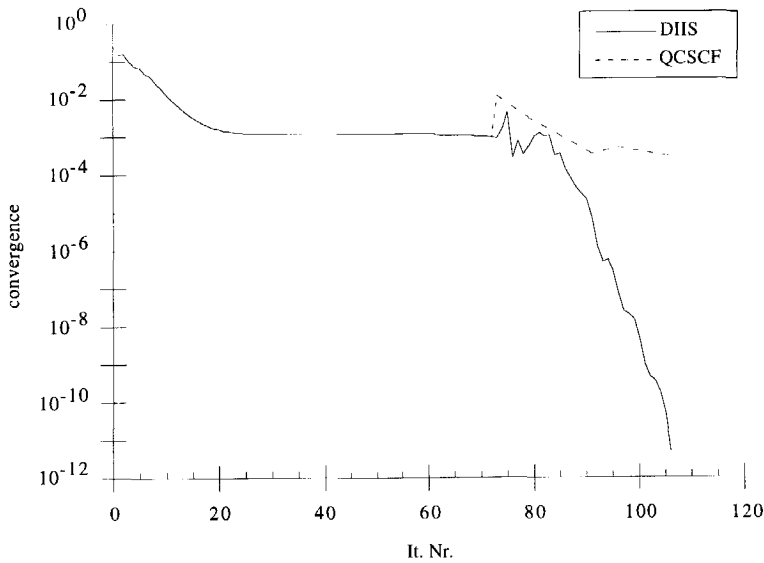


Figure 3.4.7 The results of the non-relativistic calculations on CoF_6^{2-} .

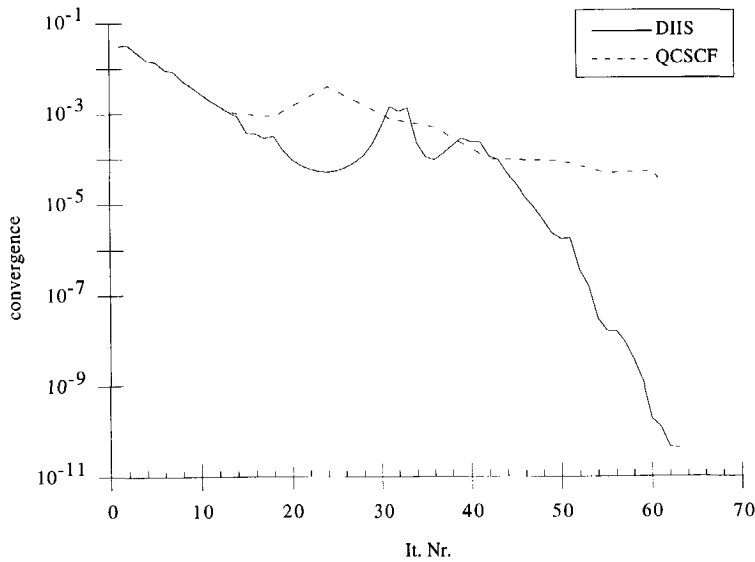


Figure 3.4.8 The results of the relativistic calculations on CoF_6^{2-} .

In the case of CoF_6^{2-} the DIIS procedure had some trouble reaching a converged result when we started the procedure at an initial convergence of 10^{-2} on the density. However it did eventually reach convergence. When we started the DIIS procedure at an initial convergence of 10^{-3} on the density it performed much better, although also in this case the DIIS procedure seems initially to have some problems. That we need a higher initial convergence here than in the other cases is caused by the high damping factor we needed to use to obtain the initial convergence. A high damping factor means that a very large part of the old density matrix is retained in the next iteration. Because of that the convergence appears to be better than it in reality is. This is nicely illustrated in figure 3.4.7. Upon starting the DIIS procedure the damping is switched off and we see the convergence drop by an order of magnitude.

The performance of the QCSCF method is a bit disappointing. For the calculations on the atoms the current implementation of the QCSCF method should work properly. On the macro iteration level the method indeed shows very fast convergence. Because each macro iteration needs on average three micro iterations the overall convergence however is poor. The calculations on B show that the performance is approximately equal to that of the non-extrapolated SCF procedure.

The non-relativistic calculation on Co^{4+} also shows a performance equal to the normal non-extrapolated procedure. But in the last iteration we see the convergence drop sharply. The last iteration of a QCSCF calculation consists of a traditional diagonalisation of the Fock matrix. This serves two purposes: It is a check to see if the QCSCF method really converged to a proper eigenstate of the Hamiltonian, and we get a set of canonical orbitals and orbital energies. We have to conclude that in this case the QCSCF method converged to a wrong state. Surprisingly the QCSCF method did perform quite well for the relativistic calculation on Co^{4+} . Although it was still outperformed by the DIIS method.

Because of the current implementation limits we expect the QCSCF method to perform even worse on our molecular test systems. The results bear this out. For the SiH_4 calculations the convergence is extremely slow and for the relativistic calculation it appears to converge towards a wrong state. For the calculations on CoF_6^{2-} we see almost no convergence gain at all. The convergence seems to remain at approximately 10^{-3} on the density.

3.5 Conclusions

Without any convergence accelerators the SCF procedure will only converge smoothly for very simple systems, like atoms. More complex systems will give rise to oscillations and will therefore converge very slowly, if at all.

The damping on the density is able to suppress those oscillations. With the damping procedure convergence can always be achieved, but the convergence can be very slow. In the case of the CoF_6^{2-} ion we needed more than 800 iterations to achieve a convergence of 10^{-10} on the density.

The Pople extrapolation procedure shows very variable results. In the calculations on the SiH_4 molecule the method performs very favourably, suggesting that for simple closed shell systems the method works quite well. In the calculations on the difficult CoF_6^{2-} molecular ion the method fails. The results for the B atom and the Co^{4+} ion do not show a clear trend. If the method works the convergence is not much better than the non-extrapolated convergence. So the Pople extrapolation method seems to have trouble with open shell systems.

The DIIS procedure shows excellent convergence behaviour. It does need a partially converged result to start, but the convergence after that is smooth and fast. An initial convergence of 10^{-2} on the density is in most cases enough to get good results. Such an initial convergence is easily reached with the damping procedure. The combination of damping and DIIS should be able to get a proper converged result in almost all cases.

The QCSCF procedure shows disappointing results. Part of this may be attributed to the current implementation limits of the method. The QCSCF method is implemented to work only with real \mathbf{X} . This is true only for a very limited set of systems. However the fact that the method also has problems with the non-relativistic calculation on the Co^{4+} ion suggests that there are other reasons as well. One of the assumptions in the derivation of the QCSCF method is that the energy hypersurface is quadratic. In general the energy hypersurface is not quadratic except to a good approximation near the absolute converged result. In our calculations we assumed that a convergence of 10^{-2} on the density was near enough to the real solution for the method to work. Apparently this is not true for all systems.

For the systems for which the method does work we see a very fast, almost quadratic, convergence on the macro iteration level. Unfortunately every macro iteration requires at least three micro iterations. As a consequence the overall performance of the QCSCF method always drags behind the performance of the DIIS procedure.

References

- 1) Relativistic Quantum Chemistry: The MOLFDIR program package, L. Visscher, O. Visser, P.J.C. Aerts, H. Merenga and W.C. Nieuwpoort, Computer Physics Communications **81** 120 (1994)

- 2) Relativistic Quantum Chemistry: The MOLFDIR program package, L. Visscher, W.A. de Jong, O. Visser, P.J.C. Aerts, H. Merenga and W.C. Nieuwpoort, in METECC-95, E. Clementi and G. Corongiu, (STEF, Cagliari, 1995)
- 3) R.C. Raffenetti, J. Chem. Phys. **58** 4452 (1973)
- 4) M. C. Zerner and M. Hehenberger, Chem. Phys. Lett. **62**(3) 550 (1979)
- 5) L. Fox, An Introduction to Numerical Linear Algebra, Clarendon Press, Oxford, 1979
- 6) Gaussian 92, Revision G.2, M. J. Frisch, G. W. Trucks, M. Head-Gordon, P. M. W. Gill, M. W. Wong, J. B. Foresman, B. G. Johnson, H. B. Schlegel, M. A. Robb, E. S. Replogle, R. Gomperts, J. L. Andres, K. Raghavachari, J. S. Binkley, C. Gonzalez, R. L. Martin, D. J. Fox, D. J. Defrees, J. Baker, J. J. P Stewart and J. A. Pople, Gaussian, Inc., Pittsburgh PA, 1992
- 7) HONDO is a molecular quantum mechanical program package developed by Dupuis and King.
- 8) GAMESS-UK is a package of ab initio programs written by M.F. Guest, J.H. van Lenthe, J. Kendrick, K. Schoffel, P. Sherwood and R.J. Harrison, with contributions from R.D. Amos, R.J. Buenker, M. Dupuis, N.C. Handy, I.H. Hillier, P.J. Knowles, V. Bonacic-Koutecky, W. von Niessen, V.R. Saunders and A.J. Stone. The package is derived from the original GAMESS code due to M. Dupuis, D. Spangler and J. Wendoloski, NRCC Software Catalogue, Vol. 1, Program No. QG01 (GAMESS), 1980
- 9) P. Pulay, Chem. Phys. Lett. **73**(2) 393 (1980)
- 10) P. Pulay, J. Comp. Chem. **3**(4) 556 (1982)
- 11) T. P. Hamilton and P. Pulay, J. Chem. Phys. **84**(10) 5728 (1986)
- 12) G. B. Bacskay, Chem. Phys. **61** 385 (1981)
- 13) G. B. Bacskay, Chem. Phys. **65** 383 (1982)
- 14) J. Douady, Y. Ellinger, R. Subra and B. Levy, J. Chem. Phys. **72**(3) 1452 (1980)
- 15) O. Visser, L. Visscher and P.J.C. Aerts, in The effects of relativity in atoms, molecules and the solid state, eds. I.P. Grant, B. Gyorffy and S. Wilson, Plenum, New York (1991)
- 16) A. Messiah, Quantum Mechanics, Volume II, North Holland Publishing Company, Amsterdam (1986)
- 17) W.J. Hehre, R.F. Stewart and J.A. Pople, J. Chem. Phys. **26** 57 (1969)
- 18) A.J.H. Wachters, PhD Thesis, Rijks Universiteit Groningen, 1971.

Chapter 4

Improving the Overall Efficiency of the MOLFDIR Program Package

In the previous chapter we described our improvements to the convergence behaviour of the MOLFDIR^{1,2} program package. Even with those improvements the amount of CPU time and the amount of disk space needed for a full four component relativistic calculation is still huge and can easily become prohibitive in the case of larger systems and systems of low symmetry. In this chapter we will describe our efforts to improve the overall efficiency of the MOLFDIR program package and thus reduce the amount of computer resources needed for a relativistic calculation.

In the first part of this chapter we will review the possibilities we have to improve the program package and make the choice of which improvements to apply. In the second part of this chapter we will give the current status of this work.

4.1 Problem Survey

The large demands the MOLFDIR program package has on the computational resources stem primarily from the enormous amount of two-electron integrals that need to be computed, stored and processed. The number of two-electron integrals is much larger than in the non-relativistic case. In the relativistic case we also need a basis set for the small component of the wave function. Because of the kinetic balance principle³ the basis set for the small component is larger and contains functions for higher l -values than the basis set for the large component. This greatly increases the number of two-electron integrals relative to non-relativistic calculations.

The large number of two-electron integrals creates two problems: Firstly the integrals have to be stored on disk. For larger and heavier systems the needed disk space is so large that it can easily become prohibitive. Secondly all the integrals have to be read in and processed at each

SCF iteration. The processing of all those integrals is the time determining step in the SCF process. Reading in all the integrals is slow and increases the wall clock time needed to complete the calculation.

So reducing the number of two-electron integrals would greatly improve the performance of the relativistic calculations with the MOLFDIR program package and would make calculations on larger systems or calculations on smaller computers more feasible.

4.2 Reduction of the Number of Two-Electron Integrals

There are basically three ways to reduce the problems associated with the large number of two-electron integrals. The first one is the so-called Direct SCF method⁴. The second one is reducing the actual number of two-electron integrals by making better use of symmetry. The third one is reducing the size of the basis set and thus reducing the number of two-electron integrals. In the following sections we will review these strategies and estimate their effectiveness.

4.3 The Direct SCF Method

In the "traditional" Hartree-Fock-Roothaan⁵ schemes the two-electron integrals are computed first and stored on disk. During the SCF cycles the integrals are read from the disk and used to build the Fock matrix. In the Direct SCF method the two-electron integrals are not stored but recomputed each time they are required. This reduces the storage requirements for a SCF calculation to almost zero.

If we would recompute all the two-electron integrals every cycle this method would show a substantial rise in the CPU time needed for a calculation. Fortunately algorithms have been devised which make the recomputation of an integral dependent on the amount of change in the density matrix elements with which that integral is multiplied. So the number of integrals that have to be calculated for a SCF cycle decreases when the convergence increases. Relatively recent implementations of this scheme, like the Direct SCF program in the Gaussian92 package⁶, show a very good performance relative to the traditional scheme.

Direct SCF programs seem to be very suited to the capabilities of modern day workstations, which have fast processors but very slow I/O channels.

A Direct SCF program for the MOLFDIR package would therefore be a welcome addition. The more so because the gain in CPU efficiency, resulting from clever integral routines, is expected to be larger in the four component case than in the normal two component case. The reason for this is twofold. The two-electron integrals over the small component of the basis set form by far the largest subset of the total number of two-electron integrals. Their contribution to the Fock-Dirac matrix however is small and does not change much from one iteration to the next. So they probably only have to be computed a few times. The second reason lies in the fact that the small and large component parts of the basis share the same exponents. So whenever the integrals over the small component basis have to be computed this can be done very efficiently.

A direct SCF program would make full relativistic SCF calculations on a routine basis much more feasible than it is now. The writing of a state of the art direct SCF program requires a major effort. Because of the limited time to our disposal we have decided against writing such a program.

4.4 The Use of Spatial Symmetry

The most promising way to reduce the number of two-electron integrals (at least for systems with high symmetry) is to make use of the available symmetry as much as possible. The old version of the MOLFDIR program package already uses the spatial symmetry to a high extend, but it can be made more efficient.

Theory

Consider a system with the pointgroup symmetry G . Also consider a set of atomic orbitals $\{\phi_i\}$ which we use to describe this system. We divide $\{\phi_i\}$ into subsets $\{\phi_i^a\}$ such that:

$$g\phi_i^a \in \{\phi_i^a\} \quad \forall g \in G, \quad 4.4.1$$

where g is a symmetry operator of the pointgroup G .

Within each subset $\{\phi_i^a\}$ we can make linear combinations of the ϕ_i^a such that the resulting functions transform according to some irreducible representation of the pointgroup G:

$$\psi_i^{\Gamma\gamma} = \mathcal{P}_{\Gamma\gamma} \phi_i^a. \quad 4.4.2$$

Where $\psi_i^{\Gamma\gamma}$ is the i^{th} symmetry adapted orbital of the subspecies γ of the irreducible representation Γ and $\mathcal{P}_{\Gamma\gamma}$ is the projection operator for the subspecies γ of the irreducible representation Γ .

Symmetry adapted orbitals belonging to different irreducible representations are always orthogonal. The Fock-Dirac operator \mathcal{F} transforms according to the total symmetric irreducible representation. So:

$$\langle \psi_i^{\Gamma} | \mathcal{F} | \psi_j^{\Omega} \rangle \neq 0 \quad \text{if and only if } \Gamma = \Omega. \quad 4.4.3$$

In other words the Fock-Dirac matrix will be block diagonal in the irreducible representations. We can now write the Fock-Dirac matrix in the basis of the symmetry adapted orbitals:

$$F_{ij}^{\Gamma\gamma} = h_{ij}^{\Gamma\gamma} + \sum_{kl} \sum_{\Omega\omega} \left(J_{ijkl}^{\Gamma\gamma\Omega\omega} - K_{ijkl}^{\Gamma\gamma\Omega\omega} \right) D_{kl}^{\Omega\omega}, \quad 4.4.4$$

where \mathbf{h} is the one-electron matrix, \mathbf{D} is the two-particle density matrix, \mathbf{J} is the coulomb interaction supermatrix and \mathbf{K} is the exchange interaction supermatrix. Note that we only need two-electron integrals of the form $(\Gamma_\gamma \Gamma_\gamma \| \Omega_\omega \Omega_\omega)$ and $(\Gamma_\gamma \Omega_\omega \| \Gamma_\gamma \Omega_\omega)$.

Symmetry requires that:

$$F_{ij}^{\Gamma_1} = F_{ij}^{\Gamma_2} \text{ etc.} \quad 4.4.5$$

So we can drop the subspecies label in equation 4.4.4:

$$F_{ij}^{\Gamma} = h_{ij}^{\Gamma} + \sum_{kl} \sum_{\Omega} \left(J_{ijkl}^{\Gamma\Omega} - K_{ijkl}^{\Gamma\Omega} \right) D_{kl}^{\Omega}, \quad 4.4.6$$

$$\text{with } J_{ijkl}^{\Gamma\Omega} = \frac{1}{N_\Gamma} \frac{1}{N_\Omega} \sum_{\gamma \in \Gamma} \sum_{\omega \in \Omega} J_{ijkl}^{\Gamma_\gamma \Omega_\omega}, \quad 4.4.7$$

where N_Γ is the dimension of the irreducible representation Γ .

The matrix elements $J_{ijkl}^{\Gamma\Omega}$ and $K_{ijkl}^{\Gamma\Omega}$ are called reduced matrix elements⁷. These reduced matrix elements all have totally symmetric integrands, because they have been averaged over all the subspecies within the relevant irreducible representation. This makes the computation of these reduced matrix elements relatively easy because we can use Pitzer's theorem⁸. Pitzer's theorem states that each integral of a set of integrals related by symmetry contributes equally to an integral with a totally symmetric integrand. In practice this means that we can compute all the matrix elements $J_{ijkl}^{\Gamma\Omega}$ and $K_{ijkl}^{\Gamma\Omega}$ from only the symmetry unique two-electron integrals over the atomic orbital basis.

Estimate of the Gain

To give an idea of the effects which the proper use of symmetry would have on the number of two-electron integrals we will give here an estimate for the CoF_6^{2-} system. This system has pointgroup symmetry O_h and consequently is a best case example because it has the highest symmetry the MOLFDIR package is able to handle.

The large component basis is a generalised contracted basis: Co (5s,5p,3d) and F (3s,2p). The small component basis was constructed from the large component basis with the kinetic balance principle: Co (6s,9p,8d,5f) and F (3s,4p,4d).

In table 4.4.1 we list the number of basis functions for each irreducible representation. In table 4.4.2 we list the number of two-electron integrals that the current package gives and the number of integrals that would result from the implementation of the symmetry supermatrix formalism⁹.

Component	e_{1g}	e_{2g}	f_g	e_{1u}	e_{2u}	f_u
large	12	5	15	12	2	14
small	42	26	63	37	24	55

Table 4.4.1 Number of basis functions for the CoF_6^{2-} system

The current version of the MOLFDIR package uses the so-called petite list¹⁰ of two electron integrals. This means that only the symmetry unique integrals are calculated and stored. Furthermore, integrals that are zero for symmetry reasons are also not calculated and stored. Integrals that are "accidentally" zero are calculated but not stored. The numbers listed in table 4.4.2 are the number of integrals that are actually stored.

For the symmetry supermatrix formalism the number of integrals we have to calculate is smaller than or equal to the number of integrals we have to calculate for the petite list because we only need symmetry unique integrals of the form $(\Gamma_\gamma \Gamma_\gamma \| \Omega_\omega \Omega_\omega)$ and $(\Gamma_\gamma \Omega_\omega \| \Gamma_\gamma \Omega_\omega)$.

	(LL LL)	(SL SL)	(SS SS)	Breit
current	220,600	6,357,851	47,940,066	12,401,379
with symmetry	79,800	2,319,387	16,898,391	4,638,774

Table 4.4.2 Number of two-electron integrals for the CoF_6^{2-} system

From table 4.4.2 we can see that the use of the supermatrix formalism gives a reduction of a factor three in the number of two-electron integrals. This result may be a bit flattered though, because the symmetry integrals will in general be complex quantities, while the integrals currently in use are all real. So the real gain depends on our ability to construct the symmetry adapted basis functions in such a way as to yield real valued integrals.

The current package stores the integrals together with their label. This label takes just as much space as the integral value. So the disk storage needed is twice that as expected on the basis of the number of integrals alone. In the symmetry supermatrix scheme the order of all the supermatrix elements is precisely defined. So we do not have to store labels for the matrix elements. This can be an advantage as well as a disadvantage. The advantage is that it halves our storage requirements relative to the current scheme. The disadvantage is that we cannot make use of the distance zeroes. We also have to store the integrals with value zero. So in practice we would save less than halve of the disk space. When generalised contracted¹¹ basis sets are used (which is normal practice) the number of distance zeroes is small. So this disadvantage will not be too severe.

4.5 The Use of Time Reversal Symmetry

In the previous section we have described the consequences of the spatial symmetry for the Hartree-Fock-Dirac calculations. Apart from this spatial symmetry the Dirac equation also shows another symmetry: the time reversal symmetry. The time reversal symmetry is not very well used in the MOLFDIR program package.

The time reversal symmetry results in an at least twofold degeneracy of each Fock-Dirac eigenvalue. The normal pointgroup symmetry cannot be used anymore and we have to use double group symmetry¹².

If we look at the basis functions that span the irreducible representations of the double groups, there are three possibilities with respect to the distribution of a basis function and its time reversed conjugate:

- i) The basis function and its time reversed conjugate are in different subspecies of the same irreducible representation.

- ii) The basis function and its time reversed conjugate are in different irreducible representations, of which the characters are each others complex conjugate. (Two such irreducible representations can be taken together to form one reducible representation.)
- iii) The basis function and its time reversed complex conjugate belong to the same (subspecies of an) irreducible representation.

In the first two cases the time reversal symmetry is in principle already contained in the symmetry adapted orbital basis defined in the previous section and there are no Fock matrix elements between a function and its time reversed conjugate. In the third case we have to take special actions to make use of the time reversal symmetry because now there are Fock matrix elements between all the functions in that irreducible representation.

General Theory

Consider a double group G^* containing (among others) two one-dimensional irreducible representations 'E and "E which have characters, that are each others complex conjugate. The projection operators \mathcal{P}'^E and \mathcal{P}''^E which produce suitable symmetry adapted functions out of a trial function are defined by:

$$\mathcal{P}'^E = \frac{1}{n} \sum_{i=1}^n (\chi_i'^E)^* g_i, \quad 4.5.1$$

$$\mathcal{P}''^E = \frac{1}{n} \sum_{i=1}^n (\chi_i''^E)^* g_i, \quad 4.5.2$$

$$\chi_i'^E = (\chi_i''^E)^*. \quad 4.5.3$$

Where n is the order of the group G.

The time reversal operator \mathcal{K} is defined by¹²:

$$\mathcal{K} = -i \begin{pmatrix} \sigma_y & 0 \\ 0 & \sigma_y \end{pmatrix} \mathcal{K}_0, \quad 4.5.4$$

where σ_y is the 2x2 Pauli matrix and \mathcal{K}_0 is the complex conjugation operator. We can now deduce the following relation between the two projection operators of equations 4.5.1 and 4.5.2:

$$\mathcal{P}^E = \mathcal{K}\mathcal{P}^E\mathcal{K}^{-1}. \quad 4.5.5$$

Now consider a function $|^E\rangle$. Operating on this function with the operator \mathcal{P}^E will return the same function $|^E\rangle$. Also:

$$\mathcal{P}^E|^E\rangle = \mathcal{K}\mathcal{P}^E\mathcal{K}^{-1}|^E\rangle = \mathcal{K}|^E\rangle. \quad 4.5.6$$

The last step in equation 4.5.6 follows from the fact that the operator \mathcal{P}^E will either project the function $|^E\rangle$ out of its object or return zero. The last option is clearly not possible.

So we have shown:

$$|^E\rangle = \mathcal{K}|^E\rangle. \quad 4.5.7$$

Now consider a matrix element of an arbitrary hermitian one-electron operator \mathfrak{h} . When we operate with the time reversal operator \mathcal{K} on this matrix element and make use of 4.5.7 we find:

$$\mathcal{K}\langle^E, i|\mathfrak{h}|^E, j\rangle = \langle^E, i|\mathcal{K}^\dagger\mathfrak{h}^\dagger\mathcal{K}|^E, j\rangle = \langle^E, i|\mathfrak{h}^\dagger|^E, j\rangle = \langle^E, i|\mathfrak{h}|^E, j\rangle. \quad 4.5.8$$

When we operate with the time reversal operator on the matrix element and do not make use of 4.5.7 we get:

$$\mathcal{K}\langle^E, i|\mathfrak{h}|^E, j\rangle = \langle^E, i|\mathcal{K}^\dagger\mathfrak{h}^\dagger\mathcal{K}|^E, j\rangle = \langle^E, i|\mathfrak{h}|^E, j\rangle^*. \quad 4.5.9$$

Combining 4.5.8 and 4.5.9 we find:

$$\langle^E, i|\mathfrak{h}|^E, j\rangle = \langle^E, i|\mathfrak{h}|^E, j\rangle^*. \quad 4.5.10$$

The Double Group D_2^*

We will limit ourselves now to the double group D_2^* . This group contains eight symmetry operators: \mathcal{E} , \mathcal{R}_z , \mathcal{C}_2 , $\mathcal{C}_2\mathcal{R}_z$, \mathcal{C}_x , \mathcal{R}_x , \mathcal{C}_y and $\mathcal{C}_y\mathcal{R}_x$ where \mathcal{R} is a rotation over 360° , which is for the double groups not equal to the identity operator. It has one two-dimensional fermion irreducible representation: $E_{1/2}$. The highest abelian subgroup for D_2^* along the subgroup chain is C_2^* . The double group C_2^* has four symmetry operators: \mathcal{E} , \mathcal{R}_z , \mathcal{C}_2 and $\mathcal{C}_2\mathcal{R}_z$. It has

two one-dimensional fermion irreducible representations: $'E_{1/2}$ and $''E_{1/2}$. The character projection operators for the symmetry adapted functions for D_2^* now become:

$$\begin{aligned}\mathcal{P}'^E &= \frac{1}{4}(\mathcal{E} - \mathcal{R} + i\mathcal{C}_z - i\mathcal{RC}_z) \\ \mathcal{P}''^E &= \frac{1}{4}(\mathcal{E} - \mathcal{R} - i\mathcal{C}_z + i\mathcal{RC}_z)\end{aligned}\tag{4.5.11}$$

In this way we obtain symmetry functions that transform simultaneously as the $E_{1/2}$ irreducible representation of D_2^* and as one of the irreducible representations of the subgroup C_2^* . The symmetry adapted functions that are obtained by applying the projection operators of equation 4.5.11 define matrix representations $D_{E,\Gamma}(\mathcal{O})$ for the operators \mathcal{O} of the group D_2^* , with Γ : $'E$ or $''E$. Now consider the effect of the operator C_y (which is not in C_2^*) on a matrix element of a one-electron operator \mathfrak{h} , which is invariant under the symmetry operations of the group D_2^* :

$$\begin{aligned}C_y\langle E, 'E, i | \mathfrak{h} | E, 'E, j \rangle &= \sum_{\Gamma, \Omega}^{\{E, ''E\}} \langle E, \Gamma, i | \mathfrak{h} | E, \Omega, j \rangle D_{\Gamma, 'E}^*(C_y) D_{\Omega, ''E}(C_y) \\ &= \langle E, ''E, i | \mathfrak{h} | E, ''E, j \rangle\end{aligned}\tag{4.5.12}$$

Because the operator \mathfrak{h} is invariant for a rotation around the y-axis we should also have:

$$C_y\langle E, 'E, i | \mathfrak{h} | E, 'E, j \rangle = \langle E, 'E, i | \mathfrak{h} | E, 'E, j \rangle.\tag{4.5.13}$$

Combining equations 4.5.12 and 4.5.13 yields:

$$\langle E, 'E, i | \mathfrak{h} | E, 'E, j \rangle = \langle E, ''E, i | \mathfrak{h} | E, ''E, j \rangle\tag{4.5.14}$$

Combining the equations 4.5.14 and 4.5.10 gives:

$$\langle E, 'E, i | \mathfrak{h} | E, 'E, j \rangle = \langle E, 'E, i | \mathfrak{h} | E, 'E, j \rangle^*\tag{4.5.15}$$

So the matrix elements have to be real. In a very similar way it can also be shown that the two-electron integrals, i.e. the matrix elements $J_{ijkl}^{\Gamma\Omega}$ and $K_{ijkl}^{\Gamma\Omega}$, are real.

The Other Double Groups

For non-abelian double groups symmetry adapted basis functions are constructed by using a projection operator that is a product of two projection operators:

$$\mathcal{P}^{\Gamma\Omega} = \mathcal{P}^{\Gamma}\mathcal{P}^{\Omega} \quad 4.5.16$$

Double group	Irreducible representation	Subgroup	Irreducible representation
T_d^*	$E_{1/2}$ $E_{5/2}$ $G_{3/2}$	S_4^*	' $E_{1/2}$ ', " $E_{1/2}$ " ' $E_{3/2}$ ', " $E_{3/2}$ " ' $E_{1/2}$ ', " $E_{1/2}$ ", ' $E_{3/2}$ ', " $E_{3/2}$ "
O^*	$E_{1/2}$ $E_{5/2}$ $G_{3/2}$	C_4^*	' $E_{1/2}$ ', " $E_{1/2}$ " ' $E_{3/2}$ ', " $E_{3/2}$ " ' $E_{1/2}$ ', " $E_{1/2}$ ", ' $E_{3/2}$ ', " $E_{3/2}$ "
O_h^*	$E_{g,1/2}$ $E_{g,5/2}$ $G_{g,3/2}$ $E_{u,1/2}$ $E_{u,5/2}$ $G_{u,5/2}$	C_{4h}^*	' $E_{g,1/2}$ ', " $E_{g,1/2}$ " ' $E_{g,3/2}$ ', " $E_{g,3/2}$ " ' $E_{g,1/2}$ ', " $E_{g,1/2}$ ", ' $E_{g,3/2}$ ', " $E_{g,3/2}$ " ' $E_{u,1/2}$ ', " $E_{u,1/2}$ " ' $E_{u,3/2}$ ', " $E_{u,3/2}$ " ' $E_{u,1/2}$ ', " $E_{u,1/2}$ ", ' $E_{u,3/2}$ ', " $E_{u,3/2}$ "
D_4^*	$E_{1/2}$ $E_{3/2}$	C_4^*	' $E_{1/2}$ ', " $E_{1/2}$ " ' $E_{3/2}$ ', " $E_{3/2}$ "
C_{4v}^*	$E_{1/2}$ $E_{3/2}$	C_4^*	' $E_{1/2}$ ', " $E_{1/2}$ " ' $E_{3/2}$ ', " $E_{3/2}$ "
D_{2d}^*	$E_{1/2}$ $E_{3/2}$	S_4^*	' $E_{1/2}$ ', " $E_{1/2}$ " ' $E_{3/2}$ ', " $E_{3/2}$ "
D_{4h}^*	$E_{g,1/2}$ $E_{g,3/2}$ $E_{u,1/2}$ $E_{u,3/2}$	C_{4h}^*	' $E_{g,1/2}$ ', " $E_{g,1/2}$ " ' $E_{g,3/2}$ ', " $E_{g,3/2}$ " ' $E_{u,1/2}$ ', " $E_{u,1/2}$ " ' $E_{u,3/2}$ ', " $E_{u,3/2}$ "
D_2^*	$E_{1/2}$	C_2^*	' $E_{1/2}$ ', " $E_{1/2}$ "
C_{2v}^*	$E_{1/2}$	C_2^*	' $E_{1/2}$ ', " $E_{1/2}$ "
D_{2h}^*	$E_{g,1/2}$ $E_{u,1/2}$	C_{2h}^*	' $E_{g,1/2}$ ', " $E_{g,1/2}$ " ' $E_{u,1/2}$ ', " $E_{u,1/2}$ "

Table 4.5.1 Subgroup chains and fermion irreducible representations correspondence for point groups with an even order principle axis

where Γ is a multi-dimensional irreducible representation of the non-abelian double group and Ω is a corresponding one-dimensional irreducible representation of the highest abelian double group in the subgroup chain.

In this way we uniquely resolve the degeneracy of the highest irreducible representation.

In the tables 4.5.1 and 4.5.2 we list the group chains that are used in the MOLFDIR program package along with the correspondence of the irreducible representations.

In table 4.5.1 we see that all non-abelian double groups, with a principal rotation axis of even order, are reduced to S_4^* , C_4^* , C_2^* or the product of one of these groups with C_i^* . The symmetry adapted functions for the double groups that are reduced to C_2^* (D_2^* and C_{2v}^*) can all obviously be constructed in such a way as to yield real valued integrals.

In a recent paper Visscher¹³ shows that the symmetry adapted functions for the double groups D_2^* and C_{2v}^* can be chosen in such a way as to give real valued integrals. In that paper it is also argued that the double groups which reduce to C_4^* or S_4^* will also have real valued one- and two-electron integrals, because the functions obtained for those groups will also define proper representation matrices for the elements of the groups D_2^* and C_{2v}^* .

Double group	Irreducible representation	Subgroup	Irreducible representation
T^*	$E_{1/2}$ ' $G_{3/2}$ " $G_{3/2}$	C_3^*	' $E_{1/2}$, " $E_{1/2}$ B, ' $E_{1/2}$ B, " $E_{1/2}$
T_h^*	$E_{g,1/2}$ ' $G_{g,3/2}$ " $G_{g,3/2}$ $E_{u,1/2}$ ' $G_{u,3/2}$ " $G_{u,3/2}$	S_6^*	' $E_{g,1/2}$, " $E_{g,1/2}$ B _g , ' $E_{g,1/2}$ B _g , " $E_{g,1/2}$ ' $E_{u,1/2}$, " $E_{u,1/2}$ B _u , ' $E_{u,1/2}$ B _u , " $E_{u,1/2}$
D_3^*	$E_{1/2}$ ' $E_{3/2}$, " $E_{3/2}$	C_3^*	' $E_{1/2}$, " $E_{1/2}$ B, B
C_{3v}^*	$E_{1/2}$ ' $E_{3/2}$, " $E_{3/2}$	C_3^*	' $E_{1/2}$, " $E_{1/2}$ B, B
D_{3d}^*	$E_{g,1/2}$ ' $E_{g,3/2}$, " $E_{g,3/2}$ $E_{u,1/2}$ ' $E_{u,1/2}$, " $E_{u,3/2}$	S_6^*	' $E_{g,1/2}$, " $E_{g,1/2}$ B _g , B _g ' $E_{u,1/2}$, " $E_{u,1/2}$ B _u , B _u

Table 4.5.2 Subgroup chains and fermion irreducible representations correspondence for point groups with an odd order principle axis

For double groups with a principal rotation axis of odd order things are more complicated. All the non-abelian double groups are reduced to C_3^* or S_6^* . The symmetry adapted functions that are constructed for these groups do not form a proper representation for the elements of D_2^* and consequently the integrals are not necessarily real valued.

For those groups we can still construct symmetry adapted basis functions which do deliver real integrals. In fact we can do so for all double groups that do not contain A or B fermion irreducible representations. To accomplish this we need to combine functions from the 'E_{n/2} and "E_{n/2} (or 'G_{n/2} and "G_{n/2}) irreducible representations in such a way that they still form proper time reversal pairs and that they form a proper matrix representation for the symmetry operators of D_2^* .

This procedure however destroys (part of) the symmetry blocking of the Fock-Dirac matrix and will thus give rise to larger **J** and **K** supermatrices. It is not a priori clear if the full use of spatial symmetry or the advantage of being able to work with real valued matrix elements will result in the most efficient calculations. It may well be that the optimal choice differs for different double groups.

For the double groups containing real one-dimensional fermion irreducible representations of type iii, using the time reversal symmetry to advantage is much more difficult. We can regard a type iii irreducible representation as a type ii reducible representation, but with real characters. The time reversal operator connects the two components of this reducible representation and the Fock-Dirac matrix will be block diagonal in the components. The problem with this picture is that we have no way to distinguish between the functions belonging to one of the components. Therefore it is very difficult to construct a set of functions that blocks the Fock-Dirac matrix. Furthermore the set of functions that block the Fock-Dirac matrix may contain linear combinations of functions which the current version of MOLFDIR cannot handle. The same arguments hold for the construction of basis functions that would yield real valued integrals.

4.6 Current Status

At this moment there is a production version of the MOLFDIR program package which makes use of the fact that the integrals for groups containing D_2^* or C_{2v}^* as a subgroup are real valued. This version of the code was programmed by Visscher¹³. The performance of his code relative to the old one is discussed in his paper for the F₂ molecule using the double group D_{4h}^* . His conclusion is that for the diagonalisation and the construction (the time

determining step) of the Fock matrix significant speedups are achieved. Significant time savings are also observed for the Coupled Cluster calculations.

A version of the MOLFDIR package that makes use of the supermatrix formalism is not yet production ready. The programs MOLFDIR, RELTWEL and MFDSCF have been adapted to make use of the supermatrix formalism and to make use of the real valued integrals for those double groups that contain D_2^* or C_{2v}^* as a subgroup. A new program MFDSRT has been written to construct the **J** and **K** supermatrices from the unsorted two-electron integrals over the symmetry adapted functions which are obtained by RELTWEL.

Because a whole chain of programs has been changed, debugging is tricky. The work has not been completed yet. So a comparison between the supermatrix formalism and the use of the petite list of integrals cannot yet be given.

References

- 1) Relativistic Quantum Chemistry: The MOLFDIR program package, L. Visscher, O. Visser, P.J.C. Aerts, H. Merenga and W.C. Nieuwpoort, *Computer Physics Communications* **81** 120 (1994)
- 2) Relativistic Quantum Chemistry: The MOLFDIR program package, L. Visscher, W.A. de Jong, O. Visser, P.J.C. Aerts, H. Merenga and W.C. Nieuwpoort, in *METECC-95*, E. Clementi and G. Corongiu, (STEF, Cagliari, 1995)
- 3) R.E. Stanton and S. Havriliak, *J. Chem. Phys.* **81** 1910 (1984)
- 4) J. Almlöf, K. Faegri Jr. and K. Korsell, *J. Comp. Chem.* **3** 385 (1982).
- 5) C.C.J. Roothaan, *Rev. Mod. Phys.* **32** 179 (1960)
- 6) Gaussian 92, Revision G.2, M. J. Frisch, G. W. Trucks, M. Head-Gordon, P. M. W. Gill, M. W. Wong, J. B. Foresman, B. G. Johnson, H. B. Schlegel, M. A. Robb, E. S. Replogle, R. Gomperts, J. L. Andres, K. Raghavachari, J. S. Binkley, C. Gonzalez, R. L. Martin, D. J. Fox, D. J. Defrees, J. Baker, J. J. P. Stewart and J. A. Pople, Gaussian, Inc., Pittsburgh PA, 1992.
- 7) G. Aissing, PhD Thesis, Rijksuniversiteit Groningen, 1988.
- 8) R. M. Pitzer, *J. Chem. Phys.* **58** 3111 (1973).
- 9) C.C.J. Roothaan, *Rev. Mod. Phys.*, **23** 69 (1951)
- 10) P.J.C. Aerts, *Chem. Phys. Lett.*, **104** 28 (1984) and references therein.
- 11) R.C. Raffanetti, *J. Chem. Phys.* **58** 4452 (1973)
- 12) J. G. Snijders, PhD Thesis, Free University of Amsterdam, 1979.
- 13) Lucas Visscher, *Chem. Phys. Lett.*, **253** 20 (1996)

Chapter 5

The Fluorine Compounds

With the help of electronic structure calculations we want to improve our understanding of scintillation in inorganic ionic crystals. In recent years our group has experimentally and theoretically studied several ionic crystals, doped with cerium^{1,2,3,4,5,6}. In such crystals the cerium ion usually acts as the luminescence centre. The luminescence is caused by a $\text{Ce}^{3+} 5d^1 \rightarrow \text{Ce}^{3+} 4f^1$ transition. We will limit our investigations to ionic crystals doped with cerium. In this chapter we will discuss the results of our calculations on several fluorine compounds containing cerium. The compounds we have investigated are: CeF_3 , $\text{LaF}_3:\text{Ce}$, $\text{LiLuF}_4:\text{Ce}$, $\text{LiYF}_4:\text{Ce}$ and $\text{LiBaF}_3:\text{Ce}$.

CeF_3 and $\text{LaF}_3:\text{Ce}$ are interesting systems to investigate for several reasons. Some of these reasons are technical; the others have a more physical background.

First the technical reasons: In CeF_3 the Ce ion is part of the host crystal and not an impurity. The positions of all the atoms are known from X-ray diffraction experiments. Any discrepancies between our calculated results and experimental results cannot be due to uncertainties about the atom positions but must come from errors or oversights in our method. Good experimental data are available for CeF_3 and $\text{LaF}_3:\text{Ce}$ on the absorption and emission frequencies^{7,8} as well as on the positions of the Ce 4f and Ce 5d levels in the band gap^{9,10}. CeF_3 and $\text{LaF}_3:\text{Ce}$ have the same crystal lattice, although somewhat different bond lengths. The experimental results for both systems are therefore very similar. In our cluster approach there is, apart from the different bond lengths, no difference between these two systems. So from a technical standpoint these two systems belong together and form an almost ideal benchmark for our methods.

From a physical standpoint CeF_3 is also a very interesting compound. It has a very high density, so consequently a high stopping power for radiation. It is extremely radiation hard¹¹. It shows very fast scintillation (~ 10 ns.). It also has a reasonably high photon yield (~ 4000 photons/MeV)¹². These properties have made CeF_3 an interesting candidate for a gamma detector for the Large Hadron Collider to be built at CERN¹³. For the above mentioned reasons it is understandable that this material has raised a considerable amount of interest in recent years from the scintillation community.

LiYF₄ crystals doped with Ce have been studied some 16 years ago because of their potential application as ultraviolet solid-state lasers¹⁴. Recently experiments have been performed in our laboratory on the scintillation properties of LiYF₄:Ce and LiLuF₄:Ce^{5,15}. The object of these experiments was to determine the suitability of these materials to provide a good thermal neutron detector. The presence of Li in these compounds is required because of its ability to convert the incident thermal neutrons into secondary charged particles. This is done through the reaction:



The crystal structures of LiYF₄ and LiLuF₄ are almost identical, which can also be seen from their almost identical spectra. Therefore we have only performed calculations on LiYF₄:Ce¹⁶.

LiBaF₃ has recently been investigated experimentally¹⁷ in our laboratory to determine its suitability to provide a detector for thermal neutrons. It was found that this scintillator exhibits cross-luminescence and self-trapped-exciton luminescence. The Li ions in the compound are needed to convert the thermal neutrons into secondary charged particles according to the reaction equation 5.0.1. To see if light output of the material could be improved by doping it with Ce, experiments have been performed on LiBaF₃:Ce crystals¹⁸. Our calculations have been performed to assist these experiments.

5.1 The Model

To improve our understanding of the crystals involved we want to calculate the Ce 4f and Ce 5d levels and their positions in the band gap of the host material. We cannot solve the Schrödinger or Dirac equation for the entire crystal, so we need to make some approximations. Our theoretical model contains two separate approximations. One approximation is concerned with the level of theory for the computations; the other is concerned with the material representation of the crystal.

The Material Model

The properties we are interested in are mainly local properties of the Ce impurity. A band structure calculation cannot describe these local properties, so we use the cluster

approximation. We represent the crystal with a cluster containing the Ce impurity and the first layer of the atoms from the host crystal. The interaction with the rest of the crystal is represented by a limited number of point charges, which are chosen so as to generate the correct Madelung potential at the cluster sites, due to the rest of the crystal¹⁹. A more thorough discussion of the cluster model can be found in chapter 2.

In figure 5.1.1 we show the Ce 5d level splitting for the Ce^{3+} ion in the field of the LaF_3 Madelung potential and for the CeF_{11} cluster in the field of the LaF_3 Madelung potential. It can easily be seen that it is essential to include the first layer of atoms of the host crystal to accurately describe the Ce 5d levels. If we replace the first layer of neighbouring atoms with point charges the calculated 5d level splitting is far too small.

The position of the band edges of the host crystal can only be a crude approximation, because of the very limited size of the cluster^{20,21}.

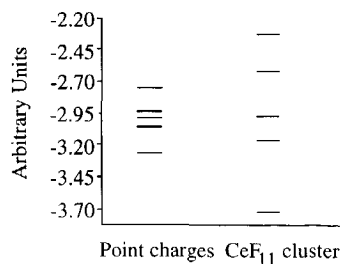


Figure 5.1.1 Point charge model results for the 5d level splitting of Ce^{3+} ion in the Madelung field of LaF_3 compared to those of a CeF_{11} cluster in the Madelung field of LaF_3 .

The Computational Model

We use ab initio molecular quantum mechanical methods to compute all the energies we need: HF SCF^{22,23}, HFD SCF^{24,25}, GVB²⁶ and CIS²⁷ (see also Chapter 2). Ce is a rather heavy atom, so we expect relativistic effects to be important. However, because of their very large demands for resources relativistic calculations are not always feasible for the systems we want to study. Fortunately, it is possible to get good results without using the relativistic variant for all the calculations. In figure 5.1.2 we show the 4f and 5d levels of the Ce ion calculated with the fully relativistic Hartree-Fock-Dirac method and with the non-relativistic Hartree-Fock method.

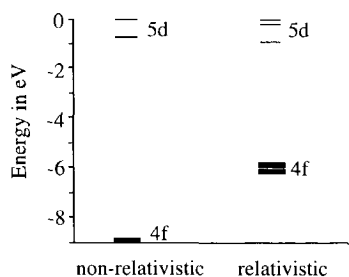


Figure 5.1.2 The 4f and 5d levels of a Ce^{3+} ion surrounded by six point charges on the x, y and z axes. (Site symmetry: O_h)

It is clear from this figure that the distance between the Ce 4f and the Ce 5d levels can only be described correctly by a relativistic formalism. The spread in the Ce 5d levels, apart from the spin-orbit interaction, however is already correctly described by a non-relativistic formalism.

The Ce 4f - 5d energy difference obeys some regularities we can use to minimise the number of relativistically correct calculations. In figure 5.1.3 we show the *experimental* energy difference between the average of the energies of the Ce 4f levels and the average of the energies of the Ce 5d levels for some crystals^{5,15,18,28,29,30,31}. It appears that for all fluorine compounds the distance between the average of the Ce 4f and the average of the Ce 5d levels is approximately the same.

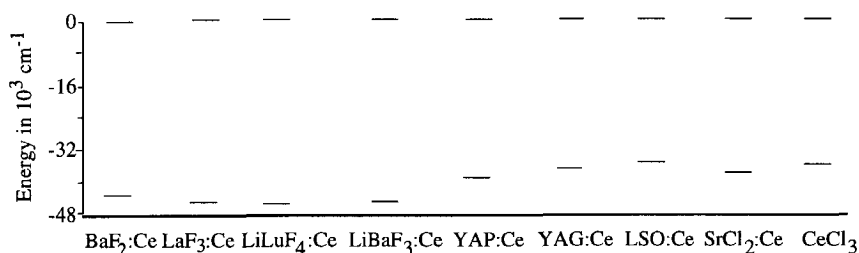


Figure 5.1.3 Energy difference between the average of the Ce 4f and the average of the Ce 5d levels.

This also seems to hold, to a somewhat lesser extent, for the oxygen compounds and the chlorine compounds. So for each type of crystal (i.e. fluorine compounds, oxygen compounds, chlorine compounds, etc.) we need one fully relativistic calculation to determine the distance between the energy of the average of the Ce 4f states and the energy of the average of the Ce 5d states and thus the distance between the average Ce 4f and 5d levels. After that we only need to perform a non-relativistic calculation on the relevant cluster to determine the Ce 5d energy levels. This can be done in several ways: by doing one Restricted Hartree-Fock calculation on the average of all Ce 5d states or by doing a Configuration Interaction Singles calculation. From the calculated Ce 5d levels we can then deduce the position of the average of the Ce 4f levels.

Recently good effective core potentials were developed for the lanthanides which contain relativistic effects³². Because these effective core potentials are to be used in non-relativistic calculations one cannot expect them to give completely relativistically correct results. The orbitals which are described explicitly will differ somewhat from the correct relativistic orbitals and the spin-orbit coupling will be missing entirely. Nevertheless they can provide an estimate for the Ce 4f - 5d energy difference. We will ascertain in this chapter how good these estimates really are.

The Band Gap

To determine the band gap and the positions of the valence and conduction band edges we have several options. To calculate the band gap we perform a Hartree-Fock calculation on the ground state of a cluster of the host material and a General Valence Bond Open Shell Singlet calculation on the first excited state of the same cluster. The difference of the total energies of these calculations is taken as a reasonable measure for the band gap. In a physical sense we are making in this calculation, a localised exciton: an excitation of a fluorine 2p electron to the 5d/6s orbital of a neighbouring Ce atom. This picture does not correspond very well with the concept of band gap as it is derived from effective one-electron band structure calculations³³. On the other hand from experiment it is known that the bottom of the conduction band in CeF_3 is formed by a hybrid of Ce 5d and Ce 6s orbitals³⁴. It is exactly such an excitation that we calculate. Because of electronic polarisation the occupied 5d/6s orbital will lower in energy and the exciton will become localised. The band gaps calculated with this procedure are in better agreement with experiment than the band gaps calculated from the band structure picture (see section 5.2).

From experiment it is known that the conduction band edge in the real crystal is formed by the metal s functions³⁵, or a 5d/6s orbital hybrid in the case of all Ce compounds. In our clusters we only have one central ion and consequently a delocalised metal s band cannot be formed. By adding a few very diffuse s functions to the basis set of the metal atom we give the system the possibility to form a set of very diffuse (delocalised) s orbitals. We assume that these very diffuse s orbitals will give a reasonable estimate for the bottom of the conduction band.

The Position of the Ce Levels in the Gap

The position of the Ce levels in the band gap is a more complex problem. We start with a Hartree-Fock calculation on a $\text{Ce}^{3+} 5d^1$ configuration. Assuming Koopmans' theorem³⁶ is valid the positions of the Ce 5d levels on an absolute scale are given by their orbital energies. The Ce 4f levels can be placed relative to the Ce 5d levels with the help of the energy difference between the average of the Ce 5d)¹ states and the average of the Ce 4f)¹ states for that type of crystal. To find the position of the Ce levels in the band gap we need to determine the positions of the valence and conduction band edges. There are two possibilities. We can assume that the orbital energy of the lowest unoccupied molecular orbital (diffuse metal s-type orbital) of the pure host crystal gives the edge of the conduction band and then place the valence band edge relative to this estimated conduction band edge with the help of the calculated value for the band gap. This procedure will shift the valence band orbitals to higher energy. We can also assume that the valence band edge is given by the orbital energy

of the highest occupied F 2p orbital and place the conduction band edge relative to this valence band edge with the help of the calculated value for the band gap.

Because the cluster we use is too small to give the fluorine atoms a chance to form a good band the F 2p band will be too narrow. Hence the highest F 2p orbitals will lie too low in energy. The absence of part of the repulsion the 2p-electrons would feel in the crystal will also place the F 2p orbitals too low. The diffuse metal s-type orbital of the host material cluster is expected to give a reasonable estimate for the conduction band edge although the error bar is not known.

The advent of good effective core potentials for the heavier elements makes possible a more solid way for calculating the positions of the localised Ce levels in the gap. Furthermore, because the core potentials describe the inner core orbitals of the elements the number of electrons that are described explicitly and consequently the number of basis functions needed is much smaller than in the all-electron case. This enables us to do calculations on a higher level of theory (CIS) than would have been possible in the all-electron case. Also, because the effective core potentials contain the relativistic effects of the core orbitals they enable us to obtain a much more accurate description of the Ce 4f orbitals in an otherwise non-relativistic calculation than we would have obtained with an all-electron basis set. As we will see a good accuracy of the Ce 4f level energies is a very important prerequisite for the success of the method.

The VB - Ce 4f distance is calculated by taking the total energy difference between a SCF calculation on the cluster in its Ce^{4+} state and a SCF or GVB calculation on the cluster in a $\text{Ce}^{3+} 4f^1$ anion np-hole state. If the anion np band is too narrow this energy difference will be too large and the Ce 4f levels will lie too high in the gap. The error will be less severe than in the last alternative method which relates the position of the Ce levels to the position of the anion np orbitals, because in this case we do not incur the error caused by the neglect of electronic relaxation in using Koopmans' theorem.

To calculate the difference between the $\text{Ce}^{3+} 4f^1$ levels and the $\text{Ce}^{3+} 5d^1$ levels we have two options. We can take the difference in total energy between a SCF calculation on the lowest $\text{Ce}^{3+} 4f^1$ state of the cluster and a SCF or GVB calculation on the lowest $\text{Ce}^{3+} 5d^1$ state of the cluster. These calculations give the distance between the lowest $\text{Ce}^{3+} 4f^1$ and lowest $\text{Ce}^{3+} 5d^1$ state. The other $\text{Ce}^{3+} 5d^1$ states can be positioned by making use of the calculated Ce 5d level splitting. The second option we have is performing a CIS calculation with as reference state the $\text{Ce}^{3+} 4f^1$ groundstate of the cluster. From this calculation we obtain directly the energy differences between the $\text{Ce}^{3+} 4f^1$ groundstate and all the $\text{Ce}^{3+} 5d^1$ states.

Finally we place the conduction band above the valence band with the amount calculated for the band gap.

5.2 CeF_3 and $\text{LaF}_3\text{:Ce}$

The CeF_3 and LaF_3 crystals belong to the spacegroup P3-C1 ^{37,38}. The pointgroup site symmetry of the Ce or La atom is C_2 . The Ce atom is surrounded by 11 fluorine atoms at various distances. So the obvious first choice of a cluster to describe the crystal with is a CeF_{11} cluster surrounded by point charges that represent the Madelung potential. We shall later see that this cluster is quite sufficient to give a good description of those features of CeF_3 that we are interested in. A picture of the cluster is given in figure 5.2.1.

Due to the relatively large size and low symmetry of the cluster we were not able to perform fully relativistic calculations. We did perform Hartree-Fock and CIS calculations. The Hartree-Fock calculations have been done with several basis sets to establish the sensitivity of the results for the basis sets used. The large basis set for Ce we have used was constructed from the one by van Piggelen³⁹ by reoptimising the exponents for the $\text{Ce}^{3+} 5d^1$ state with a Watson shell at the smallest Ce - F distance in CeF_3 . The primitive set was used both in a generalised contraction⁴⁰

and in a segmented contraction. The contraction coefficients were taken from a non-relativistic atomic calculation on Ce^{3+} in the $5d^1$ configuration with a Watson shell at the smallest Ce-F distance in CeF_3 . The basis set is listed in appendix A. The large basis set for F we have used is a (11/6) primitive set, optimised for the groundstate of F^- with a Watson shell at the smallest Ce-F distance in CeF_3 . This basis set was used in generalised contraction and in a segmented contraction. The basis set is also listed in appendix A. The small basis set for Ce is a (15/10/8) primitive set contracted to (6/5/4). This basis is listed in appendix A. The small basis set for F is a primitive (7/6) basis contracted to (2/1). The basis was optimised for the groundstate of F^- and is due to Huzinaga⁴¹.

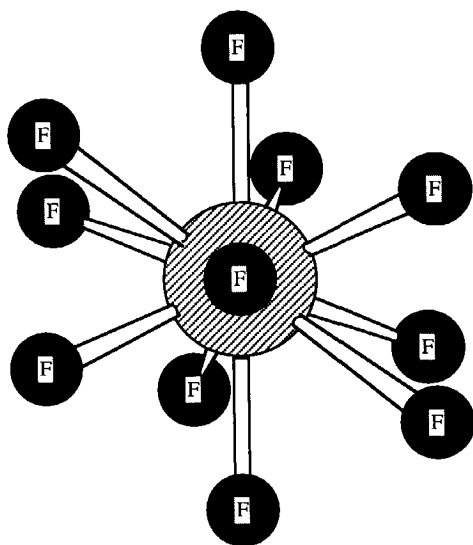


Figure 5.2.1 The CeF_{11} cluster in CeF_3
The direction of view is along the C_2 axis.

All the CIS calculations and some of the Hartree-Fock calculations were done with the ECP's and basis sets of Stevens et al^{32,42}. For the Ce atom we used a (111) contraction for the d-exponents and a (61) contraction for the f-exponents. For the F⁻ ion we changed the contraction of the basis to (211) to allow for the more diffuse negative charge state.

In table 5.2.1 we show the ionisation potential for the Ce³⁺ ion as calculated with the basis sets we have used.

	basis			exp. ^{43,44}
	large	small	ecp	
IP Ce ³⁺ 4f) ¹	N.A.	N.A.	35.75	36.72
IP Ce ³⁺ 5d) ¹	30.21	29.00	29.48	31.65

Table 5.2.1 Ionisation potentials for the Ce³⁺ ion. All entries in eV.

The calculated ionisation potentials agree within an error of 8% with the experimental ionisation potentials. The large basis set, which is significantly larger than the other basis sets only performs slightly better than the other basis sets. We may conclude that the basis sets are all flexible enough to describe the Ce⁴⁺ as well as the Ce³⁺ states.

In table 5.2.2 we show the electron affinities for the F atom as calculated with the basis sets we have used. The electron affinities were calculated by taking the difference in total energy of the neutral F atom and the singly negative F⁻ ion. The electron affinities of the large basis and the ECP basis agree reasonably with each other and are near enough to the Hartree-Fock limit to guarantee an adequate description of the F⁻ ion. The electron affinity calculated with the small basis is much worse. Because this basis was optimised for the F⁻ ion and is a minimal basis, the unfavourable result must come from an inadequate description of the neutral atom. This is supported by the fact that decontracting the last p exponent decreases the calculated electron affinity to 1.94 eV.

	basis			exp. ⁴⁵
	large	small	ecp	
EA F	1.18	4.78	0.82	3.464

Table 5.2.2 Electron affinities for the F atom. All entries in eV.

All the CIS calculations and most of the Hartree-Fock calculations have been done with the Gaussian 92²³ program package. The remaining Hartree-Fock calculations have been done with the MOLDIR program package^{24,25}.

The Results of the All Electron Hartree-Fock Calculations

The pointgroup symmetry of the Ce site is only C₂, so the 5d levels should split up into five singlets, which transform as either the A or B irreducible representations of C₂. This is exactly what we see in the results of our calculations. In Table 5.2.3 we have listed some of the results of our non-relativistic Hartree-Fock calculations on the average of the five 5d¹ states. The meaning of the basis set labels is explained in table 5.2.4. To make a comparison between the different calculations easier we shifted the orbital energy of the highest Ce 5d orbital to zero for all the calculations.

	Γ	basis set a	basis set b	basis set c	basis set a; no Mad. pot.	basis set e
5d levels	B	-1.40	-1.39	-1.07	-1.33	-1.53
	A	-1.09	-1.09	-0.83	-1.05	-1.18
	B	-0.75	-0.75	-0.53	-0.53	-0.79
	A	-0.56	-0.57	-0.19	-0.33	-0.59
	A	0.00	0.00	0.00	0.00	0.00

Table 5.2.3 Hartree-Fock energies of the Ce 5d orbitals of the CeF₁₁ cluster. All entries are in eV.
For an explanation of the basis set labels see table 5.2.4.

From the table we can see that the different basis sets yield very similar results, with one notable exception: column c. This is a calculation with two extra very diffuse s-functions on the Ce ion. The two diffuse functions form a very diffuse low lying s orbital, which is only 0.5 eV above the highest 5d orbital. They also mix very strongly with the 5d orbitals, thus affecting the nature of the 5d orbitals and their energies. The diffuse functions protrude far beyond the cluster edge and still have a significant density at the positions of the point charges surrounding the cluster. The point charges are fitted so that they represent the Madelung potential at a grid at the cluster positions¹⁹. Far beyond the cluster edge the potential generated by the point charges is not the correct Madelung potential for CeF₃. So the very diffuse s-functions feel a potential, which is not quite correct. Therefore molecular orbitals with a large contribution of those functions may show some error, as can be seen from Table 5.2.3.

basis	original basis	additions
a	large basis	none
b	large basis	2 diffuse s on Ce: 0.12 and 0.04
c	large basis	2 diffuse s on Ce: 0.10 and 0.02
e	small basis	none

Table 5.2.4 The basis sets for the CeF₃ calculations.

Surprisingly the calculations with basis b do not show the same error. Just as in the previous case the diffuse functions form a Ce s-like molecular orbital, which lies 0.5 eV above the highest Ce 5d orbital. The s-d mixing, however, is in this case much smaller. Apparently the only small difference in diffuseness of the diffuse exponents (0.02 and 0.04) is in this case crucial for the amount of mixing with the 5d orbitals which is observed. This calculation converged badly however, while all the other calculations converged smoothly; so the good results in this case may be fortuitous.

The results for the cluster without a Madelung potential are remarkably good, especially for the two lowest lying 5d levels. The splitting of the Ce 5d levels in CeF_3 seems to be primarily determined by the next nearest neighbours of the Ce ion.

The above mentioned calculations were done on the average of all five $\text{Ce } 5d^1$ states. Because there is only one set of molecular orbitals for five different states, none of these states is described optimally. To get better results one would have to do separate Hartree-Fock calculations on all five states separately. However the Hartree-Fock method only enables us to correctly calculate the lowest state of a given symmetry. In this case this means we can only calculate the two lowest $\text{Ce } 5d^1$ states; one A and one B type state. To be able to compare these results with the previous ones we calculate the total energy difference between the calculated states and the average of all $\text{Ce}^{3+} 5d^1$ states. The results are listed in Table 5.2.5.

		basis set a		basis set e	
I ⁺		average	lowest	average	lowest
5d orb. en.	B	-0.63	-0.66	-0.71	-0.72
	A	-0.33	-0.36	-0.36	N.A.

Table 5.2.5 Hartree-Fock energies of the lowest two Ce 5d orbitals of the CeF_{11} cluster in CeF_3 . All entries are in eV.

To facilitate the comparison all the energies in table 5.2.5 are calculated as the deviation of the orbital or total energy of a specific orbital or state to the average energy of the 5d orbitals or states. As one can see from Table 5.2.5 it hardly makes a difference if we use the orbital energies of the calculation on the average or if we use the total energies of the different $5d^1$ states. The electronic polarisation due to the occupation of a specific 5d orbital is very small in this case.

To determine the position of the Ce 5d levels in the gap of CeF_3 or LaF_3 we need to compute the band gap. For CeF_3 this is technically very difficult, because of the 4f and 5d levels in the gap. It is impossible to specify, within the Hartree-Fock method, the electronic configurations we want. For LaF_3 we are able to calculate the band gap by doing a Generalised Valence Bond calculation on an excited state where one electron is promoted from the highest lying F 2p orbital to the lowest lying virtual (diffuse s-function on La). The electron spins are singlet

coupled. This is strictly speaking not the first excited state of the cluster, but the energy difference between the singlet and triplet state will be small. Much smaller in any case than the errors we incur by using a finite cluster. In this way we calculated a band gap for LaF₃ of 10.14 eV, which is in good agreement with experiment³¹. We can now calculate the positions of the Ce levels in the gap in the ways noted earlier in section 5.1.

For the energy difference between the average Ce 4f and the average Ce 5d levels we have used the average of the experimental absorption lines¹⁰: 5.57 eV. The numbers we used for the Ce 5d levels were taken from the calculations with basis set a. The results are listed in Table 5.2.6 together with the results deduced from experiments^{9,10,31,46}. For convenience we shifted the conduction band to zero energy.

The column cb in table 5.2.6 contains the results obtained by placing the levels relative to the virtual conduction band like diffuse s-function on Ce.

	This work		Exp. ^{9,10,31,46}
	cb	vb	
CB	0.00	0.00	0.00
Ce 5d	-0.47	0.89	-0.14
	-1.04	0.33	-0.60
	-1.22	0.14	-0.94
	-1.57	-0.20	-1.33
	-1.87	-0.50	-1.62
Ce 4f av.	-6.81	-5.44	-6.50
VB	-10.14	-10.14	-10.00

Table 5.2.6 Positions of the Ce 4f and Ce 5d levels in the gap of CeF₃ and LaF₃:Ce. The column labelled "cb" contains the values obtained by putting the conduction band edge at the orbital energy of the virtual La 6s orbital. The column labelled "vb" contains the values obtained by placing the valence band edge at the orbital energy of the highest occupied F 2p orbital. All entries in eV.

The column vb contains the results obtained by placing the Ce levels relative to the highest occupied F 2p functions (valence band). The last procedure places the Ce levels approximately 1.4 eV higher in the gap. The levels are placed so high in the gap that three Ce 5d levels appear to be in the conduction band. The results of column cb are in good agreement with the experimental data, especially if we account for the experimental uncertainty of ± 0.5 eV in the position of the Ce 4f levels.

The Results of the ECP Calculations

The results of the non-relativistic all-electron calculations we have presented in the previous sub-section give a good description of CeF₃ and LaF₃:Ce. However we were not able to calculate the energy difference of the Ce 4f and Ce 5d levels in the gap. In this sub-section

we will present the results of our calculations on CeF_3 with the help of the ECP's and basis sets of Stevens et al^{32,42}. Because these ECP's contain relativistic effects we should be able to get a fair, totally ab initio, prediction for the $4f^1 \rightarrow 5d^1$ absorption spectrum. Moreover, because the ECP basis sets are much smaller than the all-electron basis sets we are now able to do the CIS calculations on the cluster.

To get a feeling for the accuracy of the ECP's for Ce we performed some calculations on the free Ce^{3+} ion with the ECP's of Stevens et al. We also performed fully relativistic calculations on the Ce^{3+} ion with the MOLFDIR^{24,25} package and the uncontracted version of the basis set of van Piggelen. The results are listed in table 5.2.7.

$\Delta E(4f - 5d)$	MOLFDIR (All electron)		Gaussian (ECP's)	
	HFD	HF	HF	CIS
	5.37	8.57	6.28	7.11

Table 5.2.7 $4f^1 \rightarrow 5d^1$ excitation energies of the free Ce^{3+} ion. All entries are in eV.

From the table it is clear that the ECP's perform quite acceptable. Although there is a difference with the full relativistic result of 0.91 eV, this result is much better than the totally non-relativistic one. Furthermore in ionic compounds the electronic structure of the Ce^{3+} ion is expected to be very similar to the one of the free ion. If that is true the difference in ΔE_{4f-5d} in the free ion between the full relativistic results and the ECP results should be transferable to the cluster results. Thus enabling us to correctly predict the Ce absorption spectrum from only the ECP results.

We also see a relatively large difference between the ΔE_{4f-5d} of the HF and the CIS calculations with the ECP's. The HF result is a so-called ΔSCF result. The ΔE is the difference between the total energies of the $4f^1$ and the $5d^1$ state. Both states are described with molecular orbitals, which are optimised for that state. So the electronic polarisation, which takes place when exciting the electron from the 4f to the 5d orbital is accounted for. In the CIS calculation the excited $5d^1$ state is described with molecular orbitals optimised for the $4f^1$ state. Although some of the electronic polarisation is accounted for by the mixing in of determinants describing other single excitation configurations, most of the electronic polarisation is absent. This accounts for the difference between the HF and CIS results.

The ECP calculations on CeF_3 can be divided into two sets: The calculations on the Ce^{4+} charge state, to determine the position of the Ce 4f levels relative to the valence band, and the calculations on the Ce^{3+} charge state to determine the position of the Ce 5d levels relative to the Ce 4f level. The results are listed in tables 5.2.8 and 5.2.9.

The GVB(OSS) result for $\Delta E_{\text{VB-4f}}$ was obtained by taking the total energy difference of a Hartree-Fock calculation on the Ce^{4+} ground state of the cluster and a generalised valence bond calculation on an excited state in which one electron was excited from the highest

occupied F 2p orbital to the lowest Ce 4f orbital. The two unpaired electrons were singlet spin coupled. This is the same procedure we have used to compute the band gap of the LaF₁₁ cluster; so the same arguments for the validity of the result apply as mentioned there.

The CIS calculation places the Ce 4f level much higher. The reason for this is the lack of electronic polarisation in the CIS calculation as mentioned earlier. In this case the lack of polarisation is much worse than in the previous case because the charge state of the Ce ion changes upon this excitation. The Ce orbitals used by the program to describe the (local) Ce³⁺ 4f¹ state are not able to do that very well, because they were optimised for the Ce⁴⁺ state.

	CIS		CIS
4f levels	0.00	5d levels	6.41
	0.00		7.38
	0.21		7.78
	0.30		8.19
	0.36		8.22
	0.55		
	0.59		

Table 5.2.8 Results of the CIS ECP calculations on the CeF₁₁ cluster. All entries are in eV.

Just as in the case of the free Ce ion we have calculated ΔE_{4f-5d} in two ways: as a Δ SCF result and with CIS. For the CeF₁₁ cluster the two results differ less than for the free Ce ion. The Δ SCF result is poor in comparison with the experimental result of $\Delta E_{4f-5d} = 4.88$ eV. If we assume that the difference between the full relativistic and the ECP ΔE_{4f-5d} for the free Ce ion also applies in this case we obtain $\Delta E_{4f-5d} = 5.27$ eV. This result compares much better with experiment.

	CIS	HF & GVB
$\Delta E(\text{VB}-4f)$	7.82	4.06
$\Delta E(4f-5d)$	6.41	6.18
$\Delta E(4f\text{-CB})$	9.64	N.A.

Table 5.2.9 Results of the ECP calculations on the CeF₁₁ cluster. All entries are in eV.

The CIS calculation on the Ce³⁺ 4f¹ state of the cluster gives seven 4f¹ states with a total splitting of 0.59 eV. This splitting is not caused by the spin-orbit coupling, because this effect is not included in this calculation. Experiments⁴⁷ suggest a total 4f splitting of 0.3 eV, which is mainly caused by spin-orbit splitting. The full relativistic MOLFDIR calculations on the average of the 4f¹ states of the free Ce ion support this. These calculations show a total 4f level splitting of 0.3 eV, which can only be due to spin-orbit coupling (because there is no external potential). The large 4f level splitting in the ECP calculations must be an artefact of the calculation. The ECP calculation on the free Ce ion already shows a 4f level splitting of 0.3 eV. Spin-orbit splitting is not included in these calculations and there is no external

potential, so there is no physical phenomenon that could cause this splitting. The reference state for the CIS calculation is a state in which one of the 4f orbitals is occupied. The six empty 4f orbitals see the potential of a $\text{Ce}^{3+} 4f^1$ state and are therefore not the proper orbitals to describe the excited $\text{Ce} 4f^1$ states. When they become occupied in the CIS calculation the energy of the associated states will be too high.

	This work		Exp. ^{9,10,31,46}
	Best ECP	Best of all	
CB	0.00	0.00	0.00
Ce 5d	1.00	0.59	-0.14
	0.96	0.02	-0.60
	0.56	-0.16	-0.94
	0.15	-0.51	-1.33
	-0.81	-0.81	-1.62
Ce 4f av.	-6.08	-6.08	-6.50
VB	-10.14	-10.14	-10.00

Table 5.2.10 Positions of the Ce levels in the gap of CeF_3 . All entries are in eV.

For the 5d levels we see something similar. The total 5d splitting is larger than in the SCF case and larger than experimentally measured. In this case, however one could argue that the CIS results should be better than the SCF results because in the real material the 4f - 5d

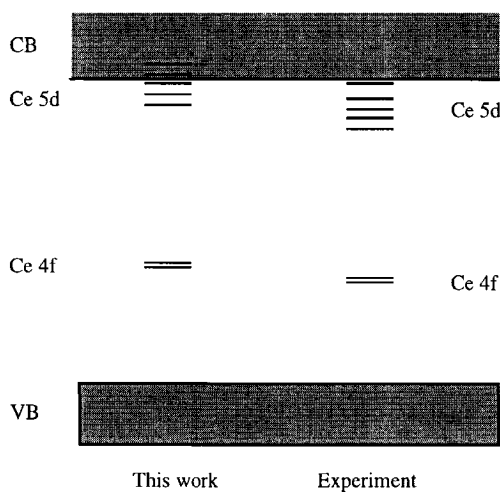


Figure 5.2.2 Localised Ce levels in the bandgap of CeF_{11}

transition goes so fast that the other electrons may not have a chance to fully adjust themselves to the new situation. In this case, however, this argument does not seem to be supported by the theoretical and experimental results.

In table 5.2.10 we list the positions of the Ce levels in the band gap of CeF_3 as we deduced them from the best ECP results we have. In this table there is a second column labelled "Best of all", in which the Ce 5d level splitting was taken from the all-electron calculation with the large Ce basis set. A pictorial representation of the best results and the experimental data is given in figure 5.2.2.

The position of the Ce 4f level is predicted quite accurately; approximately 0.5 eV too high. The calculated energy difference between the Ce 4f and Ce 5d levels is also somewhat too large. Therefore the Ce 5d levels are placed too high in the gap. The Ce 5d level splitting seems to be better described by a SCF calculation on the average of 5d states than by a CIS calculation.

We can extend our picture of the electronic levels of CeF_3 with the width of the valence band. From the orbital energies of the F^- 2p orbitals we can estimate the valence band width. In table 5.2.11 we list the estimated valence band widths for the basis sets we have used together with the experimental value⁴⁶.

	large basis	small basis	ecp basis	exp. ⁴⁶
VB width	3.2	3.5	3.2	3.0

Table 5.2.11 Valence band widths for CeF_3 . All entries are in eV.

The calculated values were obtained for a CeF_{11} cluster in the Madelung field of CeF_3 .

The calculated values agree quite well with the experimental value. The calculated values are somewhat larger than the experimental one, this in contrast with expectations. The uncertainty in the experimental values, however, is large (30%).

Conclusions

We are able to describe CeF_3 quite adequately. The band gap is calculated correctly with the GVB(OSS) calculation. The Ce 5d level splitting can be correctly computed with most of the methods we used; CIS being the only exception. The position of the Ce 4f level in the band gap can also be calculated correctly. The only significant error that remains in our calculations is the ab initio prediction of the energy difference of the Ce 4f and Ce 5d levels in the gap. The error we make here is 0.4 eV. This is less than 10% of the transition energy. For a semi-relativistic approach this is not too bad a result, although it is not yet accurately enough for our purposes.

5.3 $\text{LiLuF}_4\text{:Ce}$ and $\text{LiYF}_4\text{:Ce}$

LiYF_4 crystallises in a lattice with the $I41/\text{AS}$ spacegroup⁴⁸. The Ce impurity replaces a Y ion. The pointgroup symmetry of the Y site is S_4 . The Y ion is surrounded by eight fluorine ions. These eight fluorines fall into two groups of four. The two groups have slightly different bond lengths to the Y ion. The obvious first choice for a cluster to describe the system is a CeF_8 cluster embedded in an array of point charges that emulate the Madelung potential at the cluster sites. In figure 5.3.1 we show a picture of this cluster.

All the calculations on the CeF_8 cluster were performed with the Gaussian 92 program. We only performed non-relativistic Hartree-Fock calculations and some limited geometry optimisations. The basis sets used were the small basis sets mentioned in the previous section.

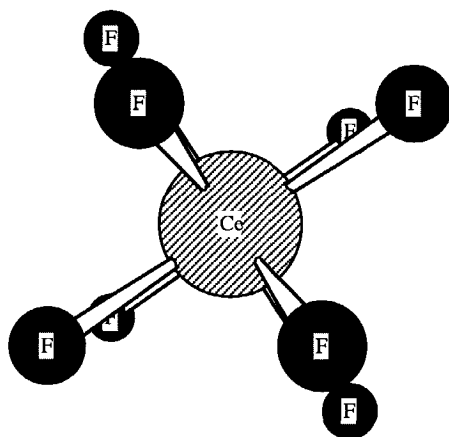


Figure 5.3.1 The CeF_8 cluster in $\text{LiYF}_4\text{:Ce}$

The Results

In table 5.3.1 we show the results of a Hartree-Fock calculation on the CeF_8 cluster with the Ce ion in its $4+$ charge state. The energies of the 5d levels were taken from the energies of the virtual 5d orbitals.

It can be seen from the first and last column of table 5.3.1 that the agreement between the calculated and experimental values is poor. This was of course to be expected. Our cluster has the host crystal geometry. The Ce ion however is substantially larger than the Y ion, so one would expect lattice relaxations to occur upon doping with Ce.

On the basis of the pointgroup symmetry of the cluster we expect four different 5d levels. The results of our calculation also show this. The experimental values however show five 5d levels. The degenerate 5d level can be splitted up by spin-orbit coupling, but the energy

difference we see between those levels in the experimental values is much too large to be explained by spin-orbit coupling. Apparently the lattice relaxation around the Ce impurity lowers the symmetry of the site.

	Γ	1	2	3	4	5
5d levels	A	0.00	0.00	0.00	0.00	0.00
	A	-0.85	-0.70	-0.59	-2.62	-0.34
	A	-0.85	-0.70	-0.59	-2.75	-0.65
	B	-2.34	-1.79	-1.41	-3.12	-1.58
	B	-3.74	-2.83	-2.17	-3.12	-2.42

Table 5.3.1 Ce 5d orbital energies of the CeF₈ cluster in LiYF₄:Ce..
All entries are in eV.

Column 1: CeF₈ cluster in the host geometry in the Madelung field of LiYF₄.

Column 2: CeF₈ cluster with 5.15% outward relaxation of the fluorines in the Madelung field of LiYF₄.

Column 3: CeF₈ cluster with 10% outward relaxation of the fluorines in the Madelung field of LiYF₄.

Column 4: CeF₈ cluster (partially optimised structure) in the Madelung field of LiYF₄.

Column 5: The experimental results^{5,15} for LiYF₄

The easiest way to model the lattice relaxation is to let the eight fluorine ions move out radially, while keeping the Madelung field fixed. If this is done we find a minimum in the total energy of the cluster for an outward relaxation of 5.15%. The virtual orbital energies are listed in table 5.3.1 under the column 2. As expected the total 5d level splitting is now reduced, although it is still too large when compared with the experimental values. We can move the fluorine ions even more outward. The column 3 of table 5.3.1 lists the 5d levels for an outward radial relaxation of 10%. Apart from the second and third level the calculated and experimental values show a reasonable agreement.

The 10% outward relaxation of the fluorine ions is found by comparing the calculated results with the experimental results and is therefore not a strictly *ab initio* result. What is worse: this method can never be used to predict the properties of a material that has not been experimentally investigated. A theoretical more sound and satisfying way would be to find the geometry of the cluster which yields the lowest total energy and compute the 5d levels at that geometry. This method does not necessarily give the correct geometry of the impurity and its surroundings in the crystal. In our calculations the cluster is embedded in an array of point charges and not in the real crystal. The forces acting on the cluster ions will be incomplete and partly incorrect, leading to a possibly incorrect optimal geometry. Nevertheless Berrondo et al.⁴⁹ have shown that good results can be obtained with the help of *ab initio* cluster geometry optimisations.

We have optimised the two bond lengths and the bond angles of the CeF_8 cluster in the field of the point charges under the constraint that the symmetry of the cluster remains S_4 . Without the last constraint the number of degrees of freedom would be much larger. This would make the optimisation significantly more difficult, if not impossible. Although in the real crystal the symmetry of the site seems to be distorted, this calculation should provide a reasonable estimate of the site geometry. The cluster was optimised for the $\text{Ce}^{3+} 5d)^1$ charge state. We subsequently did a calculation on the Ce^{4+} charge state. The energies of the virtual 5d orbitals from this calculation are listed in table 5.3.1 in the column labelled 4. As can be seen from the table the total level splitting has become much larger. Even the ordering of the levels has changed. The agreement with experiment is even worse than in the case of the calculation on the cluster in the host crystal geometry. Apparently the lack of repulsive forces from the ions not included in the cluster gives the cluster ions too much freedom to relax.

Conclusions

The present CeF_8 cluster is too small to reliably calculate the distorted geometry around a Ce impurity in LiLuF_4 . The interactions of the CeF_8 group with its direct environment are in the small cluster only represented by the interaction with the point charges. The very important repulsive forces, which limit the cluster relaxation, are completely missing. In a larger cluster these repulsive forces would be present and result in a more reliable geometry. Unfortunately, increasing the cluster size with the next shell of atoms makes the cluster too large to perform a complete geometry optimisation.

Given the experimental absorption spectrum of $\text{LiLuF}_4\text{:Ce}$ we can, to a certain extent, modify the geometry such that the calculated and experimental absorption spectra match. In this way we can obtain information about the impurity site geometry, which is not accessible by any other means.

In the case of $\text{LiLuF}_4\text{:Ce}$ we were able to reproduce the total splitting of the Ce 5d levels. We were not able to completely match the experimental results. The breaking of the S_4 pointgroup symmetry leaves too many possibilities to try by hand and the cluster proved too small to get reliable results by doing an automatic geometry optimisation.

5.4 $\text{LiBaF}_3:\text{Ce}$

The Ba site in LiBaF_3 has the very high pointgroup symmetry O_h . The next nearest neighbours of the Ba ion consist of twelve fluorine ions⁵⁰. At a slightly larger distance there are eight Li ions. We assume that the Ce impurity will occupy a Ba site. To describe the Ce impurity in LiBaF_3 we will use in first instance two systems: A Ce ion and a CeF_{12} cluster embedded in an array of point charges. In figure 5.4.1 we present a picture of the Ba site in LiBaF_3 .

The Ba site can be thought of as the centre of a cube. The twelve F ions are located at the middle of the edges of the cube and the eight Li ions are located at the corners of the cube. By translating this cube in the x, y and z axis directions one can build up the entire crystal.

The Ba ion has a formal charge of +2. The Ce ion, which replaces it has a formal charge of +3. This difference in charge has to be compensated. This can be done by either removing one

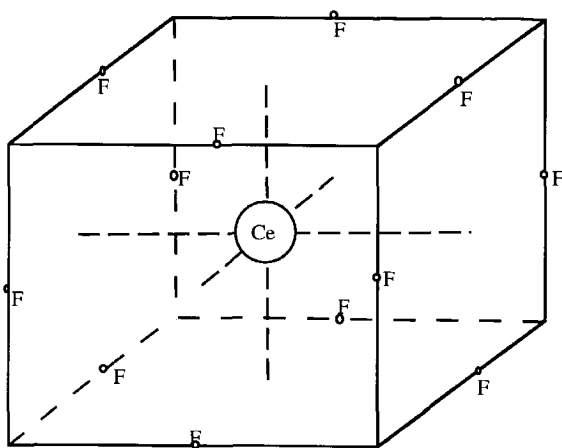


Figure 5.4.1 The CeF_{12} cluster in $\text{LiBaF}_3:\text{Ce}$

of the eight Li ions near the Ba site, or by adding an interstitial F ion near the Ba site, or by replacing one of the next nearest Ba ions by a Li ion. In this section we will determine which of these three possibilities apply to $\text{LiBaF}_3:\text{Ce}$.

Results

The Ba site has O_h pointgroup symmetry. The Ce 5d levels in the unmodified crystal will split up into a triplet (T_2) and a doublet (E) in the absence of spin-orbit coupling. The spin-orbit coupling will split up the triplet into a singlet (E_{2g}) and a doublet (F_g). In the terminology we did not account for Kramers degeneration. The spin-orbit splitting will be

small: 0.3 eV. Our Hartree-Fock calculations on the Ce ion in the cubic point charge environment and the CeF_{12} cluster show the triplet and the doublet (column 1 and 2 of table 5.4.1). The experimental absorption spectrum of Ce in LiBaF_3 shows four lines (column 7 of table 5.4.1). However we can still recognise two groups of lines and thus the cubic structure in this spectrum, so the distortion from the cubic symmetry is not too large. This distortion is due to the charge compensation and its accompanying lattice relaxation.

In column 3 of table 5.4.1 we show the Ce 5d level splitting as it is obtained by a calculation on the CeF_{12} cluster, with one of the Li ions deleted from the surrounding point charges. The symmetry is now reduced and we get a singlet and two doublets. This spectrum does not resemble the experimental one; neither quantitatively nor qualitatively. Although the lattice relaxation following the removal of the Li ion may lower the site symmetry further and thus split up the lowest doublet it seems unlikely that the charge compensation is realised in this way.

	1	2	3	4	5	6	7
Ce 5d levels	0.00	0.00	0.00	0.00	0.00	0.00	0.00
	0.00	0.00	-0.23	-1.76	-0.14	-0.21	-0.39
	0.00	0.00	-0.23	-2.61	-0.47	-0.74	-0.91
	-0.30	-0.54	-0.75	-2.97	-0.67	-1.12	-1.12
	-0.30	-0.54	-0.75	-2.97	-0.67	-1.12	-

Table 5.4.1 Ce 5d orbital energies of several CeF_x clusters in $\text{LiBaF}_3\text{:Ce}$. All entries in eV.

Column 1: Ce^{3+} ion in the Madelung field of LiBaF_3 .

Column 2: CeF_{12} cluster in the Madelung field of LiBaF_3 .

Column 3: CeF_{12} cluster in the Madelung field of LiBaF_3 with one of the Li point charges deleted.

Column 4: CeF_{12} cluster + extra F^- ion on one of the cubic axes in the Madelung field of LiBaF_3 .

Column 5: CeF_{12} cluster in the Madelung field of LiBaF_3 with one of the point charges of the nearest neighbouring Ba ions replaced by a Li ion point charge.

Column 6: $\text{CeF}_{12}\text{LiBa}_4$ (optimised structure) in the Madelung field of LiBaF_3 .

Column 7: Experimental results¹⁸ for $\text{LiBaF}_3\text{:Ce}$.

In column 4 of table 5.4.1 we show the Ce 5d level splitting as it is obtained by a calculation on the CeF_{12} cluster with an extra F ion added on one of the cubic axes. The pointgroup symmetry is reduced and we get a doublet and three singlets.

We now have a spectrum which at least qualitatively matches the experimental data. The calculated total splitting is much too large. The total splitting is very sensitive to the distances between the Ce ion and its neighbours. The lattice relaxation, which will undoubtedly occur on introducing the interstitial F ion and which we did not account for, may very well decrease the splitting.

In column 5 of table 5.4.1 we show the Ce 5d level splitting as it is obtained by a calculation on the CeF_{12} cluster where in the array of point charges the +2 charge of a nearest Ba ion was

replaced by the +1 charge of a Li ion. The pointgroup symmetry is reduced and now we also get a doublet and three singlets.

We again have a spectrum which at least qualitatively matches the experimental data. The calculated total splitting is still much too small.

From the above mentioned results we can conclude that the charge compensation in $\text{LiBaF}_3:\text{Ce}$ is realised by either an interstitial F ion or the replacement of a Ba ion by a Li ion.

The last option is the most likely. The interstitial F ion would be in a very cramped position, which would probably result in extensive lattice relaxation. The energy barrier for such a process would be rather high. Replacing the Ba ion with a Li ion is much easier. There is more than enough space for the small Li ion at the Ba site.

Assuming that the Ba ion is indeed replaced by a Li ion we optimised the structure of our cluster for this situation. The optimal geometry of the Ce site was first determined with the HADES⁵¹ program. The HADES program lets the lattice relax over very long distances. In the subsequent Hartree-Fock calculations we only used the modified coordinates of the CeF_{12} cluster. We did not change the Madelung point charges. During the optimisation the four F ions above the Ce ion move down toward the Ce and a little bit outward. The Li ion moves upward. The Ce ion also moves upward a bit. All the other ions move only marginally. A pictorial representation of the optimisation is shown in figure 5.4.2.

The optimal geometry was confirmed by minimising the Hartree-Fock total energy of some clusters with respect to the ion coordinates in the field of the Madelung point charges. The smallest cluster we have used for this optimisation is the $\text{CeF}_{12}\text{Li}_8$ cluster. The geometry optimisation of this cluster gives basically the same results as the HADES optimisation, with one significant difference: The four F ions above the Ce ion move significantly outward. This is due to the lack of repulsion at the cluster edge and therefore is an artefact of the limited cluster size. If we extend the cluster with the four Ba ions around the Ce ion at the same z-coordinate, i.e. use a $\text{CeF}_{12}\text{Li}_8\text{Ba}_4$ cluster, this lack of repulsion is corrected for. We then get approximately the same optimised geometry as with the HADES program. The displacement

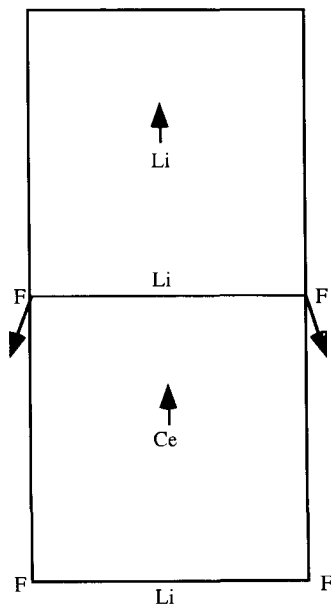


Figure 5.4.2 Side view of a unit cell of $\text{LiBaF}_3:\text{Ce}$. The arrows indicate the direction in which the ions will move upon relaxation.

of the ions is much larger in the HADES case than in the Hartree-Fock optimisation case but the direction of the displacements is the same. It is a well-known fact that the HADES method over-estimates the displacements, so these results are in agreement with general experience.

The Ce 5d orbital energies belonging to the optimised cluster are listed in column 6 of table 5.4.1. The agreement with the experimental values is quite satisfactory.

Conclusions

We were able to calculate the experimental Ce 5d level splitting quantitatively correct. The structure of the experimental absorption spectrum can be reproduced by assuming that the charge compensation in $\text{LiBaF}_3\text{:Ce}$ is realised by replacing a neighbouring Ba ion of the Ce impurity with a Li ion.

Molecular cluster calculations, even on the relatively low level performed here, are very useful in obtaining valuable information that is inaccessible by experimental means.

References

- 1) J. Andriessen, P. Dorenbos and C.W.E. van Eijk, *Mat. Res. Soc. Symp. Proc.*, **348** 355 (1994)
- 2) J. Andriessen, A. Sobolev, A. Kuznetsov, H. Merenga, P. Dorenbos and C.W.E. van Eijk, in *Proceedings of the International Conference on Inorganic Scintillators and their Applications*, eds. P. Dorenbos and C.W.E. van Eijk, p130, Delft University Press, Delft, 1996
- 3) R. Visser, J. Andriessen, P. Dorenbos and C.W.E. van Eijk, *J. Phys.: Condens. Matter*, **5** 5887 (1993)
- 4) P. Dorenbos, J.T.M. de Haas, C.W.E. van Eijk, N.N. Ryskin, E.V. Zharikov and A.A. Kiryukhin, in *Proceedings of the International Conference on Inorganic Scintillators and their Applications*, eds. P. Dorenbos and C.W.E. van Eijk, p365, Delft University Press, Delft, 1996
- 5) C.M. Combes, P. Dorenbos, C.W.E. van Eijk, C. Pedrini and J.Y. Gesland, in *Proceedings of the International Conference on Inorganic Scintillators and their Applications*, eds. P. Dorenbos and C.W.E. van Eijk, p396, Delft University Press, Delft, 1996
- 6) J.C. van 't Spijker, P. Dorenbos, C.W.E. van Eijk, K. Kramer and H.U. Güdel, in *Proceedings of the International Conference on Inorganic Scintillators and their Applications*, eds. P. Dorenbos and C.W.E. van Eijk, p411, Delft University Press, Delft, 1996
- 7) W.W. Moses, S.E. Derenzo, M.J. Weber, F. Cerrina and A. Ray-Chaudhuri, *IEEE Trans. Nucl. Sci.* (1993)

- 8) A.J. Wojtowicz, M. Balcerzyk, E. Berman and A. Lempicki, *Phys. Rev. B*, **49** 14880 (1994)
- 9) K.H. Park and S.J. Oh, *Phys. Rev. B*, **48** 14833 (1993)
- 10) W.W. Moses, S.E. Derenzo, M.J. Weber, A. Ray-Chaudhuri and F. Cerrina, *J. Luminescence*, **59** 89 (1994)
- 11) M. Kobayashi et al., *Nucl. Instr. and Meth. A*, **302** 443 (1991)
- 12) W.W. Moses and S.E. Derenzo, *IEEE Trans. Nucl. Sci.*, **NS-36** 173 (1989)
- 13) P. Lecoq, in *Proceedings of the International Conference on Inorganic Scintillators and their Applications*, eds. P. Dorenbos and C.W.E. van Eijk, p52, Delft University Press, Delft, 1996
- 14) D.J. Ehrlich, P.F. Moulton and R.M. Osgood Jr., *Opt. Lett.* **4** 184 (1979)
- 15) C.M. Combes, P. Dorenbos, C.W.E. van Eijk, C. Pedrini, H.W. den Hartog, J.Y. Gesland and P.A. Rodnyi, *J. of Luminescence Eng.*, To be published.
- 16) J. Andriessen, H. Merenga, C.M. Combes, P. Dorenbos and C.W.E. van Eijk, in *Proceedings of the International Conference on Inorganic Scintillators and their Applications*, eds. P. Dorenbos and C.W.E. van Eijk, p142, Delft University Press, Delft, 1996
- 17) M.J. Knitel, P. Dorenbos, J.T.M. de Haas and C.W.E. van Eijk, in *Proceedings of the International Conference on Inorganic Scintillators and their Applications*, eds. P. Dorenbos and C.W.E. van Eijk, p81, Delft University Press, Delft, 1996
- 18) C.M. Combes, private communications.
- 19) J. Almlöf and U. Wahlgren, *Theoret. Chim. Acta*, **28** 161 (1973)
- 20) Gerrard Aissing, *Interstitial transition metals in silicon*, PhD thesis, University of Groningen (1988)
- 21) J. Sauer, *Chem. Rev.*, **89** 199, (1989)
- 22) C.C.J. Roothaan, *Rev. Mod. Phys.* **32** 179 (1960)
- 23) Gaussian 92, Revision G.2, M. J. Frisch, G. W. Trucks, M. Head-Gordon, P. M. W. Gill, M. W. Wong, J. B. Foresman, B. G. Johnson, H. B. Schlegel, M. A. Robb, E. S. Replogle, R. Gomperts, J. L. Andres, K. Raghavachari, J. S. Binkley, C. Gonzalez, R. L. Martin, D. J. Fox, D. J. Defrees, J. Baker, J. J. P Stewart and J. A. Pople, Gaussian, Inc., Pittsburgh PA, 1992.
- 24) *Relativistic Quantum Chemistry: The MOLFDIR program package*, L. Visscher, O. Visser, P.J.C. Aerts, H. Merenga and W.C. Nieuwpoort, *Computer Physics Communications* **81** 120 (1994)
- 25) *Relativistic Quantum Chemistry: The MOLFDIR program package*, L. Visscher, W.A. de Jong, O. Visser, P.J.C. Aerts, H. Merenga and W.C. Nieuwpoort, in *METECC-95*, E. Clementi and G. Corongiu, (STEF, Cagliari, 1995)
- 26) Bobrowicz and Goddard, Chapter 2 of *Modern Theoretical Chemistry*, Volume 3, H.F. Schaefer III, ed. (1977)
- 27) J.B. Foresman, M. Head-Gordon, J.A. Pople and M.J. Frisch, *J. Phys. Chem.*, **96** 135 (1992)
- 28) H. Merenga, J. Andriessen and C.W.E. van Eijk, *Radiation Measurement*, **24** 343, (1995)
- 29) H. Suzuki, J.A. Tombello, C.L. Melcher and J.S. Schweitzer, *IEEE Trans. Nucl. Sci.*, **40** 380 (1993)
- 30) O.T. Antonyak and N.S. Pidzyrilo, *Opt. Spectrosc. (USSR)*, **60** 743 (1986)

- 31) S. Sato, J. of the Phys. Soc. Japan, **41** 913 (1976)
- 32) Thomas R. Cundari and Walter J. Stevens, J. Chem. Phys. **98** 5555 (1993)
- 33) F. Bloch, Z. Phys., **57** 545 (1929)
- 34) A.J. Wojtowicz et al., Conference Record NSS&MIC, IEEE, Norfolk, 1994, p123
- 35) A.J. Wojtowicz, in Proceedings of the International Conference on Inorganic Scintillators and their Applications, eds. P. Dorenbos and C.W.E. van Eijk, p95, Delft University Press, Delft, 1996
- 36) T. Koopmans, Physica, 's Grav., **1** 104, (1933)
- 37) A.K. Cheetham, B.E.F. Fender, H. Fuess and A.F. Wright, Acta Crystallographica B **32** 94 (1976)
- 38) B. Maximov and H. Schulz, Acta Crystallographica B **41** 88 (1985)
- 39) H.U. van Piggelen, W.C. Nieuwpoort and G.A. van der Velde, J. Chem. Phys., **72** 3727 (1980)
- 40) R.C. Raffanetti, J. Chem. Phys. **58** 4452 (1973)
- 41) S. Huzinaga, Ed., J. Andzelm, M. Klobukowski, E. Radzio-Andzelm, Y. Sakai, H. Tatewaki, in Gaussian Basis Sets for Molecular Calculations, Elsevier, Amsterdam, 1984.
- 42) W.J. Stevens, H. Basch, M. Krauss, J. Chem. Phys. **81** 6026 (1984)
- 43) C.E. Moore, Analysis of Optical Spectra, NSRDS-NBS 34, Office of Standard Reference Data, National Bureau of Standards, Washington D.C.
- 44) R.J. Lang, Can. J. Res. Sect. A, **14** 127 (1936)
- 45) E.F. Carr, J. Chem. Phys., **38** 1540, (1963)
- 46) C. Pedrini, D. Bouttet and C. Dujardin, in Proceedings of the International Conference on Inorganic Scintillators and their Applications, eds. P. Dorenbos and C.W.E. van Eijk, p103, Delft University Press, Delft, 1996
- 47) G. H. Dieke, in Spectra and Energy Levels of Rare Earth Ions in Crystals, H.M. Crosswhite and H. Crosswhite eds., Interscience Publishers, New York,
- 48) R.E. Thoma, C.F. Weaver, H.A. Friedman, H. Insley, L.A. Harris and H.A. Yakel Jr., J. Phys. Chem. **65** 1096 (1961)
- 49) M. Berrondo, J.F. Rivas-Silva and J.B. Czirr, in Proceedings of the International Conference on Inorganic Scintillators and their Applications, eds. P. Dorenbos and C.W.E. van Eijk, p144, Delft University Press, Delft, 1996
- 50) W.L.W. Ludekens and A.J.E. Welch, Acta Cryst., **5** 841 (1952)
- 51) A.H. Harker, HADES II/PC: The Harwell Automatic Defect Evaluation System for Personal Computers, 1989, (Harwell: Publications Office)

Chapter 6

The Oxygen Compounds

In this chapter we will describe the results of our work on three rather complex oxygen compounds: $\text{La}_2\text{Hf}_2\text{O}_7\text{:Ce}$, $\text{Lu}_2\text{SiO}_5\text{:Ce}$ and CeAlO_3 .

$\text{La}_2\text{Hf}_2\text{O}_7\text{:Ce}$ and even more so $\text{Lu}_2\text{Hf}_2\text{O}_7\text{:Ce}$ are interesting candidates for scintillators. They have a high density and a large number of high Z atoms. The corresponding materials with vanadium and tungsten instead of hafnium do not show any luminescence¹. Blasse² suggests that this is caused by the transference of the excited Ce 4f electron to a neighbouring vanadate or tungstate group. In the case of the hafnates this transfer is not expected to occur³. Hence $\text{Lu}_2\text{Hf}_2\text{O}_7\text{:Ce}$ should show Ce luminescence. In our laboratory this material will be experimentally investigated. The calculations reported here were done to assist those experiments.

Lutetium-ortho-silicate (LSO) doped with Ce is a very interesting material. It has an unexpectedly high density and it already gives a large light output (25,000 photons/MeV) for a small concentration of Ce impurities (0.1 at %)⁴. Consequently LSO:Ce and derivatives have attracted a lot of attention in recent years^{5,6,7}.

Recently XPS results³¹ became available on CeAlO_3 . The structure of this material is very near the geometry used in our laboratory for some simplified model calculations on $\text{YAlO}_3\text{:Ce}$ ⁸. This gave us the opportunity to check those results against experiment.

6.1 Computational Details

In section 5.1 we gave an overview of the methods we can use to calculate the properties of the fluorine compounds we were interested in. The properties of the oxygen compounds can be calculated in the same way.

For the calculations we have used several basis sets. Some were optimised by ourselves, with the help of the program ASCF⁹, others were taken from the literature. The Ce and O basis sets used for the calculations on $\text{La}_2\text{Hf}_2\text{O}_7\text{:Ce}$ were optimised by ourselves. These basis sets were primarily used in a general contraction¹⁰. The exponents of the basis and the contraction were optimised for the ion in the charge state in which it occurs in the ionic compound, with a Watson shell to make the system neutral again. These basis sets are listed in appendix A.

For the relativistic calculations on LSO:Ce and CeAlO_3 we used a kinetically balanced general contracted basis, based on the primitive set of van Piggelen¹¹. For the oxygen ion we used a kinetically balanced general contracted basis, based on a primitive set for O^- of Huzinaga¹². The basis sets are listed in appendix A. For the non-relativistic calculations on LSO we used mainly the small segmented contracted basis set for Ce, already mentioned in chapter 5 and a segmented contracted version of the O^- basis set of Huzinaga. In the cases where we also had Si atoms in our cluster we used a small segmented contracted basis set. This basis set is listed in appendix A. Some LSO calculations were also performed with the ECP's of Stevens et al^{13,14} for Ce and Si.

The quality of the Ce basis sets has already been discussed in section 5.2. The Hartree-Fock and experimental ionisation potentials for the Si atom are listed in table 6.1.1.

	basis		Exp. ¹⁵
	small	ECP	
1st IP	11.5	11.8	8.2
2nd IP	17.3	17.6	16.3
3rd IP	26.7	26.9	33.5
4th IP	44.5	N.A.	45.1

Table 6.1.1 The first four ionisation potentials for the Si atom. All entries are in eV.

The fourth ionisation potential cannot be calculated with the ECP's. With the ECP's, the Si atom only has four electrons, so a calculation on Si^{4+} is impossible. The results obtained with the two basis sets are virtually the same. The fourth ionisation potential is the energy difference of the $\text{Si}^{3+} \{ \text{Ne} \} 3s^2 3p^1$ and the $\text{Si}^{4+} \{ \text{Ne} \} 3s^2$ states. For these states the correlation energy should be approximately equal. We therefore expect the Hartree-Fock method to perform well. Comparison of our calculated fourth ionisation potential with the experimental one confirms this. The agreement of the other calculated ionisation potentials with experiment is much poorer. We will use the Si basis sets to describe Si ions in LSO. If we assume LSO to be completely ionic all the Si ions will have a +4 charge. We may conclude from our results that the Si basis sets are adequate for this task.

Making and testing a basis set for the O^{2-} ion is a difficult task because the O^{2-} ion is not stable in vacuum. This is also immediately evident from table 6.1.2. This table lists the first

ionisation potential and the first electron affinity of the oxygen atom. It is clear that the basis set optimised by ourselves (labelled optimal) gives the best results, at least for the more negatively charged states. This best result is still not very good compared with the experimental result. The small basis by Huzinaga performs a little less good than our own, but the difference is not so great. The ECP basis for O^0 performs not so good and will probably not yield reliable results for O^{2-} ions.

	basis			Exp. ¹⁶
	small	optimal	ECP	
$E_{\text{tot}} O^+$	-74.3703	-74.3574	-15.1849	N.A.
$E_{\text{tot}} O^0$	-74.8084	-74.8045	-15.6205	N.A.
$E_{\text{tot}} O^-$	-74.7776	-74.7836	-15.5808	N.A.
IP O	11.9	12.2	11.8	13.6
EA O	-0.8	-0.6	-1.1	1.5

Table 6.1.2 Total energies, ionisation potentials and electron affinities of the oxygen atom. The total energies are in atomic units and the electron affinities are in eV.

All the CIS and most of the Hartree-Fock calculations were done with the Gaussian92¹⁷ package. All the relativistic calculations and the remaining Hartree-Fock calculations were done with the MOLFDIR^{18,19} program package.

6.2 $\text{La}_2\text{Hf}_2\text{O}_7\text{:Ce}$

$\text{La}_2\text{Hf}_2\text{O}_7$ is a solid which crystallises in a lattice with the FD3-MZ spacegroup²⁰. The lanthanum site has the pointgroup symmetry D_{3d} .

The calculations were done on the lanthanum compound and not on the lutetium compound because structural data were only available for the lanthanum compound. Both compounds are expected to have the same crystal structure although the ion distances may vary somewhat because of the different ion sizes of lanthanum and lutetium.

The Ce impurity is expected to occupy a lanthanum site. The Ce ion and the La ion both have the same formal charge and approximately the same ion size, so we do not expect large lattice relaxations upon doping with Ce.

The first shell of neighbours around the La^{3+} site consists of eight O ions (six at a distance of 2.6 Å and two at a distance of 2.3 Å). So the obvious first choice of cluster to describe $\text{La}_2\text{Hf}_2\text{O}_7\text{:Ce}$ would be a CeO_8 cluster. The cluster is shown in figure 6.2.1.

Unfortunately, no experimental work has yet been carried out so far on this material. We have therefore no check on the results we will obtain for this material, except for a few general notions, which seem to apply for all oxygen compounds. On the other hand, we can also consider this as a big challenge. Theory should be able to predict beforehand the results of experiments. If our predictions are later confirmed by experiment, it would mean the ultimate proof of our methods.

The Results of the Hartree-Fock Calculations

To describe the oxygen anions accurately we need a rather diffuse basis set, optimised for the (in vacuum not stable) -2 charge state of the oxygen. This makes the oxygen compounds much harder to treat than the fluorine or chlorine compounds. The diffuse oxygen basis protrudes far outside the cluster in places where the crystal potential is not correctly described anymore. This can give rise to spurious oxygen states in the band gap. This seriously hampers the determination of the Ce levels in the gap and the determination of the band edges.

In our Hartree-Fock calculations on the CeO_8 cluster these problems indeed occurred. When we performed the calculation with the van Piggelen basis for the Ce ion and the Huzinaga basis for the O ion it was impossible to obtain reasonable Ce 5d states. There were very low lying O states and a very strong mixing of the Ce 5d orbitals and the O orbitals. This made it impossible to occupy or even recognise the Ce 5d orbitals.

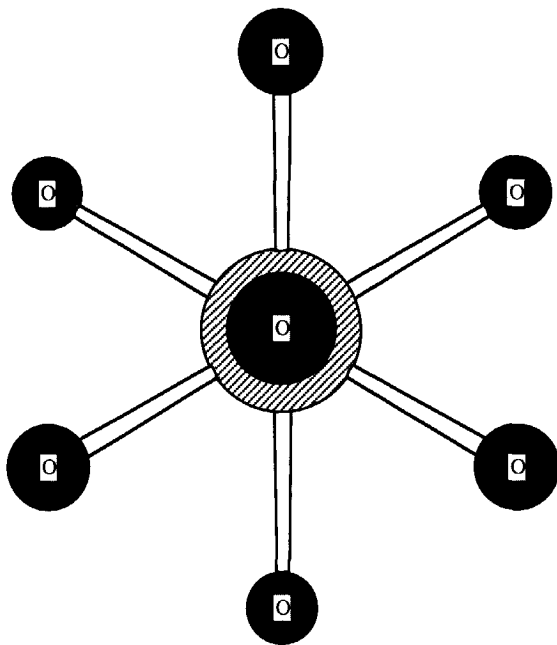


Figure 6.2.1 The CeO_8 cluster in $\text{La}_2\text{Hf}_2\text{O}_7\text{Ce}$
The direction of view is along the C_3 axis (O-Ce-O)

We reoptimised the van Piggelen basis for the Ce^{3+} ion with a Watson shell at half the distance of the nearest O ion and generalised contracted this basis to (6/5/4). This resulted in a basis that was more compact than the original one. We also optimised a new basis for the O^{2-} ion with a Watson shell at half distance. This basis was generalised contracted to (3/3). The results of the cluster calculations with these basis sets was better than the previous ones. But the Ce 5d orbitals still showed a very strong mixing with the O orbitals.

We then reoptimised the O basis for the O^{2-} ^2P state with the Watson shell at half distance. The basis was then generalised contracted for the O^{2-} state to (3/3). This procedure resulted in a very compact O basis. The results of the cluster calculations with this basis show "good" Ce 5d orbitals. There is still some mixing with O orbitals, but this is on an acceptable level. Apparently we need a very compact O basis to get valid results. To study this in a more systematic way we decontracted the most diffuse p-exponent and varied it in the cluster calculations, the results are listed in table 6.2.1.

The O content of the Ce 5d orbitals increases with a decreasing exponent. The highest lying Ce 5d orbital shows significantly more O mixing than the others. When the exponent has decreased to 0.115803 the O content of the Ce 5d orbitals has become very high. In the case of an exponent of 0.105803 the highest Ce 5d orbital consists primarily of O functions.

The lowest total energy is obtained for the exponent 0.115803. This suggests that this is the best basis set for the O^{2-} ion in the cluster. The O content of the Ce 5d orbitals for this basis, however is high and that may lead to an inaccurate calculated 5d level splitting.

exponent	Γ	0.145803	0.135803	0.125803	0.115803	0.105803
E_{tot}	-	-9182.972	-9183.040	-9183.084	-9183.094	-9183.058
5d levels	A_{1g}	0.00	0.00	0.00	0.00	0.00
	E_g	-1.73	-1.64	-1.51	-1.29	-0.72
	E_g	-2.96	-2.88	-2.75	-2.53	-1.68

Table 6.2.1 Total energies and Ce 5d orbital energies for the CeO_8 cluster as a function of the most diffuse O p exponent. The total energies are in Atomic Units. The 5d orbital energies are in eV. The spin-orbit splitting is not included.

From table 6.2.1 we can see that when the exponent becomes smaller than 0.125803 the positions of the Ce 5d levels change faster with the decreasing exponent then before. Therefore the best basis for the O^{2-} ion in the CeO_8 cluster seems to be the one with the p-exponent 0.125803. This is the O basis set which was labelled "optimal" in the previous section. The 5d level splitting calculated with this basis should be the most reliable result for the Ce 5d splitting.

To be able to calculate the 4f-5d absorption spectrum of $\text{La}_2\text{Hf}_2\text{O}_7\text{:Ce}$ we need the Ce 4f - 5d energy difference. To calculate this value we have used the ECP and basis set of Stevens et

al. for the Ce ion. For the oxygen ion we have tried the three different basis sets already mentioned in section 6.1. Some of the results of these calculations are listed in table 6.2.2. From table 6.2.2 it becomes clear that the results are very sensitive to the basis set used for the oxygen ions. Much more so than in the case of the fluorine and chlorine compounds.

	small	optimal	ecp
5d levels	0.00		0.00
	-0.63		-0.24
	-0.63	N.A.	-0.24
	-2.19		-1.75
	-2.19		-1.75
$\Delta E(4f-5d)_{\text{low}}$	4.49	3.78	4.61
$\Delta E(\text{vb}-4f)$	2.18	1.21	4.05

Table 6.2.2 The relative positions of the Ce 4f and 5d levels of the CeO_8 cluster in $\text{La}_2\text{Hf}_2\text{O}_7\text{:Ce}$. For the Ce ion we used the ECP basis set of Stevens et al. For the oxygen ions we used the basis sets denoted in the column headers.

The energies of the Ce 5d orbitals calculated with the optimal O basis set are missing from the table because we were unable to identify them. There are ten alpha spin orbitals which show a significant Ce 5d occupation and which all are strongly mixed with oxygen p orbitals. If we occupy the lowest orbital with a significant Ce 5d content, this orbital remains strongly mixed with the oxygen orbitals. The Mulliken orbital analysis for this orbital shows that only 20% of the electron is on the Ce ion. We can also see from table 6.2.2 that $\Delta E(4f-5d)_{\text{low}}$ for the optimal oxygen basis deviates significantly from the values for the other two basis sets. This holds particularly for the value of $\Delta E(\text{vb}-4f)$.

The overlap populations of the Ce d with the oxygen p functions of the optimal O basis are large. This means that the Ce 5d orbitals can use oxygen p functions for their description and vice versa. Under these circumstances it is very hard to determine the orbital character from the function coefficients. Consequently it makes the gross Mulliken population analysis unreliable. It can also explain why, in this case, the use of a different Ce basis can have such a huge effect. The effect can be seen by comparing table 6.2.1 with 6.2.2. The Ce ECP basis is more diffuse than our reoptimised van Piggelen basis and can be used better by the O atoms to describe their orbitals. Therefore the Ce 5d and O 2p orbital mixing will be larger in the ECP case and the "real" Ce 5d orbitals have become unrecognisable.

Given the above observations and the results on the quality of the O basis sets listed in table 6.1.2 we conclude that the results obtained with the small O basis are the most reliable results of table 6.2.2.

So the energy difference between the lowest Ce 4f and the lowest Ce 5d level is 4.49 eV. If we correct this value with the correction we found to be necessary for the free ion (section 5.2) we obtain: $\Delta E(4f-5d)_{\text{low}} = 3.58 \text{ eV}$.

The lowest Ce 4f level is 2.18 eV above the valence band edge, which is estimated from the orbital energy of the highest occupied oxygen level.

We also performed Hartree-Fock calculations on the LaO_8 cluster with the small basis sets and extra diffuse s-functions on the La ion, to obtain the band gap. We found a band gap of 6.6 eV. Oxygen compounds usually have a band gap in the order of 6 eV, so this value seems reasonable.

Conclusions

Calculations on clusters containing O^{2-} ions are complicated by the diffuse basis sets needed for the O^{2-} ions. The diffuse O orbitals protrude far beyond the cluster edge where they feel a potential that deviates significantly from the correct crystal potential. Because of this there are low lying O states in the band gap, which seriously hamper the determination and occupation of both the Ce 5d levels and the conduction band edge.

By carefully adjusting and balancing the basis sets it is still possible to get reasonable looking results. We were able to get a reasonable estimate for the band gap, the valence band \rightarrow Ce 4f distance (table 6.2.2, first column) and the Ce 4f \rightarrow Ce 5d distance (table 6.2.2, first column). The only remaining problem is that the two most reliable results we have obtained for the Ce 5d level splitting differ significantly and we have no objective way of determining which one is

better, although the results of the third column of table 6.2.1 seem somewhat more trustworthy than the results from the first column of table 6.2.2.

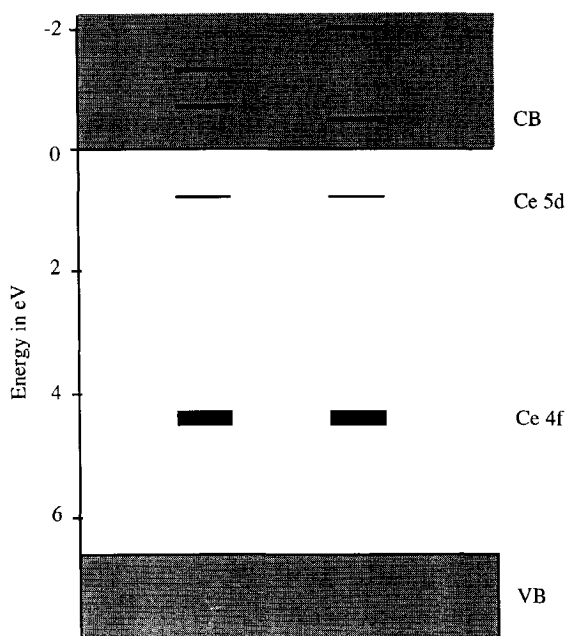


Figure 6.2.2 The band gap and local Ce levels in $\text{La}_2\text{Hf}_2\text{O}_7\text{:Ce}$

So we finally arrive at two possible level schemes for $\text{La}_2\text{Hf}_2\text{O}_7\text{:Ce}$. They are depicted in figure 6.2.2. Note that if the Ce 4f levels are indeed this high above the valence band edge, the difference in Ce 5d level splitting between the two results may not really matter. In that case we could probably only observe the lowest Ce 5d level.

6.3 $\text{Lu}_2\text{SiO}_5\text{:Ce}$

LSO crystallises in the same structure as Yttrium-ortho-silicate (YSO)²¹. These materials have very low symmetry and belong to the spacegroup $\text{P}121/\text{M}1^{22}$. Because structural data for LSO was not available we used the structural data for YSO in our calculations. Both materials are believed to have the same structure although the lattice parameters will be slightly different because of the different radii of the Y^{3+} and Lu^{3+} ions (0.89 Å and 0.85 Å respectively).

There are two different Lu sites. The Ce impurity is believed to occupy a Lu site. So there also are two possible different kinds of Ce impurities in LSO, which may have different luminescence behaviour.

The pointgroup site symmetry of both Lu sites is C_1 . We will call the sites: site 1 and site 2. In figure 6.3.1 we show a picture of site 1. The Lu ion has seven O ions at small distances around it. The average distance between the Lu and the O ions is 2.32 Å for this site. The conformation of the O ions can be viewed as a disturbed octahedron and an extra O^{2-} ion. In

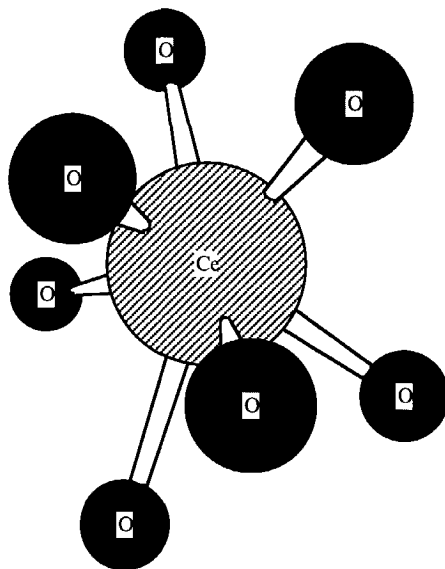


Figure 6.3.1 The CeO_7 cluster (site 1) in LSO:Ce .

figure 6.3.2 we see a picture of site 2. Here the Lu ion is surrounded by six O ions. The average Lu - O distance is 2.22 Å for this site. The conformation of the O ions can be viewed as a distorted octahedron.

The clusters shown in figures 6.3.1 and 6.3.2 are the clusters we used for only some of our calculations. It is not a priori clear that these clusters will give a proper description of LSO. Most of the O^{2-} ions around the central site are covalently bonded to Si atoms. So to make the above clusters we have had to break covalent Si - O bonds. This may introduce severe errors into description of the affected O^{2-} ions and thus into the calculated observables.

Therefore we have decided to construct a cluster in which the SiO_4^{4-} groups were treated as undividable units. We then get a $\text{LuO}_2(\text{SiO}_4)_4$ cluster. This cluster is an extended version of the cluster for site 2. The cluster is shown in figure 6.3.3. Also this cluster has its drawbacks.

The cluster O^{2-} ions which are furthest away from the central Lu ion are much further away than a lot of other ions which are not included in the cluster. This may give problems with the fitted Madelung potential for the cluster. The alternative is to include all ions up to a distance of 9 Bohr from the central Lu ion. This would result in a $\text{Lu}_8\text{Si}_4\text{O}_{26}$ cluster. The effort required to do a Hartree-Fock SCF calculation on this cluster is tremendous and can certainly not be done on a routine basis.

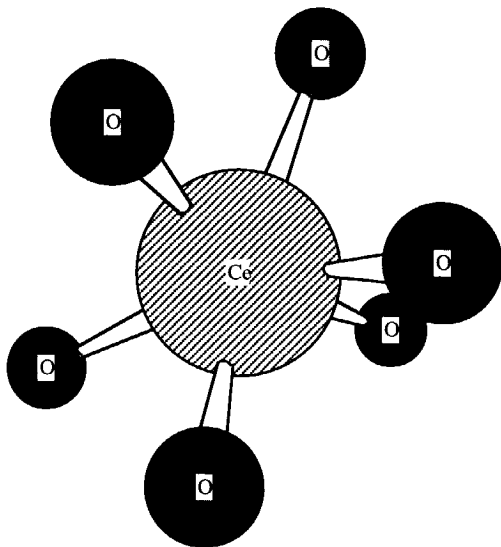


Figure 6.3.2 The CeO_6 cluster (site 2) in LSO:Ce .

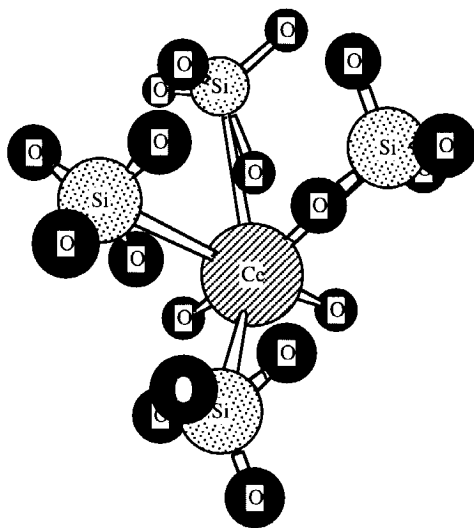


Figure 6.3.3 The $\text{CeO}_2(\text{SiO}_4)_4$ cluster (site 2) in LSO:Ce .

The average distance between the Lu ion and its neighbouring O ions is rather small. Ce has a larger estimated ionic radius than Lu¹⁶. So we expect significant lattice relaxation in LSO upon doping with Ce. Based on the Lu-O distances we expect a significantly higher occupation of site 1 than site 2.

Determination of the Cluster Embedding

In all previous cases we embedded the clusters only in an array of point charges generating the correct Madelung potential at the cluster sites²³. In the case of LSO there is a complication. It can be argued that LSO cannot be regarded as a completely ionic material because the SiO₄⁴⁻ groups contain covalent bonding. The consequence of that is that the Si and O ions which are part of a SiO₄ group may have smaller charges than +4 and -2 respectively. To study the sensitivity of the cluster results for variations of the Madelung potential we performed Hartree-Fock calculations on the three smallest above mentioned clusters (with the Lu ion replaced by a Ce ion) with a Madelung potential based on Lu₂³⁺O²⁻(Si⁴⁺O₄²⁻) (labelled mad4) and a Madelung potential based on Lu₂³⁺O²⁻(Si³⁺O₄^{1.75-}) (labelled mad3). The geometry of all the clusters was relaxed in the sense that all ions, except the Ce ion, were moved outward radially by 10%. This was needed to get reasonably recognisable Ce 5d orbitals²⁴. The results of these calculations are listed in table 6.3.1.

	CeO ₇ (site 1)		CeO ₆ (site 2)		CeO ₂ (SiO ₄) ₄	
	mad3	mad4	mad3	mad4	mad3	mad4
5d levels	0.00	0.00	0.00	0.00	0.00	0.00
	-0.45	-0.78	-0.33	-0.67	-0.37	-0.60
	-1.25	-1.07	-2.25	-1.49	-2.52	-2.73
	-1.57	-1.35	-2.30	-1.60	-2.72	-2.93
	-2.17	-1.85	-2.49	-1.84	-2.85	-3.05

Table 6.3.1 Orbital energies of the virtual Ce⁴⁺ 5d orbitals of LSO:Ce. The calculations labelled mad4 were done with a Madelung potential based on a totally ionic description of LSO:Ce. The calculations labelled mad3 were done with 25% smaller charges for the Si and O ions which are part of a SiO₄ group. All entries are in eV and relative to the highest Ce 5d level.

In the case of the large CeO₂(SiO₄)₄ cluster the differences in Ce 5d splitting due to the different Madelung potentials is small (only 0.2 eV). The Ce ion in the centre of the cluster is shielded from the point charges by the other ions in the cluster. For the large cluster this shielding already works so well that the difference in Madelung potential only results in marginal differences in the Ce 5d level splitting. In the CeO₇ cluster this shielding is less effective. Still the differences between the two calculations are not very large. This in

contrast to the results for the CeO_6 cluster, which do differ markedly for the two different Madelung potentials.

The results on the CeO_6 cluster seem to imply that the potential mad3 is the best choice, because the mad3 results of the CeO_6 and the $\text{CeO}_2(\text{SiO}_4)_4$ clusters agree better with each other than the mad4 results. On the other hand, because of its odd shape, it is not a priori clear that the results of the $\text{CeO}_2(\text{SiO}_4)_4$ cluster should be better than those of the CeO_6 cluster. Consequently the mad3 potential does not necessarily need to be better than the mad4 potential.

In the case of the small clusters, i.e. CeO_6 and CeO_7 , there is an inconsistency in the charge of the quantum-mechanically treated cluster and equivalent clusters in the environment when we use the potential mad3. Therefore it seems best to use the potential based on the formal charges²⁵, i.e. the potential mad4.

The Effects of Cluster Size

As explained earlier the choice of the cluster to model this system is not trivial. To study the effect different choices of cluster have on the results, we performed a number of calculation on the host material and extracted from those calculations the Lu 4f band width, the valence band width and the band gap. The calculations were performed on the LuO_7 cluster (site 1), the LuO_6 cluster (site 2), the $\text{LuO}_2(\text{SiO}_4)_4$ cluster (site 2) and the $\text{Lu}_8\text{O}_{10}(\text{SiO}_4)_4$ cluster (site 2). The results are listed in table 6.3.2.

	LuO_7	LuO_6	$\text{LuO}_2(\text{SiO}_4)_4$	$\text{Lu}_8\text{O}_{10}(\text{SiO}_4)_4$	Exp. ^{26,27}
4f band	0.19	0.10	0.11	2.20	3.1
VB	9.93	8.34	7.25	11.74	5.0
gap 1	11.76	11.69	12.87	9.90	6.5
gap 2	3.25	3.47	5.43	N.A.	N.A.

Table 6.3.2 Selected crystal properties of LSO, calculated with different clusters. Gap 1 was calculated from the (virtual) orbital energies. Gap 2 was calculated from a HF calculation on the first excited state. All entries are in eV.

For the three smaller clusters we see a very narrow Lu 4f band. In these clusters we only have one Lu ion and therefore a band cannot be formed. What we see is only the ligand field splitting between the lowest and highest Lu 4f level. In the largest cluster we have eight Lu ions and a band can be formed. Because the Lu 4f orbitals are rather core-like the overlap between the Lu 4f orbitals on different sites will be small and the band will be narrow. The calculated band width of 2.2 eV confirms this. The experimental value²⁶ is somewhat larger, but this is to be expected.

The calculated valence band width is very large. It is larger for site 1 than for site 2. Surprisingly the $\text{LuO}_2(\text{SiO}_4)_4$ cluster gives a significantly smaller valence band width than the LuO_6 cluster. The largest cluster shows the largest valence band width.

The calculated valence band widths are all much larger than the experimental one²⁶. There are two main reasons for this. First the experimental value is rather inaccurate. In the XPS spectrum for LSO the O 2p band only shows up as a tail of the Lu 4f peak. The width of the O 2p peak can only be estimated by comparison with similar compounds (CeAlO_3 and LuAlO_3). But because there are two oxygen p bands in LSO (one of the oxygens bonded to silicon and one of the free oxygens) the total oxygen p band width for LSO will be larger than for the similar compounds. The second reason has already been mentioned in section 6.2. Because of their diffuseness the (outer) O 2p functions reach beyond the cluster edge and therefore feel a wrong potential. This effect will broaden the O 2p band.

In the $\text{LuO}_2(\text{SiO}_4)_4$ cluster most of the O ions, and therefore most of the O 2p orbitals, are involved in covalent bonds to Si ions. This limits the freedom of the O 2p orbitals to find regions of low potential outside the cluster. The calculated valence band width for this cluster is consequently smaller than for the smaller clusters.

In the $\text{Lu}_8\text{O}_{10}(\text{SiO}_4)_4$ cluster we have ten non-bonded O ions and consequently the valence band width is larger than for the other three clusters. However if we ignore the three deepest O 2p levels the valence band width reduces to 7.2 eV. This is reasonable because these orbitals would have a very small weight in the XPS spectrum (only 3 orbitals of a total of 78). This corrected value agrees well with the calculated value for the $\text{LuO}_2(\text{SiO}_4)_4$ cluster.

The band gap as estimated from the orbital energies is as usual much too large. The values for the three smaller clusters agree reasonably with each other. The value for the largest cluster is somewhat smaller. For this cluster the lowest unoccupied molecular orbital is a mixture of Si 4s, O 3p, Lu 6s and Lu 5p orbitals. It should be a Si 4s orbital. Because of the strong admixture of O 3p orbitals this orbital lies too low in energy and so the calculated band gap is smaller than it should be.

The band gap calculated as the difference of the total energies of the ground state and first excited state of the cluster is much smaller, because the electronic polarisation is now accounted for. For the two smallest clusters the highest occupied molecular orbital of the first excited state consists of a Lu 6s like function strongly mixed with a O 3p type function. This strong mixing is possible because the O 3p orbitals lie too low in energy (again as a consequence of the fact that they spill significantly over the edge of the cluster). Because of this the calculated band gap is far too small. For the $\text{LuO}_2(\text{SiO}_4)_4$ cluster the results are better. The highest occupied molecular orbital for the first excited state is now a Si 4s function. The mixing with O 3p functions is much less.

Above we have seen how some crystal properties vary with cluster size. Our main interest, however, lies in the 4f - 5d distance and 5d level splitting of Ce impurities in LSO. To study the effect of cluster size on these properties we performed calculations on the CeO_7 , CeO_6 and $\text{CeO}_2(\text{SiO}_4)_4$ clusters. The ligands were moved 10% radially outwards. Some of the results are listed in table 6.3.3.

	$\text{CeO}_7(1)$	$\text{CeO}_6(2)$	$\text{CeO}_2(\text{SiO}_4)_4(2)$	Exp. ⁴
5d levels	1.85	1.84	3.05	
	1.07	1.17	2.45	
	0.78	0.35	0.33	1.23
	0.50	0.24	0.12	0.71
	0.00	0.00	0.00	0.00

Table 6.3.3 Ce 5d level splitting for LSO:Ce . The ligands were moved 10% radially outwards. All entries are in eV and relative to the lowest Ce 5d level.

From this table we can see that the two sites give rise to significantly different absorption spectra. The two different sized clusters for site 2 agree well on the three lowest Ce 5d levels. The two highest Ce 5d levels however differ enormously. The two highest Ce 5d levels of the large cluster are probably not very accurate because they lie amidst a set of low lying O 3p orbitals and also are mixed with O 3p orbitals. Because experimentally only the three lowest absorption lines were measured it is at this stage impossible to say which of the two clusters performs better. Furthermore the experimental data seem to suggest that site 1 is the preferred site for Ce ion²⁸, leaving no experimental way to distinguish between the site 2 clusters CeO_6 and $\text{CeO}_2(\text{SiO}_4)_4$.

So it seems that the Ce 5d level splitting can very well be calculated with the help of the small clusters, because the differences between the results of the small and larger cluster are not experimentally verifiable.

Estimation of Lattice Relaxation

As mentioned before the Lu - O distances in LSO are rather small. The Ce^{3+} ion is substantially larger than the Lu^{3+} ion, so we expect lattice relaxations to occur upon doping LSO with Ce. As a first ansatz to the relaxation we determined the radially outward relaxation giving the lowest total energy for the clusters. The results are given in table 6.3.4. The results for the CeO_7 and $\text{CeO}_2(\text{SiO}_4)_4$ clusters are very similar, although they refer to different sites. As expected the relaxation is larger for site 2. Calculations for the CeO_6 cluster at 5%, 10% and 15% radially outward relaxation showed the lowest total energy for 15% relaxation. We expect the optimal relaxation to lie between 10% and 15%, near 15%.

Because the larger cluster for site 2 is expected to give a more reliable result we did not think it necessary to determine the optimal relaxation more accurately.

Because there are no repulsive forces to stop the ions from moving outwardly, the relaxation is overestimated. Furthermore the relaxation probably is not purely radial and we should perform a completely unrestricted geometry optimisation. The three above mentioned clusters are not very suitable for a geometry optimisation because of their very limited size. A more suitable cluster, however, would require a prohibitive amount of computer resources.

relaxation (%)	CeO ₇ (1)	CeO ₆ (2)	CeO ₂ (SiO ₄) ₄ (2)	Exp.
	8.0	15.0	9.4	N.A.
5d levels	1.60	2.25	2.86	
	0.93	1.57	2.48	
	0.57	0.33	0.32	1.23
	0.21	0.22	0.08	0.71
	0.00	0.00	0.00	0.00

Table 6.3.4 Ce 5d level splitting for LSO:Ce. The clusters are at their optimal relaxation, except for the CeO₆ cluster. All entries are in eV and relative to the lowest Ce 5d level.

To get a reasonable estimate of the relaxation we used a simplified model system. We used the LuO₆ cluster, representing site 2. We saturated the O ions with twelve H ions (two H for each O ion) and optimised the H positions. The hydrogen ions should mimic the repulsive forces of the direct surroundings of the cluster. Thus we have a LuO₆H₁₂ cluster representing site 2 in LSO. With this cluster it is not quite clear how the Madelung potential should be constructed, so we left it out. We can now optimise the positions of the O ions. If this system would be a perfect model for LSO all the O ions would remain at their initial positions. The system is not a perfect model and so the O ions are displaced, but not very much. The displacements are listed in table 6.3.5. Surprisingly the relaxation is almost radial. The smallest Lu - O distance changes 1%, the others only 0.6%. The changes in the angles and dihedrals are very small.

The LuO₆H₁₂ cluster now has its optimal geometry. We now replace the Lu³⁺ ion by a Ce³⁺ ion and reoptimise the positions of the O ions. These displacements of the O ions are also shown in table 6.3.5. We now have found the geometry relaxation due to the replacement of Lu³⁺ by Ce³⁺. Again the relaxation is almost radial. The smallest Ce - O distance changes 2.1% and the other bond distances change 1.6%. The changes

	host	optimal LuO ₆	optimal CeO ₆
R ₁	2.17	2.19	2.24
R ₂	2.26	2.27	2.31
R ₃	2.24	2.26	2.29
R ₄	2.24	2.26	2.29
R ₅	2.24	2.25	2.29
R ₆	2.23	2.24	2.28

Table 6.3.5 Results of the geometry optimisation of (Lu/Ce)O₆H₁₂. Only the (Lu/Ce) bond lengths are shown. All the angles changed less than 0.2°. All dihedrals changed less than 0.3°. All entries in Å.

in the angles and dihedrals are very small.

The relaxations calculated with this simplified model are much smaller than the optimal radial relaxations calculated previously. It is possible that the O - H interaction is so strong that the relaxation is underestimated. Andriessen et al.²⁸ performed a geometry optimisation on LSO:Ce with the semi-classical MOLSTAT code²⁹ and found a relaxation of 4%. They conclude that their relaxation may be somewhat too small because the displacement of the O ions is smaller than the difference in ionic radii between the Lu³⁺ and Ce³⁺ ion.

Keeping all this in mind we decided that a 5% radial relaxation should be a reasonable model for the Ce impurity site in LSO. We performed calculations on the small clusters for sites 1 and 2 with the small O basis and the Ce ECP basis. The results of these calculations are listed in table 6.3.6.

The calculated $\Delta E(4f \rightarrow 5d)$ for the CeO₇ cluster is somewhat too large compared with experiment. If we correct the calculated value for the error we know the ECP makes in the free ion case (section 5.2) we get $\Delta E(4f \rightarrow 5d) = 3.23$, which is a bit too small, but within 10% of the experimental value. The calculated $\Delta E(4f \rightarrow 5d)$ for the CeO₆ cluster is far too small. In this cluster the Ce 5d and O p orbitals mix very strongly. This makes it impossible to find a pure 5d¹ state. The mixing with the artificially low O p orbitals lowers the energy of the 5d¹ like state and thus reduces $\Delta E(4f \rightarrow 5d)$.

The distance between the valence band edge and the Ce 4f level also varies greatly between the two clusters. A population analysis of the occupied orbitals of the two clusters suggest that CeO₇ results is more reliable than the CeO₆ result. The latter is again plagued by strong mixing with O orbitals.

For the CeO₇ cluster the Ce 4f levels lie under the valence band edge. Although this is not impossible³⁰ we have to date not seen any other Ce³⁺ case where this is so^{26,31}.

Note that for the CeO₇ cluster the Ce 4f and Ce 5d levels span a range of 5.56 eV. So the levels just barely fit in the band gap. If by any chance the Ce 4f level lies above the valence band edge one

or more of the Ce 5d levels would shift into the conduction band edge. This would nicely account for the inability to measure all five Ce 5d levels in absorption experiments.

	CeO ₇ (1)	CeO ₆ (2)	Exp. ⁴
5d levels	2.33		
	1.37		
	1.04	0.59	1.23
	0.57	0.41	0.71
	0.00	0.00	0.00
$\Delta E(4f \rightarrow 5d)$	4.14	1.89	3.42
$\Delta E(VB \rightarrow 4f)$	-1.45	0.59	

Table 6.3.6 Results for the small LSO:Ce clusters with 5% radial relaxation. The Ce 5d levels were taken from virtual orbital energies. The energy differences are ΔSCF results. All entries are in eV.

The Relativistic calculations

Finally we performed some relativistic Hartree-Fock-Dirac calculations on the small cluster representing site 2 in LSO:Ce. Because of the absence of any symmetry this small CeO_6 cluster is already too large to perform a full four-component HFD calculation in our usual basis sets. It was possible however to perform a calculation in which we neglected the two-electron integrals (i.e. the matrix elements of the operator g_{ij}) containing small-component basis functions.

To estimate the effects of this omission we also performed calculations on the same cluster with and without the two-electron integrals containing small-component basis functions, using a much more severe contracted version of our usual primitive basis sets. For the large component of the basis we ignored the small differences in the orbitals due to the different j values for a specific l value. For the small component part of the basis we made the thresholds for conserving the atomic balance less severe. The results of these calculations are listed in table 6.3.7.

The ΔE 's give the energy differences between the average of the Ce 4f and the average of the Ce 5d levels. There are two ΔE_{av} 's. The first one is calculated by directly subtracting the total energies of the Ce 4f¹ and the Ce 5d¹ calculations; i.e.:

$$\Delta E_{av}^1 = E_{4f)^1} - E_{5d)^1}. \quad 6.3.1$$

The second one is calculated by:

$$\Delta E_{av}^2 = E_{4f)^1}^{4f \text{ basis}} - E_{5d)^1}^{5d \text{ basis}} + E_{\text{Ce}^{4+}}^{5d \text{ basis}} - E_{\text{Ce}^{4+}}^{4f \text{ basis}}. \quad 6.3.2$$

The two ΔE_{av} 's are not equal because of the so-called Basis Set Superposition Error (BSSE)³².

The calculations on the Ce 4f¹ state and the Ce 5d¹ state were not performed in exactly the same function space. Therefore their total energies are formally not comparable and ΔE_{av}^1 will contain an error. The BSSE can become quite large. In this case the two primitive basis sets only differ in the removal of the f-exponents for the "Ce 5d" basis set. Nevertheless the error is quite large for the severely contracted basis set, implying that this basis does not provide a very adequate description of Ce ion in the cluster. In equation 6.3.2 we try to correct for the BSSE. Although the correction is calculated for a different charge state of the cluster (and can therefore not be completely correct) the value for ΔE_{av}^2 should be much better than the value for ΔE_{av}^1 . The term ΔE_{low} gives the energy difference between the lowest Ce 4f level and the lowest Ce 5d level. Its value is based on ΔE_{av}^2 .

	Severely contracted basis		Exp. ⁴	normal basis
	LL int. only	Full		LL int. only
5d levels	4.64	4.88		2.13
	3.79	4.00		1.93
	0.63	0.65	1.23	0.77
	0.30	0.31	0.71	0.12
	0.00	0.00	0.00	0.00
ΔE_{av}^1	-10.09	-10.52	N.A.	5.61
ΔE_{av}^2	7.05	4.63	N.A.	4.40
ΔE_{low}	5.65	4.07	3.42	3.85

Table 6.3.7 Ce 5d orbital energies and Ce 4f \rightarrow 5d transition energies for the CeO_6 cluster (site 2) in LSO:Ce. ΔE_{av} is the energy difference between the average of the 4f and the average of the 5d levels. ΔE_{av}^1 is the "pure" value. ΔE_{av}^2 has been corrected for BSSE. All entries are in eV.

Looking at table 6.3.7 we notice that there is a huge difference between the results for the severely contracted basis and our usual basis. Obviously the basis set cannot be contracted this way without unwanted effects. This also becomes clear from the enormous differences between ΔE_{av}^1 and ΔE_{av}^2 for this basis set. The effect of ignoring part of the two-electron integrals does not seem to effect the Ce 5d level splitting much. However the total energy difference between the Ce 4f)¹ state and the Ce 5d)¹ state are affected very strongly.

If we assume that the 4f - 5d distance calculated with the normal basis set will decrease if we would do a fully relativistic calculation (just as with the smaller basis) the calculated 4f - 5d distance would be too small compared to experiment. This is (in part) due to the strong mixing of the Ce 5d and O p orbitals. As explained earlier this is an artefact caused by the O p functions spilling over the edge of the cluster to regions with an ill-defined potential. This artefact is expected to be larger in the relativistic case. The small component of the basis is larger and contains functions of higher angular momentum than the large component and thus should be more affected. And the large component basis is already larger than the basis set for a non-relativistic calculation, because the orbitals for the two different j values belonging to an l value differ.

Conclusions

Although the combination of the need for a diffuse O^{2-} basis set and the use of a small cluster surrounded by point charges give rise to artificially low lying O^{2-} levels which can have unphysical interactions with the central Ce ion, it is possible to obtain reasonably accurate results from cluster calculations.

Because of the low symmetry (C_1) and size of LSO it is impossible to do a reliable geometry optimisation of the impurity sites. Previous results indicate however that the relaxation is relatively small.

There are two possible impurity sites. Experiments indicate that only one of those sites is actually occupied. Because of the geometry of the sites and the shape of the absorption spectra we conclude that the preferred site for the Ce impurity is site 1.

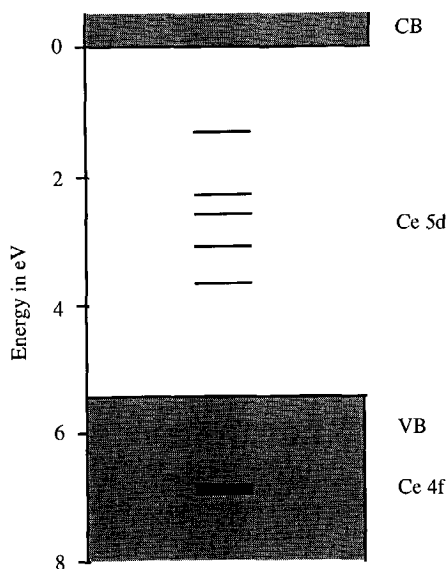


Figure 6.3.4 The band gap of LSO:Ce. The gap was taken from table 6.3.2. The Ce levels were taken from table 6.3.6. For the 4f - 5d distance the free ion corrected value was taken.

Using the best results we have obtained, we arrive at the level scheme for LSO:Ce as depicted in figure 6.3.4. The valence band \rightarrow Ce 4f distance was taken from table 6.3.6. For the 4f \rightarrow 5d distance we have used the corrected value from table 6.3.6. The Ce 5d level splitting was also taken from table 6.3.6. The gap was taken from the calculation on the $\text{LuO}_2(\text{SiO}_4)_4$ cluster.

6.4 CeAlO_3

CeAlO_3 crystallises in a lattice with the $P4/mmm$ space group symmetry³³. At first sight this seems to imply a rather low point group symmetry for the Ce site. Close inspection of the coordinates of the occupied sites, however, shows that they only deviate 2% from the values for pure O_h point group symmetry. Therefore a CeO_{12} cluster with O_h point group symmetry should be a fair model for CeAlO_3 . A picture of this cluster is shown in figure 6.4.1. To preserve the O_h symmetry for the charge density the position of the point charges, which emulate the Madelung potential, should also show O_h symmetry. So the entire crystal should be slightly deformed..

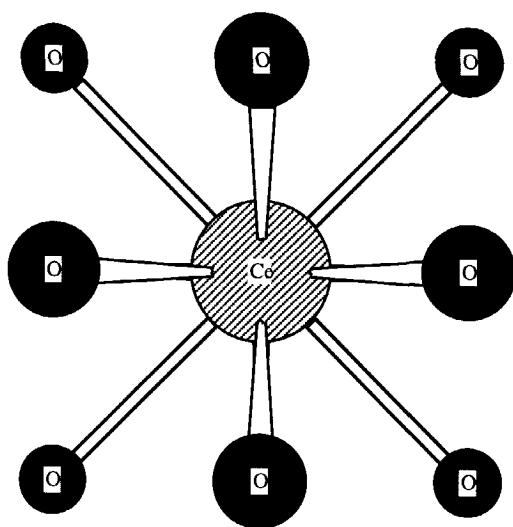


Figure 6.4.1 The CeO_{12} cluster in CeAlO_3 .
The direction of view is along one of the fourfold axes.

The Results

We have performed a fully relativistic four-component Hartree-Fock-Dirac calculation on the CeO_{12} cluster embedded in an array of point charges, emulating the Madelung potential of CeAlO_3 . From the orbital energies obtained in this way we estimated several band widths and band gaps. The results are listed in table 6.4.1.

The band widths in the first column of table 6.4.1 were calculated by taking the difference of the lowest and highest orbital energy for that band.

Since there is only one Ce ion in the cluster and consequently a band cannot be formed, the listed values for the Ce 4f and 5p bands only give an upper limit to the ligand field splitting.

The ligand field splitting is much smaller than the band width, as can be seen by comparing the calculated values with the experimental band widths.

The calculated band widths for the O 2s and 2p bands are both much larger than the experimental ones. But this is not a fair comparison. The experimental band widths are the widths of the peaks in the spectrum at half the height of the peak, while the calculated band widths are the maximum widths of the peaks. If we take the eigenvalue spectrum of the calculation and convolute it with gaussian functions with exponents of -40,000 and then measure the widths of the peaks at half maximum we obtain the values listed in the second column of table 6.4.1.

For the oxygen 2s and 2p bands these values agree much better with the experimental ones. For the Ce bands the values in the second column of table 6.4.1 just give the width the gaussian function with which we convoluted the spectrum. They have no physical meaning.

	calc.		exp. ²⁶
	plain	convoluted	
width Ce 4f	0.3	1.1	2
width O 2p	9.5	4.1	4
width O 2s	2.0	3.3	4
width Ce 5p _{3/2}	0.0	1.1	3
width Ce 5p _{1/2}	0.0	1.1	2
ΔE Ce 4f, O 2p	1.6		2.8
ΔE O 2p, O 2s	20.0		18.1
ΔE Ce 4f, Ce 5p _{3/2}	14.2		15.6

Table 6.4.1 Theoretical and experimental band widths and band distances of CeAlO₃. All entries are in eV.

In the experimental values there is an uncertainty because the O 2s and Ce 5p bands overlap and the width of the bands can only be measured on functions for the separate bands, which were fitted to the spectrum. To a lesser extent the same problems pertain to the determination of the positions of these bands.

We also listed the energy distances between some of the bands in table 6.4.1. The experimental values were obtained by measuring the distances between the tops of the peaks. The theoretical values were obtained by calculating the average of all the eigenvalues for each band, and then taking the difference between two such averages. Although not perfect, the theoretical results are quite good. The observed differences are smaller than 2 eV and could be caused by either the neglect of correlation or the deficiencies of the cluster model.

For completeness sake we have also calculated the Ce 4f - 5d distance and the Ce 5d level splitting, although there are to our knowledge, no experimental data available to check these results. The results are given in table 6.4.2.

The Ce 5d orbital energies are obtained from a four-component Hartree-Fock-Dirac calculation on the average of all Ce³⁺ 5d¹ states of the cluster. The Ce 4f - 5d difference is calculated as the direct total energy difference between the Ce³⁺ 4f¹ groundstate calculation and the Ce³⁺ 5d¹ groundstate calculation. So this value may contain a considerable error due to BSSE (see section 6.3). Nevertheless the values all lie in the expected range for an oxygen compound (see also section 5.1).

	Energies
5d levels	0.0
	-0.4
	-1.7
$\Delta E(4f \rightarrow 5d)$	4.2

Table 6.4.2 The Ce 5d level splitting and the CE 4f- \rightarrow 5d transition energy for CeAlO₃. All entries are in eV.

Conclusions

We have performed a fully relativistic four-component calculation on the CeO₁₂ cluster, embedded in an array of point charges. This cluster served as a model for CeAlO₃. As far as the computational model is concerned this calculation is close to the best we can do for this system. It is encouraging to see that the results are in good agreement with the experimental data. This shows that the cluster model is still a good model even when the materials studied, are not completely ionic anymore.

The problems we have had in the previous sections of this chapter with low lying oxygen states seem to be less severe here. This is due to the very high point group symmetry of the cluster. Because of the high symmetry the diffuse oxygen p functions are limited in their freedom to combine into functions, which have their main density in regions of low potential outside the cluster.

References

- 1) G. Blasse, Prog. Solid State Chem., **18** 79 (1988)
- 2) G. Blasse, W. Schipper and J.J. Hamelink, Inorganica Chim. Acta, **189** 77 (1991)
- 3) W.J. Schipper, J.J. Piet, H.J. De Jager and G. Blasse, Mat. Res. Bull., **29** 23 (1994)
- 4) H. Suzuki, J.A. Tombello, C.L. Melcher and J.S. Schweitzer, 13 IEEE Trans. Nucl. Sci., **40** 380 (1993)
- 5) C.L. Melcher, J.S. Schweitzer, C.A. Peterson, R.A. Manente and H. Suzuki, in Proceedings of the International Conference on Inorganic Scintillators and their Applications, eds. P. Dorenboos and C.W.E. van Eijk, p309, Delft University Press, Delft, 1996

- 6) M.J. Weber, S.E. Derenzo, C. Dujardin and W.W. Moses, in Proceedings of the International Conference on Inorganic Scintillators and their Applications, eds. P. Dorenbos and C.W.E. van Eijk, p325, Delft University Press, Delft, 1996
- 7) W. van Schaik, M. Raukas, S. Basun, U. Happek and W.M. Yen, in Proceedings of the International Conference on Inorganic Scintillators and their Applications, eds. P. Dorenbos and C.W.E. van Eijk, p380, Delft University Press, Delft, 1996
- 8) J. Andriessen, P. Dorenbos and C.W.E. van Eijk, *Mat. Res. Soc. Symp. Proc.*, **348** 355 (1994)
- 9) H.U. van Piggelen, Ab initio calculations on the electronic states of $4f^n$ ions with applications to $[\text{EuO}_6]^{9-}$, PhD Thesis, Groningen (1978)
- 10) R.C. Raffanetti, *J. Chem. Phys.* **58** 4452 (1973)
- 11) H.U. van Piggelen, W.C. Nieuwpoort and G.A. van der Velde, *J. Chem. Phys.*, **72** 3727 (1980)
- 12) S. Huzinaga, Ed., J. Andzelm, M. Klobukowski, E. Radzio-Andzelm, Y. Sakai, H. Tatewaki, in *Gaussian Basis Sets for Molecular Calculations*, Elsevier, Amsterdam, 1984.
- 13) W.J. Stevens, H. Basch, M. Krauss, *J. Chem. Phys.* **81** 6026 (1984)
- 14) Thomas R. Cundari and Walter J. Stevens, *J. Chem. Phys.* **98** 5555 (1993)
- 15) C.E. Moore, Analysis of Optical Spectra, NSRDS-NBS 34, Office of Standard Reference Data, National Bureau of Standards, Washington D.C.
- 16) L.M. Branscombe, in *Atomic and Molecular Processes*, ed. D.R. Bates, Academic Press, New York (1962)
- 17) Gaussian 92, Revision G.2, M. J. Frisch, G. W. Trucks, M. Head-Gordon, P. M. W. Gill, M. W. Wong, J. B. Foresman, B. G. Johnson, H. B. Schlegel, M. A. Robb, E. S. Replogle, R. Gomperts, J. L. Andres, K. Raghavachari, J. S. Binkley, C. Gonzalez, R. L. Martin, D. J. Fox, D. J. Defrees, J. Baker, J. J. P Stewart and J. A. Pople, Gaussian, Inc., Pittsburgh PA, 1992.
- 18) Relativistic Quantum Chemistry: The MOLFDIR program package, L. Visscher, O. Visser, P.J.C. Aerts, H. Merenga and W.C. Nieuwpoort, *Computer Physics Communications* **81** 120 (1994)
- 19) Relativistic Quantum Chemistry: The MOLFDIR program package, L. Visscher, W.A. de Jong, O. Visser, P.J.C. Aerts, H. Merenga and W.C. Nieuwpoort, in *METECC-95*, E. Clementi and G. Corongiu, (STEF, Cagliari, 1995)
- 20) A.W. Sleight, *Inorganic Chemistry*, **7** 1704 (1968)
- 21) J. Felsche, *Structure and bonding*, **13** 99 (1973)
- 22) N.G. Batalieva and Y.A. Pyatenko, *Kristallografiya* **16** 905 (1971)
- 23) J. Almlöf and U. Wahlgren, *Theoret. Chim. Acta*, **28** 161 (1973)
- 24) H. Merenga, J. Andriessen and C.W.E. van Eijk, *Radiation Measurements*, **24** 343 (1995)
- 25) G.J.M. Janssen, Localized 3d-like States in Transition Metal Compounds, PhD Thesis, University of Groningen, 1986

-
- 26) D. Bouttet, C. Dujardin, C. Pedrini, W. Brunat, D. Tran Minh Duc and J.Y. Gesland, in Proceedings of the International Conference on Inorganic Scintillators and their Applications, eds. P. Dorenbos and C.W.E. van Eijk, p111, Delft University Press, Delft, 1996
- 27) J. Becker, A.N. Belsky, D. Bouttet, C. Dujardin, A.V. Gektin, A. Hopkirk, S.N. Ivanov, I.A. Kamenskikh, N.Y. Kirikova, V. Klimenko, V.N. Kolobanov, V.N. Makhov, P. Martin, V.V. Mikhailin, I.H. Munro, C. Mythen, P.A. Orekhanov, C. Pedrini, A. Schroeder, D.A. Shaw, N. Shiran, I.N. Shpinkov, A.N. Vasil'ev and G. Zimmerer, in Proceedings of the International Conference on Inorganic Scintillators and their Applications, eds. P. Dorenbos and C.W.E. van Eijk, p118, Delft University Press, Delft, 1996
- 28) J. Andriessen, A. Sobolev, A. Kuznetsov, H. Merenga, P. Dorenbos and C.W.E. van Eijk, in Proceedings of the International Conference on Inorganic Scintillators and their Applications, eds. P. Dorenbos and C.W.E. van Eijk, p130, Delft University Press, Delft, 1996
- 29) A.N. Varaskin, Sov. J. Struct. Chem., **32** 162 (1991)
- 30) G.K. Wertheim, A. Rosencwaig, R.L. Cohen and H.J. Guggenheim, Phys. Rev. Lett., **27** 505 (1971)
- 31) C. Pedrini, D. Bouttet, C. Dujardin, A. Belsky and A. Vasil'ev, in Proceedings of the International Conference on Inorganic Scintillators and their Applications, eds. P. Dorenbos and C.W.E. van Eijk, p103, Delft University Press, Delft, 1996
- 32) S.F. Boys and F. Bernardi, Mol. Phys., **19** 553 (1970)
- 33) M. Tanaka, T. Shishido, H. Horiuchi, N. Toyota, D. Shindo and T. Fukuda, J. of Alloys and Compounds, **192** 87 (1993)

Chapter 7

The Chlorine Compounds

In this chapter we will report the results of our investigations on some chlorine compounds: $\text{SrCl}_2\text{:Ce}$ and CeCl_3 .

SrCl_2 is the very first chloride we investigate. It has a very high symmetry. This makes it relatively easy to do a full relativistic calculation on it. Good experimental data on the absorption and luminescence spectra of $\text{SrCl}_2\text{:Ce}$ are available¹. There is no experimental data available on the position of the Ce impurity levels in the gap, so we can check only a part of our calculations with experiment. Still, because of its high symmetry, this system enables us to calculate the correct relativistic energy distance between the average Ce 4f and the average Ce 5d states.

CeCl_3 is an interesting material to investigate. Just like in CeF_3 the Ce ions are not impurities, but part of the "host" lattice. So we do not have to worry about lattice relaxations. The atomic positions are known fairly accurate. Technically it is a much more difficult system to treat than CeF_3 because the chlorine ions are much larger and diffuser than the fluorine ions. There is experimental data available about the absorption spectra², the luminescence spectra³ and the position of the localised Ce levels in the gap⁴. All these facts make CeCl_3 a good benchmark system for our methods.

7.1 Computational Details

In section 5.1 we gave an overview of the methods we can use to calculate the properties of the fluorine compounds we were interested in. The properties of the chlorine compounds can be calculated in the same way.

All the CIS and most of the Hartree-Fock calculations were done with the Gaussian92⁵ package. All the relativistic calculations and the remaining Hartree-Fock calculations were done with the MOLFDIR^{6,7} program package.

For the relativistic calculations we used the same basis sets for Ce as mentioned in chapter 6. For Cl we used a basis set based on the basis set of Huzinaga⁸ for Cl⁻. The basis set was generalised contracted⁹ to (4,3/4,5,4). The contraction coefficients were based on a relativistic calculation on the Cl⁻ ion. The small component of the basis set was constructed by way of the extended kinetic balance¹⁰ requirement. For the non-relativistic calculations we used the same small Ce basis set as mentioned in the previous chapters. For Cl we used the basis set of Huzinaga⁸ as given. We also performed calculations with the basis sets and ECP's of Stevens et al^{11,12}.

EA Cl	basis		exp. ¹³
	Huzinaga 2.6	ecp 2.4	
			3.6

Table 7.1.1 The electron affinity of the Cl atom. All entries are in eV.

In table 7.1.1 we show the electron affinity of the chlorine atom calculated with the basis sets we have used, together with the experimental value¹³. The two basis sets give approximately equally good results. They should both be flexible enough to provide an adequate description of the Cl⁻ ion. The SCF results are smaller than the experimental results. This is due to the neglect of correlation in the SCF method. The correlation energy contribution of the neutral atom is different from the one of the negative ion¹⁴.

The Sr basis set we used was the Sr²⁺ basis given by Huzinaga⁸. To this basis set we added two diffuse s-functions with exponents: 0.03 and 0.01. The experimental¹⁵ and calculated second and third ionisation potentials for Sr are listed

	Calc.	Exp.
2nd IP	9.96	11.03
3rd IP	42.04	43.60

Table 7.1.2 Ionisation potentials of the Sr atom. All entries are in eV.

in table 7.1.2. For the second ionisation potential correlation effects are not very important, because we go from a {Kr} 5s)¹ to a {Kr} configuration. The calculated value has an error of 1.1 eV (10%). The calculated third ionisation potential shows a larger error, because here correlation effects are more important. From these value we can conclude that the basis set is flexible enough to adequately describe the Sr²⁺ ion.

All clusters were surrounded by a set of point charges, which were fitted to generate the Madelung potential at the cluster sites¹⁶.

7.2 $\text{SrCl}_2\text{:Ce}$

The crystal belongs to the spacegroup FM3-M^{17} . The pointgroup symmetry of the Sr site is very high: O_h . The obvious first choice of a cluster consists of the Sr ion and its next nearest neighbour Cl ions. This results in a SrCl_8^{6-} cluster. The cluster is shown in figure 7.2.1.

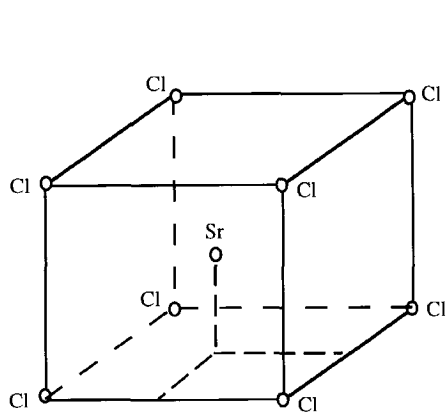


Figure 7.2.1 The SrCl_8 cluster.

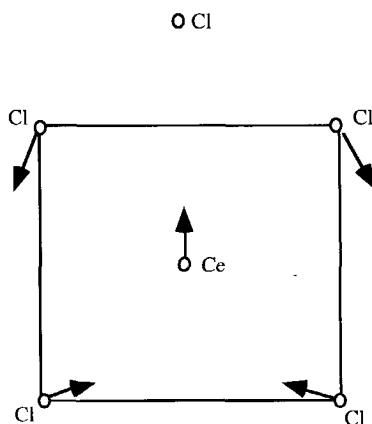


Figure 7.2.2 $\text{SrCl}_2\text{:Ce}$
Sideview of a unitcell with a Ce impurity and an extra Cl ion. The arrows indicate the direction of the lattice relaxation due to the Ce impurity and the extra Cl ion.

The Ce impurity very likely occupies a Sr site. The formal charge of the Ce ion is +3, while the formal charge of the Sr ion is +2. When a Ce^{3+} ion replaces a Sr^{2+} ion the extra charge has to be compensated. The absorption spectrum of $\text{SrCl}_2\text{:Ce}^{18}$ suggests that the impurity site has a C_4 type pointgroup symmetry. One of the ways to accomplish this is to put an extra Cl ion on the 100 axis through the Ce ion¹⁹. This is done in analogy with previous calculations in our group on $\text{BaF}_2\text{:Ce}^{20}$. Of course after replacing the Sr ion with a Ce ion and adding the extra Cl ion the lattice will relax. We tried to estimate this relaxation with the HADES program²¹. Because we did not have HADES interaction parameters for Sr and Cl we had to extrapolate them from other known parameters. This finally gave us two sets of interaction parameters and consequently two different relaxed structures. The relaxed clusters have C_{4v} pointgroup symmetry. In figure 7.2.2 we show how the lattice relaxes. The two relaxed structures only differ in the amount of displacement of the ions, not in the directions of the displacements. The distortion of the eight original Cl ions from the cubic symmetry is only

small. The largest contribution to the distortion from the cubic symmetry comes from the extra interstitial Cl ion. In figure 7.2.2 we give a rough sketch of the distortion, introduced by the extra Cl^- ion.

Results of the Relativistic Calculations

We have performed four-component relativistic calculations on the CeCl_8 cluster in the host crystal geometry. These calculations should provide us with a good estimate of the Ce 4f - 5d energy difference in chlorine compounds. To check the dependence of the results on the Ce - Cl distance we also performed a fully relativistic calculation on the same cluster but with a 8% smaller Ce - Cl bond distance. This is approximately the average expected relaxation of the crystal after replacing the Sr^{2+} ion with the Ce^{3+} ion and neglecting the charge compensation. The results are listed in table 7.2.1. Because of the cubic pointgroup symmetry the Ce 5d levels split up into a doublet and a triplet. The triplet lies higher in energy than the doublet. The triplet is again split up into a singlet and a doublet by the spin-orbit interaction, but this splitting is small.

	MOLFDIR		ECP's	Exp. ¹
	Host geom.	8% inward	Host geom.	
5d levels	0.00	0.00	0.00	0.00
	-0.15	-0.16	0.00	-0.15
	-0.15	-0.16	0.00	-0.26
	-1.46	-2.26	-1.27	-1.76
	-1.46	-2.26	-1.27	-
$\Delta E_{\text{av}} 1$	5.16	5.33	N.A.	N.A.
$\Delta E_{\text{av}} 2$	4.96	4.73	5.26	4.78
ΔE_{low}	4.32	3.61	4.85	3.80

Table 7.2.1 Ce 5d orbital energies and Ce 4f -> 5d transition energies for the CeCl_8 cluster in $\text{SrCl}_2:\text{Ce}$. ΔE_{av} is the energy difference between the average of the 4f and the average of the 5d levels. ΔE_{av}^1 is the "pure" value. ΔE_{av}^2 has been corrected for BSSE. All entries are in eV.

The ΔE 's give the energy differences between the average of the Ce 4f and the average of the Ce 5d levels. There are two ΔE_{av} 's. The first one is calculated by directly subtracting the total energies of the Ce 4f)¹ and the Ce 5d)¹ calculations; i.e.:

$$\Delta E_{\text{av}}^1 = E_{4f)^1} - E_{5d)^1} \quad 7.2.1$$

The second one is calculated by:

$$\Delta E_{av}^2 = E_{4f^1}^{4f \text{ basis}} - E_{5d^1}^{5d \text{ basis}} + E_{Ce^{4+}}^{5d \text{ basis}} - E_{Ce^{4+}}^{4f \text{ basis}}. \quad 7.2.2$$

The two ΔE_{av} 's are not equal because of the so-called Basis Set Superposition Error (BSSE)²². The calculations on the Ce 4f¹ state and the Ce 5d¹ state were not performed in exactly the same function space. Therefore their total energies are formally not comparable and ΔE_{av}^1 will contain an error. The BSSE can become quite large. In this case the error is relatively small because the two primitive basis sets only differ in the removal of the f-exponents for the "Ce 5d" basis set. In equation 7.2.2 we try to correct for the BSSE. Although the correction is calculated for a different charge state of the cluster (and can therefore not be completely correct) the value for ΔE_{av}^2 should be much better than the value for ΔE_{av}^1 . The term ΔE_{low} gives the energy difference between the lowest Ce 4f level and the lowest Ce 5d level. Its value is based on ΔE_{av}^2 .

As expected decreasing the Ce - Cl bond length increases the 5d level splitting between the doublet and the triplet. The spin-orbit splitting hardly changes, indicating that the Ce 5d orbitals do not significantly change. The change in ΔE_{av} as a consequence of the decreasing bond length is small, giving further evidence that ΔE_{av} is roughly equal for all chlorine compounds.

Comparing the calculated spectra with the experimental spectrum we see that the agreement is poor, but this was to be expected. The experimental spectrum clearly shows that the Ce site has C_{4v} symmetry instead of O_h pointgroup symmetry. This is due to the charge compensation that must follow the replacement of a Sr²⁺ ion by a Ce³⁺ ion. In our calculations up to now we neglected this. Although ΔE_{low} significantly differs between the calculated and experimental result, ΔE_{av} shows a reasonable agreement.

It is also possible to assume that the experimental spectrum is caused by a Ce ion in a C_{3v} type environment. The deviation of O_h symmetry is then small and the cluster in the host geometry should provide an adequate description of the Ce site. This interpretation is consistent with the assumption that the lattice relaxation in SrCl₂:Ce on doping with Ce is mainly caused by the different sizes of the Sr²⁺ and Ce³⁺ ions, and that charge compensation only has a minor influence on the direct environment of the Ce impurity site. In the remainder of this section we will assume that the Ce impurity site has C_{4v} pointgroup symmetry.

We have also performed calculations on the CeCl₈ cluster in the host geometry with the ECP's of Stevens et al^{11,12}. This should provide us with a further check on the validity of the ECP's. These results are also listed in table 7.2.1. The Ce 5d levels again split into a triplet and a doublet. This time the triplet is not split up by spin-orbit interaction. All electrons that are treated explicitly are treated on a non-relativistic level, so the spin-orbit interaction is absent. The difference in the total 5d level splitting between the relativistic and the non-relativistic calculation is in part due to the absence of the spin-orbit splitting in the latter. The other main reason for this difference is given by the fact that for the ECP calculation the

orbital energies are those of the virtual Ce 5d orbitals of the calculation on the Ce^{4+} charge state. If the 5d orbitals are occupied the splitting will increase somewhat.

The ECP value for ΔE_{av} is too large. If we correct the value with the correction factor we found for the free ion (section 5.2) we get: $\Delta E_{\text{av}} = 4.35\text{eV}$, which is too small. Apparently in this case the correction for the free ion does not carry over to the cluster.

If we compare the fully relativistic calculation with the ECP calculation in more detail the reason for this becomes clear. The main difference between the two calculations is not in the description of the Ce 4f orbital, but in the description of the Ce 5d orbital. The Ce 5d orbital is spatially rather extended and thus very sensitive to the direct environment of the Ce ion. It is therefore understandable that the free ion correction does not carry over very well to all sorts of different clusters.

The ECP value for ΔE_{low} combines the errors in ΔE_{av} and the 5d splitting, so its value does not compare very favourably with the full relativistic value of ΔE_{low} .

Charge Compensation and Lattice Relaxation

The Ce^{3+} ion has a higher positive charge than the Sr^{2+} ion it replaces in the crystal. In analogy with the $\text{BaF}_2\text{:Ce}$ case we assume that this extra charge is compensated by putting an extra Cl ion near the Ce impurity. The extra Cl ion is placed on one of the fourfold symmetry axes of the unperturbed cluster. This assures that the resulting Ce site has the C_{4v} symmetry the experiments¹ indicate. Because of the different sizes of the Ce and Sr ions and the extra Cl ion the positions of the other ions near the Ce impurity will be modified. We tried to estimate this lattice relaxation with the HADES program. We did not have the proper HADES interaction parameters for SrCl_2 . We obtained parameters by extrapolating the parameters for $\text{SrF}_2\text{:La}$ and KCl. This gave us two sets of parameters. We performed the relaxation for each set of parameters. Both sets of parameters yielded the same type of relaxation; i.e. the direction of the displacements of the ions was equal. The amount of displacement, however, differed significantly between the two sets of parameters. Thus we were finally left with two relaxed structures for the Ce impurity site.

In our subsequent quantum mechanical calculations we use the modified positions of the Ce impurity and its surrounding nine Cl ions. The positions and values of the Madelung point charges surrounding the cluster were kept frozen in the host crystal geometry. The Ce 5d level splittings calculated in this way with the non-relativistic Hartree-Fock method are listed in table 7.2.2.

The orbital energies in table 7.2.2 calculated with the small basis are the energies of the five occupied 5d orbitals in a calculation on the average of all Ce^{3+} 5d)¹ states. The orbital energies calculated with the ECP basis are the energies of the five virtual 5d orbitals of a calculation on the Ce^{4+} state. As can be seen from table 7.2.2 the choice of basis set or the use

of virtual versus occupied orbitals does not seem to matter very much in this case. Differences in geometry have a much larger effect. The difference in geometry seems to mainly effect the splitting between the former doublet and the former triplet. The splittings of the doublet and triplet due to the symmetry lowering are much less sensitive to the differences in geometry.

	geometry 1		geometry 2		Exp. ¹
	small basis	ECP	small basis	ECP	
5d levels	0.00	0.00	0.00	0.00	0.00
	-0.19	-0.17	-0.17	-0.16	-0.15
	-0.19	-0.17	-0.17	-0.16	-0.26
	-1.12	-1.17	-1.77	-1.73	
	-1.78	-1.69	-2.23	-2.14	-1.76

Table 7.2.2 Ce 5d orbital energies of the relaxed CeCl_9 clusters in the Madelung field of SrCl_2 . Geometry 1 is the structure derived from the optimisation with the SrF_2 parameters. Geometry 2 is the structure derived from the optimisation with the KCl parameters. All entries are in eV.

In the calculated 5d levels we still see a degeneracy between the second and third level. This degeneracy can be lifted by inclusion of the spin-orbit interaction. The relativistic calculations on the clusters in the host geometry gave a spin-orbit splitting between these levels of 0.15 eV. Assuming that the spin-orbit splitting would be the same for the relaxed clusters the degenerate levels at -0.19 eV would split up into a level at -0.12 eV and a level at -0.27 eV. These levels are in reasonable agreement with the experimental data.

When we compare the calculated Ce 5d levels with the experimental ones we observe that there is an good agreement for the three highest lying levels, especially when we take into account the spin-orbit splitting. From the two lowest lying Ce 5d levels only one can be deduced from the experiment: The transition of the lowest 4f orbital to one of those 5d orbitals is missing from the luminescence-excitation spectrum. The total Ce 5d level splitting of the calculation on geometry 1 compares very well with the total splitting found in the excitation spectrum. We therefore conclude that geometry 1 gives a good description of the direct environment of the Ce impurity in SrCl_2 .

Results of the CIS Calculations

We have also performed a CIS calculation on the CeCl_9 cluster in $\text{SrCl}_2\text{:Ce}$. In the previous section we showed that according to the Hartree-Fock method the cluster in geometry 1 showed the best agreement with experiment. Therefore we decided to do the CIS calculation on the CeCl_9 cluster in geometry 1. The calculation was performed with the ECP basis of

Stevens et al. The results are summarised in table 7.2.3. All energies are given in eV. The energies of the $4f \rightarrow 4f$ spectrum are given relative to the Hartree-Fock groundstate. All the other energies are given relative to the highest $Ce\ 5d)^1$ state. This makes the comparison with our previous results easier.

	$4f \rightarrow 4f$	$4f \rightarrow 5d$	$Ce^{3+} \rightarrow Ce^{2+}$
energies	0.00	0.00	-0.99
	0.00	-0.40	-0.74
	0.00	-0.40	-0.74
	0.04	-1.69	-0.39
	0.13	-1.72	-0.32
	0.24		-0.28
	0.24		-0.28
			-0.21
			-0.21

Table 7.2.3 Many electron energy levels for the $CeCl_9$ cluster in $SrCl_2:Ce$. All energies are in eV. The $4f \rightarrow 4f$ energies are given relative to the groundstate. All other energies are given relative to the highest $Ce^{3+}\ 5d)^1$ state.

The $Ce\ 4f)^1$ levels show a total splitting of 0.24 eV. Just as in the CeF_3 case this is mainly an artefact of the calculation. The splitting cannot be caused by spin-orbit interaction because this effect is not described by this method and the crystal field cannot have such a large effect on a core orbital as the $4f$ orbital.

The $Ce\ 5d)^1$ levels show a reasonable agreement with experiment. There are however some remarkable differences with the Hartree-Fock results. The second and third level (from above) are lying almost twice as low in the CIS case as in the Hartree-Fock case. The fourth level is at a completely different position. These differences have to do with another remarkable feature of the CIS results: The very low lying $Ce^{2+}\ 4f)^1 5d)^1$ states. Some of the Ce^{2+} states have total energies comparable with the $Ce^{3+}\ 5d)^1$ states. Because of their closeness in energy the two configurations will mix significantly. Analysis of the CIS wave functions for the three $Ce^{3+}\ 5d)^1$ states that differ most between the Hartree-Fock and the CIS calculations show that these states only consist for 70% of determinants with a $Ce^{3+}\ 5d)^1$ configuration. The remaining determinants in these wave functions have a $Ce^{2+}\ 4f)^1 5d)^1$ configuration. The Hartree-Fock method is basically a one-determinant method. Therefore configuration mixing cannot occur there and we only have pure $Ce^{3+}\ 5d)^1$ states.

The extra Cl ion near the Ce impurity has 3p levels well above the valence band and in the gap. The excitation energy from one of those 3p levels to one of the $Ce\ 5d$ levels is much smaller than a valence band $\rightarrow Ce\ 5d$ excitation. This makes the Ce^{2+} levels lie so unexpectedly low.

Nevertheless the Ce^{2+} levels, as given by the CIS calculation, may be too low relative to the Ce^{3+} levels. The errors made by the CIS method in the two types of excitations may differ

substantially. The Ce^{3+} levels consist of excitations from the lowest occupied Ce 4f orbital to the other Ce 4f orbitals and the Ce 5d orbitals. The two main errors in these excitations are the error in the position of the lowest Ce 4f orbital, due to the non-relativistic treatment of this orbital, and the error in the description of the excited states, due to the lack of polarisation. The Ce^{2+} levels consist of excitations from the Cl_{extra} 3p orbitals to the Ce 5d orbitals. The error in the position of the Ce 4f orbital does not matter here. The lack of polarisation is expected to be worse here, because the local charge state of the Ce ion changes with these excitations. The Ce^{2+} excitation energies will also show an error, due to the difference in the correlation energy contributions to the ground state and the excited states. We will address some of these errors again in the next sub-section, where we will determine the positions of all the levels in the band gap.

Position of the Ce Levels in the Gap

Now that we have calculated the splitting of the Ce 5d levels to a reasonable accuracy there remains the task of determining the position of the Ce levels in the band gap of SrCl_2 . We will start by computing the relative position of all the levels we expect to be in the band gap. All the calculations we did for this purpose were done on the CeCl_9 cluster in geometry 1. We calculated the energy difference between the lowest Ce 4f and the Ce 5d levels by taking the total energy difference from a Hartree-Fock calculation on the $\text{Ce}^{3+} 4f^1$ state and a Hartree-Fock calculation on the $\text{Ce}^{3+} 5d^1$ state. The energy difference between the lowest Cl_{extra} 3p orbital and the lowest Ce 4f orbital was calculated by taking the total energy difference from Hartree-Fock calculations on the Ce^{4+} and the " $\text{Ce}^{3+} 4f^1 \text{Cl}_{\text{extra}} 3p^{\text{hole}}$ " state. The energy difference between the lowest Cl_{extra} 3p orbital and the lowest Ce^{2+} state was calculated by taking the total energy difference of the Hartree-Fock calculations on the $\text{Ce}^{3+} 4f^1$ and the " $\text{Ce}^{2+} 4f^1 5d^1 \text{Cl}_{\text{extra}} 3p^{\text{hole}}$ " state. The Ce 5d level splitting was taken from the Hartree-Fock calculation with the small basis sets (table 7.2.2). The splitting of the Cl_{extra} 3p orbitals was taken from the orbital energies of a Hartree-Fock calculation on the Ce^{4+} state. The splitting of the Ce^{2+} levels was taken from the CIS calculation (table 7.2.3). The results are listed in table 7.2.4. All the energies are given relative to the highest Ce 5d¹ level. The lowest Ce 4f¹ level lies at -6.44 eV. The lowest Ce 5d¹ state lies at -1.78 eV. This means that the lowest Ce 4f \rightarrow Ce 5d transition lies at 4.66 eV. If we assume that for the cluster in the relaxed geometry we have the same error in the ECP results (relative to the fully relativistic MOLFDIR results) as for the cluster in the host crystal geometry the transition energy becomes 4.13 eV. This compares reasonably well with the experimental value of 3.80 eV.

If we assume that the ECP error is only in the position of the Ce 4f level and not in the positions of the Ce 5d levels all the other levels in table 7.2.4 are unaffected by this

correction. If we assume that the ECP error is only in the Ce 5d levels, all the other levels will go up by 0.53 eV.

	Ce ³⁺		Cl _{extra}	Ce ²⁺
levels	0.00		-3.63	2.01
	-0.19	3p	-3.63	2.01
5d	-0.19		-3.63	1.93
	-1.12			1.93
	-1.78			1.90
4f	-6.44			1.83
				1.48
				1.48
				1.22

Table 7.2.4. Energy levels in the gap of SrCl₂:Ce.
All entries are in eV and relative to the highest Ce 5d level.

Note that in the Hartree-Fock case the Ce²⁺ levels lie much higher relative to the Ce 5d levels, than in the CIS case. In absolute value they lie lower, which is consistent with the lack of polarisation in the CIS calculation.

We calculated the band gap of SrCl₂ by doing a Hartree-Fock calculation on the SrCl₈ cluster in the host geometry and a GVB(OSS) calculation on the same cluster in which one Cl 3p electron was excited to a Sr s orbital. The basis set of the Sr ion was extended with two diffuse s-type functions with exponents 0.03 and 0.01. The remaining unpaired Cl 3p electron and the excited electron were singlet spin coupled. The band gap can be found by subtracting the total energies of these two calculations. We found a band gap of 8.4 eV. Comparing this number with experiment is impossible, because we could not find experimental data on the band gap of SrCl₂. However for the chlorides for which the band gap was measured² it is always about 6 eV, so we may assume that the calculated band gap is somewhat too large.

To position the Ce levels in the band gap we can use the methods explained in section 5.1. There is one complicating factor. It is obvious that we should calculate the relative positions of all the Ce levels and the extra Cl levels from the results on the relaxed cluster. It is less clear if the position of those levels in the gap, and therewith the positions of the valence and conduction bands, should be estimated from the results on the cluster in the host geometry or in the relaxed geometry. The positions of the valence and conduction bands are given by the host crystal. Near the Ce impurity the potential is different from the potential in the pure host and consequently the bands will be distorted (band bending). If we determine the positions of the bands from the cluster in the host geometry this band bending is completely ignored. On the other hand if we try to determine the positions of the band edges from the cluster in the relaxed geometry, the band bending may very well be exaggerated.

Determining the band edges from calculations on the relaxed cluster turned out to be technically impossible. We were not able to get a converged result for those configurations, which would enable us to determine the band gap and the VB - Ce 4f distance.

The two methods explained in section 5.1 based on the orbital energies of the levels are possible for both clusters, except that the band gap could only be calculated for the cluster in the host geometry. Table 7.2.5 lists the VB - Ce 4f distance for all the possible methods.

	Host geom.			Geometry 1		
	vb	cb	Δ SCF	vb	cb	Δ SCF
Δ (VB \rightarrow Ce 4f)	6.13	-4.96	0.13	6.95	0.01	N.A.

Table 7.2.5 Energy difference between the VB edge and the Ce 4f¹ level for SrCl₂:Ce. Positive values mean the 4f level is above the VB. All entries are in eV.

For the valence and conduction band methods we used the calculations with the small basis sets, where the Sr basis was augmented with two very diffuse s-functions, with exponents 0.03 and 0.01 for the calculations on the cluster in the host geometry and the Ce basis was augmented with diffuse s-function, with exponents 0.111 and 0.032 for the calculations on the cluster in geometry 1. To position the Ce 4f level relative to the Ce 5d levels the corrected value of the ECP calculations was used.

The valence band method yields approximately the same result for both clusters, because the difference between the VB and the Ce 5d levels is approximately the same for both clusters. The result is implausible. We must conclude that the valence band method does not give acceptable results. Part of the reason is that the eight Cl⁻ ions see a Ce³⁺ ion instead of a Sr²⁺ ion. Because of the extra positive charge the Cl 3p band will lie much too low. This even holds for the cluster with the extra Cl⁻ ion because the extra anion is relatively far away.

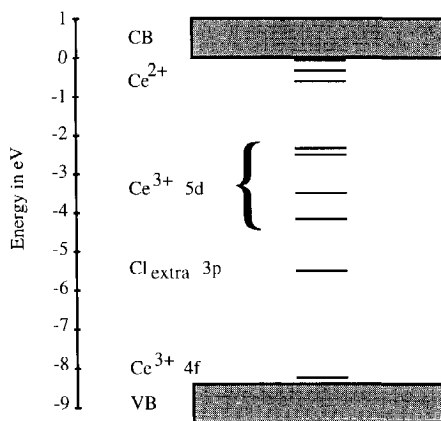


Figure 7.2.3 Energy levels in the band gap of SrCl₂:Ce

The conduction band method yields very different results for the two clusters. In the relaxed cluster all the occupied-orbital energies are higher than in the host cluster, while the Ce 6s orbital energy is the same. The result for the relaxed cluster was obtained under the

assumption that the band gap for this cluster is equal to the band gap for the cluster in the host geometry. This assumption may be wrong, so the reasonable looking value obtained with the conduction band method for the cluster with geometry 1 may be due to a lucky cancellation of errors. The ΔSCF value for the cluster with the host geometry looks reasonable and is probably the most reliable estimate we can currently obtain.

If we assume that the ΔSCF value for the VB - Ce 4f distance is correct and if we use the corrected ECP value for the Ce 4f - Ce 5d distance and if we assume that the ECP error in the Ce 4f - Ce 5d distance is completely caused by the error in the Ce 5d level positions, we find the levels in the gap as shown in figure 7.2.3. In spite of the many uncertain assumptions this is about the best estimate we can make.

We also estimated the valence bandwidth from the energies of the Cl 3p orbitals. The results are listed in table 7.2.6.

	Relativistic calc. on host geom.		Calc. with ECP basis	
	4f basis	5d basis	Host gem.	Geom. 1
band width	2.2	2.4	2.5	2.8

Table 7.2.6 Calculated valence bandwidths for $\text{SrCl}_2\text{:Ce}$. All entries are in eV.

All the calculated values for the cluster in the host geometry are very similar. The calculated value for the cluster in geometry 1 is somewhat larger.

Conclusions

With the HADES program we can get a reasonable estimate for the lattice relaxation around the Ce impurity in SrCl_2 . The Ce 5d level splitting can be calculated with acceptable accuracy. Given the uncertainty in the geometry of the impurity site the results are quite good. It is also possible that the Ce site has C_{3v} symmetry instead of C_{4v} symmetry. That interpretation has the advantage that we do not have the problem of an unexplained, experimentally not seen, Ce 5d level.

The semi-relativistic calculations with the ECP basis on the clusters in the host crystal geometry are able to reproduce the fully relativistic cluster results within an error of approximately 10%. The calculated energy difference between the Ce 4f and Ce 5d levels in the relaxed cluster still contains an error of 10% after correcting for the ECP error found for the host geometry cluster.

To give a reliable estimate for the positions of the Ce levels in the band gap remains a very difficult task. There are technical difficulties, which prevent us from calculating all the states we would like to. Experimental data, other than the luminescence and luminescence-excitation spectrum on the Ce impurity in SrCl_2 are not available. Therefore we have no

check on the final result, nor on the assumptions we have made to reach that result. More work, theoretical as well as experimental is needed to improve on these results.

7.3 CeCl_3

Although the chemical formula for CeCl_3 suggests that it may be very similar to CeF_3 it actually has quite a different structure. CeCl_3 has a higher spacegroup symmetry than CeF_3 . CeCl_3 belongs to the spacegroup $\text{P6}_3/\text{M}^{23}$. The Ce site has a pointgroup symmetry C_{3h} .

A Ce ion in CeCl_3 is surrounded by nine Cl ions; all at virtually the same distance. The next shell of ions consists of eight Ce ions. We have performed calculations on the CeCl_9 cluster and the CeCl_9La_8 cluster. In the last mentioned cluster we replaced all non-centre Ce ions by La ions. This makes the calculations a lot easier because we do not have the eight 4f electrons and their associated basis sets. In the figures 7.3.1 and 7.3.2 we show a top view and a side view of the CeCl_9Ce_8 cluster.

It is clear to see that the structure of CeCl_3 is very open. The Ce - Cl bond length is rather large, so the overlap between the Ce 5d orbitals and the Cl orbitals will be small. We therefore expect a relatively small 5d level splitting. The nine Cl ions surrounding the Ce ion lie almost on a sphere. Such a spherical surrounding will also keep the 5d level splitting small. It will also make the electron distribution more sensitive for non-spherical polarisation effects. This could make it harder to obtain good accurate results.

Results of the Hartree-Fock Calculations

The smallest cluster we can use to describe CeCl_3 is a CeCl_9 cluster. This cluster has C_{3h} pointgroup symmetry. Unfortunately this system is already too large to do a completely relativistic calculation. So we can only do non-relativistic calculations. The results of our Hartree-Fock calculations on the CeCl_9 cluster are listed in table 7.3.1, together with the results deduced from the absorption spectrum by Sato². The basis sets used are listed in table 7.3.2.

The C_{3h} pointgroup symmetry will split the 5d levels into two doublets and a singlet. This can be seen in column a of table 7.3.1. In this column the Ce 5d levels are listed as found by a calculation on the CeCl_9 cluster with the small basis sets. As expected the total 5d level splitting is small. In this case the polarisation of the Cl ions may be important. The small basis sets may not be flexible enough to describe this polarisation properly.

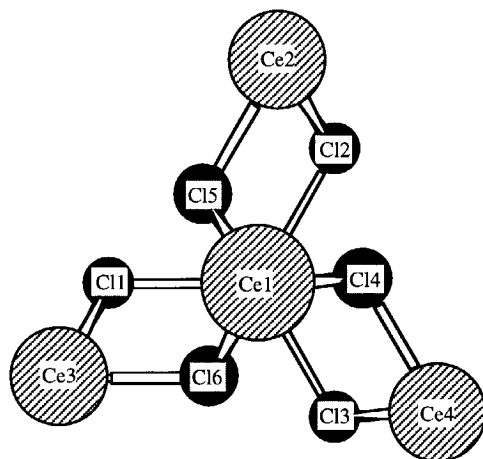


Figure 7.3.1 Top view of the CeCl_9Ce_8 cluster in CeCl_3

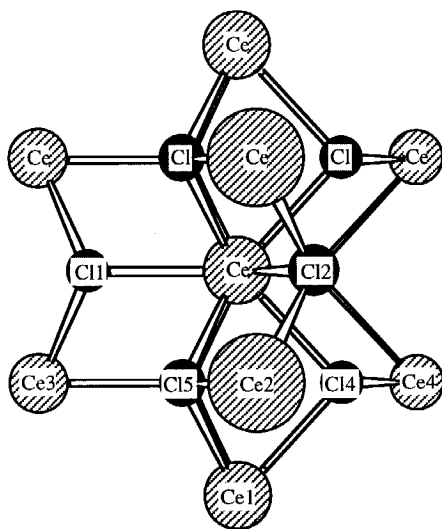


Figure 7.3.2 Side view of the CeCl_9Ce_8 cluster in CeCl_3

Therefore we extended the Cl basis set with a polarisation function: A d-function with exponent 0.457⁴. The results obtained with these basis sets are listed in column b of table 7.3.1. The total 5d splitting decreases somewhat, as expected, while the second level goes down. If we make the Cl basis even more diffuse this trend continues. Column c of table 7.3.1 lists the results obtained by using very large basis sets optimised for the Ce^{3+} and the Cl- charge states of the ions. The Cl basis set contained two polarisation d-functions with exponents 0.7 and 0.17.

	Theory					Exp. ²
	basis a	basis b	basis c	basis d	basis b, no pot.	
5d levels	0.00	0.00	0.00	0.00	0.00	0.00
	-0.17	-0.33	-0.34	-0.43	-0.30	-0.30
	-0.64	-0.56	-0.45	-0.65	-0.42	-0.70
						-1.20

Table 7.3.1 Ce 5d level energies of the CeCl_9 cluster in CeCl_3 . All entries are in eV.

If we use even more diffuse d-functions on the Cl ion it becomes impossible to obtain reasonable results. In that case the Cl 3d orbitals lie very low in energy and mix very strongly with the Ce 5d orbitals. This is an artefact caused by the very limited size of the cluster and the point charges surrounding the cluster. The effect is already somewhat visible in the calculation with basis set c.

	original basis	additions Ce basis	additions Cl basis
basis a	small basis sets	none	none
basis b	small basis sets	none	d-polarisation function; exp.: 0.457
basis c	large basis sets	none	d-polarisation functions; exp.: 0.7 and 0.17
basis d	small basis sets	4f polarisation functions	none

Table 7.3.2 The all-electron basis sets for the SCF calculations on CeCl_3 .

In the previous calculations we have seen the effect of polarisation functions on the Cl ion. We can also use polarisation functions on the Ce ion. To study this effect we extended the small basis set for Ce with the 4f functions and performed a Hartree-Fock calculation on the $\text{Ce}^{3+} 4f_{\text{av}}^{0.5} 5d_{\text{av}}^{0.5}$ state of the CeCl_9 cluster. With the orbitals thus found we evaluated the correct energy expressions for the different $\text{Ce}^{3+} 5d^1$ states of the cluster. The results are listed in column d of table 7.3.1. When we compare column d with column a we notice that the total 5d level splitting is not affected. The second level however, lies much lower in energy with the 4f functions included.

In the last theory column of table 7.3.1 we list the results of the calculation with the basis sets b, but without the point charges, which emulate the Madelung potential. Just as in the CeF_3 case we see that the 5d level splitting is mainly determined by the next nearest neighbours of the central Ce ion. The external potential has only a marginal effect on the 5d level splitting. If we compare the theoretical results with the experimental results the agreement is very poor. The calculated 5d splitting is only half the experimental one. What is more, the experimental results show four absorption lines (and not three) with the smallest distance between the lines being 0.3 eV. This absorption spectrum seems to conflict with the Ce_{3h} pointgroup symmetry of the Ce site.

To check the structural data we have used, we performed a completely relativistic calculation on the Ce^{3+} ion embedded in an array of point charges, emulating the Madelung potential of CeCl_3 . The results of this calculation, together with the experimental results are listed in table 7.3.3.

The gap between the $^2F_{7/2}$ quartet and the $^2F_{5/2}$ triplet is caused by spin-orbit interaction and is primarily determined by the ion itself and not by its environment. The splitting within the levels belonging to one term is caused by the ligand field. The calculated ligand field splitting is somewhat larger than the experimental one.

	Theory	Exp. ²⁴
4f levels	0.00	0.00
	-0.02	-0.01
	-0.05	-0.02
	-0.06	-0.03
	-0.29	-0.28
	-0.32	-0.29
	-0.35	-0.30

Table 7.3.3 The energies of the Ce^{3+} 4f levels in the Madelung field of CeCl_3 . All entries are in eV.

This is a result from the fact that the environment of the Ce ion is completely represented by point charges. The point charges generate a stronger field than the smeared out charge distributions of the real Cl ions and consequently the level splitting will also be larger. However this is only a small effect. Because all the electrons of the Ce ion react to the ligand field (and to each other) the 4f electron in Ce^{3+} only feels 28% of the ligand field²⁵. This effect is called shielding. The Hartree-Fock-Dirac method, used to obtain the theoretical results, accounts only for part of this shielding. The factor two difference between the calculated and measured values is caused by shielding effects not treated by the HFD method. Although the match between the calculated and the experimental results is not perfect, the results clearly indicate that the structural data we have used is approximately correct and that the Madelung field and its associated higher order fields are correctly represented. This leads to the conclusion that there is something wrong with either the experiment of Sato or its interpretation.

The analysis of the structure of CeCl_3 and the results of the calculations on the CeCl_9 cluster showed that the Ce 5d level splitting is small and that polarisation in the Cl shell around the

central Ce ion is important. In the CeCl_9 cluster the Cl ions are on the outside of the cluster and are therefore not properly described. This may affect their charge density and thus also the calculated Ce 5d level splitting. To describe the Cl ions better we should include the next shell of ions in the cluster. This would result in a CeCl_9Ce_8 cluster. In practice a calculation on this cluster would be very difficult. The total number of basis functions would be very large on account of the nine Ce ions. We also have nine loose 4f electrons. It is not a priori clear what the spin coupling between these nine electrons should be. To circumvent these problems we have used a CeCl_9La_8 cluster instead, because La^{3+} and Ce^{3+} are equally large. For the Cl ions this substitution should not matter much. They should feel approximately the same potential and repulsion forces as with the Ce ions. The results of the Hartree-Fock calculations on the CeCl_9La_8 cluster are summarised in table 7.3.4.

The calculations were done with the small basis sets, without polarisation functions.

The first column of the table lists the virtual orbital energies of the Ce 5d orbitals from the calculation on the Ce^{4+} charge state. The second column contains the differences in total energy of the

	Orb. en.	ΔSCF
5d levels	0.00	0.00
	-0.15	-0.18
	-0.68	-0.67

Table 7.3.4 Ce 5d level energies of the CeCl_9La_8 cluster in CeCl_3 . All entries are in eV.

different $\text{Ce}^{3+} 5d)^1$ states. The results of both methods differ very little. The extra relaxation of the charge density due to the actual occupation of one of the Ce 5d orbitals is very small. In regard of the almost spherical distribution of the Cl ions around the Ce ion this is not really surprising.

If we compare the results of table 7.3.4 with column a of table 7.3.2 we notice that there is virtually no difference. The large CeCl_9La_8 cluster does not provide a better description of the central Ce ion than the small CeCl_9 cluster. It follows that to describe the local properties of a Ce ion in CeCl_3 we can suffice with calculations on the CeCl_9 cluster.

Results of the ECP Calculations

Unfortunately the CeCl_9 cluster is too large and has too low a pointgroup symmetry to allow a fully relativistic four component calculation. To get a theoretical estimate for the Ce 4f - 5d distance and the VB - Ce 4f distance we have to resort to the use of the semi-relativistic ECP basis sets. For the Ce ion we used a (111) contraction for the d-exponents and a (61) contraction for the f-exponents. We have totally decontracted the Cl basis set to allow for the negative charge state of the ion in the cluster.

In table 7.3.5 we show the Ce 5d level splitting calculated with the CeCl_9 cluster and the ECP basis set. The column labelled SCF contains the orbital energies of the virtual Ce 5d orbitals of the calculation on the Ce^{4+} charge state of the CeCl_9 cluster. The column labelled CIS

contains the results of the CIS calculation on the CeCl_9 cluster in the $\text{Ce}^{3+} 4f^1$ reference state.

The SCF values are, as expected, approximately equal to the orbital energies calculated with the small basis sets without the polarisation functions. The results of the CIS calculation are surprising. We seem to have lost the C_{3h} point group symmetry.

	SCF	CIS	Exp.
5d levels	0.00	0.00	0.00
	-0.22	-0.27	-0.30
	-0.65	-0.29	-0.70
		-0.52	-1.20
		-1.02	

Table 7.3.5 Ce 5d level splitting of the CeCl_9 cluster in CeCl_3 . All entries are in eV.

The reference state for the CIS

calculation is the $\text{Ce}^{3+} 4f^1$ state of the cluster. If we look at the virtual Ce 5d orbitals from that calculation we see that the 5d level splitting has increased and that the symmetry is broken: The highest lying doublet has split up by 0.3 eV. The Ce 5d levels are polarised by the non-spherical distribution of the $4f^1$ electron. Performing a CIS calculation on this state will obviously give similar results, because the CIS method lacks the ability to reverse this polarisation.

Actually the Ce 5d level splitting calculated with the CIS method compares quite well with the experimental results from Sato². Assuming that the experimental results are correct this result seems to indicate that the $\text{Ce } 4f^1 \rightarrow \text{Ce } 5d^1$ transitions are so fast that the Ce 5d orbitals do not get a chance to relax to the altered electron distribution during this transition.

The remaining quantities we need to be able to determine the position of the Ce levels in the gap are listed in table 7.3.6. The gap was calculated by taking the difference in total energy of a SCF calculation on the groundstate of the LaCl_9^{6-} cluster and a GVB calculation on the first excited state of the same cluster. We used the small basis sets for La and Cl. The basis set for La was extended with two very diffuse s-type functions with the exponents 0.03 and 0.01. All the other calculated values were obtained from calculations on the CeCl_9 cluster with the ECP basis sets.

	ΔSCF	CIS	Exp.
4f \rightarrow 5d	5.39	6.42	3.80
VB \rightarrow 4f	0.51	4.89	0.00
gap	7.32	N.A.	N.A.

Table 7.3.6 Excitation energies for CeCl_3 . All entries are in eV.

As in all previous cases the CIS values are larger than the ΔSCF values, because the CIS method lacks part of the electronic polarisation. We can remedy this by including multi-excitation configurations in the CI. We can do this either by directly including those configurations in the CI or by doing Møller-Plesset perturbation theory²⁶ on the final CIS

wave function. Both methods are very time consuming for systems as large as ours. So it seems worthwhile to look for alternatives like the ΔSCF method.

The ΔSCF value for the $4f \rightarrow 5d$ transition is much larger than the experimental value. There are two reasons for this. The first reason we have encountered before. Even though the ECP's contain relativistic effects, the electrons are still treated on a non-relativistic level. Therefore the energies contain an error relative to the full relativistic energies. For the free ion we found (section 5.2) a difference between the completely relativistic results and the ECP results of 0.91 eV. For the CeCl_8 cluster in SrCl_2 we found a difference of only 0.3 eV.

The second error in the ΔSCF value for the $4f \rightarrow 5d$ transition energy comes from the fact that the SCF method is not able to reproduce the experimental 5d level splitting. We only managed to get a reasonable result with the CIS method. This gives an additional correction factor with a maximum value of 0.4 eV. The smallest value for the $4f \rightarrow 5d$ transition we can get with the help of the two above mentioned corrections is 4.08 eV. This value compares reasonably with the experimental value of 3.8 eV.

In the XPS spectrum⁴ of CeCl_3 the Ce 4f levels are seen as a shoulder on the flank of the valence band peak. The calculated value of $\Delta E_{\text{VB-4f}} = 0.5$ eV is a bit on the large side, but not too bad.

The calculated band gap is the difference between the valence band edge and the edge of the band formed by the Ce 6s orbitals.

The actual conduction band in CeCl_3 is formed by a hybrid of the Ce 5d and the Ce 6s orbitals²⁷. The real conduction band in CeCl_3 should therefore lie somewhat lower than a pure Ce 6s band. In this light the calculated value of 7.3 eV for the band gap seems a reasonable result. (Chlorine compounds usually have a band gap in the order of 6 eV.).

	Theory	Experiment
CB	0.00	0.00
5d levels	-1.70	
	-1.98	-2.32
	-1.99	-2.62
	-2.22	-3.02
	-2.72	-3.52
lowest 4f	-6.81	-7.32
VB	-7.32	-7.32

Table 7.3.7 The levels in the gap of CeCl_3 . All entries are in eV.

In table 7.3.7 we list our best results for the positions of the conduction and valence band and the levels in the gap of CeCl_3 . The Ce 5d level splitting has been taken from the CIS calculation. The Ce 4f - 5d transition energy is the ΔSCF value from table 7.3.6 corrected for both the relativistic error and the SCF error. The VB - Ce 4f transition energy was also taken from table 7.3.6. The experimental values were taken from references 2 and 4. Because the

experimental band gap is unknown we have used the calculated band gap in the column with experimental results.

From the orbital energies of all the calculations we have performed we can estimate the width of the valence band (Cl 3p band). These values, together with the experimental one, are listed in table 7.3.8. The different basis sets we have used all yield approximately the same valence band width. The valence band width calculated with the CeCl_9La_8 cluster differs from the value calculated with the CeCl_9 cluster. This is understandable, because the chlorine ions have different environments in the two clusters. The band width calculated with the smaller cluster agrees better with experiment than the band width calculated with the large cluster. Both clusters are far too small to give reliable band information. The larger cluster does not necessarily provide better results²⁸, because the different errors still vary wildly with the cluster size. Because of a lucky cancellation of errors it is possible that a small cluster yields results which seem to be better than those of a large cluster.

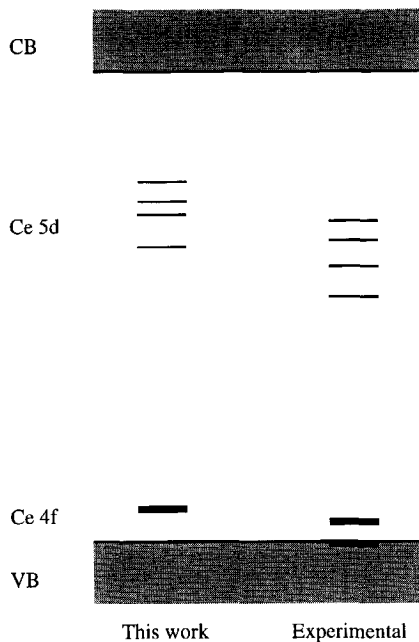


Figure 7.3.3 The band gap of CeCl_3 .

VB width	CeCl_9			CeCl_9La_8	Exp.
	small basis	large basis	ECP's	small	
	3.2	3.1	3.2	2.9	3.5

Table 7.3.8 Valence band widths for CeCl_3 . All entries are in eV.

In figure 7.3.3 we give a pictorial representation of the band gap and the localised levels. For this picture we have used the values from table 7.3.7.

Conclusions

The experimental absorption spectrum measured by Sato leaves some doubt about its correctness. The spectrum does not show the C_{3h} pointgroup symmetry. The absorption

spectrum is caused by a $\text{Ce } 4f^1 \rightarrow \text{Ce } 5d^1$ transition. The electron distribution of the Ce 4f orbital is not spherical. If the electronic transition is so fast that the Ce 5d orbitals have no time to adjust to the changing electron distribution this experimental outcome is possible (Although this effect is not observed in the other materials studied in this thesis.).

Our calculations confirm this. The SCF method yields Ce 5d energy levels that are consistent with the C_{3h} pointgroup symmetry of the Ce site, but do not agree with experiment. The CIS calculations, which use Ce 5d orbitals polarised by the occupied Ce 4f orbital, yield results that are comparable to experiment.

The lowest $\text{Ce } 4f^1 \rightarrow \text{Ce } 5d^1$ transition can be calculated with an accuracy of 10%. The position of the Ce 4f level relative to the valence band can be calculated within an accuracy of 0.5 eV. Given the fact that we use a semi-relativistic formalism to describe effects that are relativistic these are very reasonable results.

Our method is capable of predicting the positions of localised impurity levels in the gap of inorganic crystals within a reasonable accuracy.

References

- 1) O.T. Antonyak and N.S. Pidzyrailo, *Opt. Spectrosc. (USSR)*, **60** 743 (1986)
- 2) S. Sato, *J. of the Phys. Soc. Japan*, **41** 913 (1976)
- 3) A.S. Voloshinovskii, P.A. Rodnyi, O.T. Antonyak and N.S. Pidzyrailo, *Phys. Solid State* **36** 239 (1994)
- 4) K.H. Park and S.J. Oh, *Phys. Rev. B*, **48** 14833 (1993)
- 5) Gaussian 92, Revision G.2, M. J. Frisch, G. W. Trucks, M. Head-Gordon, P. M. W. Gill, M. W. Wong, J. B. Foresman, B. G. Johnson, H. B. Schlegel, M. A. Robb, E. S. Replogle, R. Gomperts, J. L. Andres, K. Raghavachari, J. S. Binkley, C. Gonzalez, R. L. Martin, D. J. Fox, D. J. Defrees, J. Baker, J. J. P Stewart and J. A. Pople, Gaussian, Inc., Pittsburgh PA, 1992.
- 6) *Relativistic Quantum Chemistry: The MOLFDIR program package*, L. Visscher, O. Visser, P.J.C. Aerts, H. Merenga and W.C. Nieuwpoort, *Computer Physics Communications* **81** 120 (1994)
- 7) *Relativistic Quantum Chemistry: The MOLFDIR program package*, L. Visscher, W.A. de Jong, O. Visser, P.J.C. Aerts, H. Merenga and W.C. Nieuwpoort, in *METECC-95*, E. Clementi and G. Corongiu, (STEF, Cagliari, 1995)
- 8) S. Huzinaga, Ed., J. Andzelm, M. Klobukowski, E. Radzio-Andzelm, Y. Sakai, H. Tatewaki, in *Gaussian Basis Sets for Molecular Calculations*, Elsevier, Amsterdam, 1984.
- 9) R.C. Raffanetti, *J. Chem. Phys.* **58** 4452 (1973)
- 10) R.E. Stanton and S. Havriliak, *J. Chem. Phys.* **81** 1910 (1984)
- 11) W.J. Stevens, H. Basch, M. Krauss, *J. Chem. Phys.* **81** 6026 (1984)

- 12) Thomas R. Cundari and Walter J. Stevens, *J. Chem. Phys.* **98** 5555 (1993)
- 13) E.F. Carr, *J. Chem. Phys.*, **38** 1540 (1963)
- 14) A. Szabo and N.S. Ostlund, *Modern Quantum Chemistry*, McGraw-Hill Publishing Company, New York (1982)
- 15) C.E. Moore, *Analysis of Optical Spectra*, NSRDS-NBS 34, Office of Standard Reference Data, National Bureau of Standards, Washington D.C.
- 16) J. Almlöf and U. Wahlgren, *Theoret. Chim. Acta*, **28** 161 (1973)
- 17) W.R. Busing, *Trans. of the Am. Cryst. Assoc.*, **6** 57 (1970)
- 18) O.T. Antonyak, I.V. Kityk and N.S. Pidzyrailo, *Opt. Spectrosc. (USSR)*, **63** 311 (1987)
- 19) H. Merenga, J. Andriessen and C.W.E. van Eijk, in *Proceedings of the International Conference on Inorganic Scintillators and their Applications*, eds. P. Dorenbos and C.W.E. van Eijk, p138, Delft University Press, Delft, 1996
- 20) R. Visser, J. Andriessen, P. Dorenbos and C.W.E. van Eijk, *J. Phys.: Condens. Matter*, **5** 5887 (1993)
- 21) A.H. Harker, *HADES II/PC: The Harwell Automatic Defect Evaluation System for Personal Computers*, (Harwell: Publication Office), (1989)
- 22) S.F. Boys and F. Bernardi, *Mol. Phys.*, **19** 553 (1970)
- 23) T. Kojima, T. Inoue and T. Ishiyama, *J. of the Electr. Soc. of Japan*, **19** 383 (1951)
- 24) G. H. Dieke, in *Spectra and Energy Levels of Rare Earth Ions in Crystals*, H.M. Crosswhite and H. Crosswhite eds., p193, Interscience Publishers, New York.
- 25) R.P. Gupta and S.K. Sen, *Phys. Rev. A*, **7** 850 (1973)
- 26) C. Møller and M.S. Plesset, *Phys. Rev.*, **46** 618 (1934)
- 27) A. Wojtowicz et al., *Conference Record NSS&MIC, IEEE, Norfolk, 1994*, p123
- 28) G. Aissing, *Interstitial Transition Metals in Silicon*, PhD Thesis, Rijksuniversiteit Groningen, 1988

Chapter 8

Summary and Concluding Remarks

In the first section of this chapter we will present a summary of this thesis together with the main conclusions we arrived at. In the second section we will discuss some of the problems which still remain with the cluster calculations and give some suggestions on how to continue this research. We will also briefly discuss what else is needed to come to a complete understanding of scintillation in ionic compounds.

8.1 Summary

The scintillation process in ionic compounds can be divided into three stages¹:

- i) The creation of hot electrons and holes by the ionising radiation and their subsequent thermalisation.
- ii) The migration through the crystal of the excitations created in the first stage.
- iii) The de-excitation of the excitations at luminescence centres.

In this thesis we are only concerned with the third stage of the scintillation process in ionic compounds doped with cerium. In these compounds the cerium ion usually acts as the luminescence centre. The light emitted by the cerium ion originates from an electronic transition from a $\text{Ce}^{3+} 5d)^1$ state to a $\text{Ce}^{3+} 4f)^1$ state. It is believed that the positions of the cerium levels relative to the bands of the host are important for the luminescence behaviour of the crystal².

The work described in this thesis is aimed at the calculation of the positions of these $\text{Ce}^{3+} 4f$ and $5d$ levels in ionic compounds. We describe the material with a cluster of ions³, embedded in an array of point charges, emulating the Madelung potential⁴. Because cerium is a rather heavy atom ($Z=58$) relativistic effects are important and the calculations should preferably be done within a relativistic computational model.

In the theoretical chemistry group of the university of Groningen a program package called MOLFDIR^{5,6} was developed, which can perform four-component Hartree-Fock-Dirac

calculations on arbitrary molecules. Due to the relatively large size and low symmetry of our clusters this program package required prohibitive amounts of computer resources for our calculations. So we decided to optimise the program package.

Optimisation of the MOLFDIR Package

We implemented a number of convergence accelerators into the SCF part of the program: Damping on the density, Aitken extrapolation⁷, Pople's extrapolation, DIIS⁸ and a partial implementation of the QCSCF method⁹. The results of the test runs we performed with these methods show that damping on the density to obtain an initial convergence of at least 10^{-2} on the density, followed by the DIIS procedure, almost always gives superior results. In all cases the program converged at least three times as fast as the original program, while the overhead of the DIIS procedure was minimal. The other convergence accelerators had systems on which they performed well, but they were less reliable and performed overall considerably less than the DIIS procedure.

The second thing we did to optimise the MOLFDIR program was to look if we could restructure the code that calculates the integrals and if we could make better use of symmetry. Making better use of symmetry is indeed possible, but does not yield computational savings as big as we had hoped. The reason lies in the fact that for double groups with an odd principle axis we cannot define a representation for all the irreducible representations such that all the integrals remain real-valued. The implementation of the new scheme has not yet been completed.

Results of the Calculations

After these optimisations we investigated a number of fluorine, oxygen and chlorine compounds. For these investigations we used a combination of non-relativistic calculations, non-relativistic calculations with ECP's¹⁰ containing relativistic corrections, and completely relativistic calculations.

The results of these calculations show clearly that the full four-component relativistic Hartree-Fock-Dirac calculations are the most accurate calculations we can perform. This is especially evident in the calculated position of the Ce 4f levels and thus in the Ce 4f-5d energy distance. The Ce 5d level splitting seems to be only marginally affected by relativistic effects and is already adequately described by the non-relativistic Hartree-Fock method.

Full four-component Hartree-Fock-Dirac calculations are not always possible, because of their huge demands on the computational resources. The only realistic alternative we have is

to perform non-relativistic Hartree-Fock calculations, where we describe the cores of the atoms with ECP's which contain relativistic effects. These calculations give much better results than "pure" non-relativistic Hartree-Fock calculations, but still fail to give correct relativistic results. In the free cerium ion there is an error of approximately 0.9 eV in the calculated position of the Ce 4f levels.

The Fluorine Compounds

The calculations on the fluorine compounds show good results.

For CeF_3 the Ce 5d level splitting is quite accurately predicted. The VB - Ce 4f distance and the Ce 4f - 5d distance is somewhat less accurate, because of the errors we make for the Ce 4f orbitals, due to the ECP's. But even these values are within 0.4 eV of the experimental values.

In $\text{LiBaF}_3\text{:Ce}$ extensive lattice relaxation is expected upon doping with cerium. By a suitable choice of cluster we are able to calculate this lattice relaxation. The resulting Ce 5d level splitting agrees well with experiment, indicating that our prediction of the lattice relaxation is also correct.

The results for $\text{LiLuF}_4\text{:Ce}$ are also reasonable. In this material also extensive lattice relaxation is expected upon doping with cerium. Judging from the experimental results the lattice relaxation or a Jahn-Teller distortion¹¹ breaks the original S_4 symmetry of the impurity site. A reliable geometry optimisation without symmetry restrictions is at the moment beyond our capabilities, so an accurate Ce 5d spectrum could not be obtained. By making use of a geometry optimisation which leaves the S_4 symmetry intact we were able to calculate the total spread of the Ce 5d levels correctly.

The Chlorine Compounds

The results for the chlorine compounds are somewhat less good than those for the fluorine compounds. This is caused by the large ionic radius of the chlorine ion and its large polarisability. The results, however, are still acceptable.

For $\text{SrCl}_2\text{:Ce}$ we are able to give a reasonable estimate of the lattice relaxation upon doping with Cerium with the HADES¹² program. Given the uncertainties linked with this HADES calculation the resulting Ce 5d level splitting agrees quite well with experiment. For the other

calculated observables, like the positions of the cerium levels in the band gap, experimental data is, to our knowledge, not yet available.

For CeCl_3 the calculated band gap, the position of the cerium 4f level relative to the valence band edge and the average cerium 4f - 5d distance agree within an error of 0.4 eV with the experimental results. Given the fact that most of the calculations were only semi-relativistic this can be considered a good result. There remains a problem with the Ce 5d level splitting in CeCl_3 which is far too small when compared with experiment. Because there is some doubt about the correctness of the experimental absorption spectrum a second independent absorption or luminescence-excitation spectrum experiment on CeCl_3 , or even better $\text{LaCl}_3:\text{Ce}$, would be desirable.

The Oxygen Compounds

The calculations on the oxygen compounds gave serious problems and the results are not always usable. But reasonable results can be achieved by a careful choice of the cluster and the basis sets. The problems with the oxygen compounds are partially caused by the need for a rather diffuse basis set to describe the O^{2-} ion. These basis sets are so diffuse that they protrude far beyond the cluster edge into the region where the point charges are located, which generate the Madelung potential at the cluster sites. These functions feel a potential and field which significantly deviate from the crystal potential and field. As a consequence they give rise to artificially low lying states in the band gap of the cluster. The low lying oxygen states seriously hamper the determination of the Ce 5d levels and the calculation of the conduction band edge. Another reason for the problems is the in general low pointgroup symmetry and the fact that cerium usually replaces an ion with a much smaller ion radius.

Despite these problems we were able to obtain reasonable looking results for $\text{La}_2\text{Hf}_2\text{O}_7:\text{Ce}$. It is not yet possible to check the results against experiment.

$\text{LSO}:\text{Ce}$ is a very complicated material because of its low symmetry. The lutetium sites have only C_1 pointgroup symmetry. It is possible to calculate observables of the host material with a reasonable accuracy. The calculated band gap, valence band width and Lu 4f band width agree reasonably with experiment. The calculations on the system with the impurity are less accurate. This is to a large extent due to the fact that we were not able to reliably calculate the lattice relaxation in this material. Nevertheless the calculated absorption spectrum for the Cerium impurity site does not compare too badly with the experimental data. The first Ce 4f \rightarrow 5d transition is predicted within 0.4 eV of the experimental value.

Our completely relativistic calculation on cubic CeAlO_3 shows that the results on oxygen compounds can be as accurate as our calculations on fluorine compounds. All the calculated values agree well with experiment. The cerium site in cubic CeAlO_3 has a high pointgroup symmetry (O_h) and the Ce - O distance is large (2.65 Å). Apparently, if these conditions are fulfilled accurate results for oxygen compounds are possible.

Final Conclusion

In conclusion we can say that our procedure to calculate the positions of local cerium levels relative to the valence band edge of ionic host materials works reasonably well. In many cases we are able to predict the levels with an error less than 0.5 eV. The combination of small cluster size and poor embedding of the cluster in the lattice can cause problems. These problems are the most severe for clusters with a low pointgroup symmetry and diffuse basis sets on the ligands.

8.2 Recommendations

In light of the above stated conclusion it is obvious on what point further research should be concentrated. The embedding of the quantum mechanically treated cluster of ions should be improved in such a way that even the diffuse functions of the cluster always will feel a reasonably correct potential. A set of point charges is not enough to ensure this. We need at least a projection operator which will prevent the diffuse functions from occupying the neighbouring core regions. By using, for instance, a pseudo potential for the ions neighbouring the cluster of ions¹³ we can ensure this. However, it may be that even more elaborate schemes are needed, which embed the cluster in the wave function and potential of a band structure calculation^{14,15}.

The need for such an embedding becomes more pressing when the ligands become heavier. The heavier the anions are the larger they are. When the anions become larger, they will also need larger and more diffuse basis sets to describe them. As a consequence the problems we already experienced with the oxygen compounds will become more severe, and we could reach a stage in which no useful results can be obtained. This can, to some extent, already be seen when we compare our calculations on the chlorine compounds with our calculations on the fluorine compounds.

In this thesis we have only considered materials doped with cerium. But cerium is not the only dopant which can act as a luminescence centre. Experiments are also performed with materials doped with, among others, neodymium^{16,17} and praseodymium^{3,18,19,20,21,22}. These ions have in their +3 charge state a partially filled 4f shell. So the 4f \rightarrow 5d excitation spectra are much more complicated than for cerium. Moreover for these excitation spectra correlation effects are important and we cannot suffice with Hartree-Fock calculations anymore. Accurate quantum mechanical calculations on a correlated level require larger basis sets (and functions for higher l-values) than Hartree-Fock calculations²³. So for these systems the problems already encountered for the oxygen compounds will also be more severe. So developing an embedding that can handle and solve these problems is very important if we want to investigate a broader range of systems.

As explained earlier scintillation can be thought of as to occur in three separate stages. In this thesis we were only concerned with the electronic structure of the luminescence centres in scintillators, which is part of the third stage. To obtain a more complete understanding of scintillation we have to understand all three stages and not only the third.

Recently a few papers^{24,25} were published that give a phenomenological description of the first stage.

Of the second stage: the migration of the holes, electrons and excitons through the lattice to the luminescence centres very little is known. The performance of a scintillator is to a large extent determined by the efficiency of this stage. A better and more quantitative understanding of this stage would enormously benefit the search for better scintillators.

The methodology described in this thesis can only describe static situations and is thus not very well suited to study a dynamic process like the migration of the excitations through the crystal. The migration of excitations through the crystal should be studied with methods which are capable to describe the dynamics of the process.

References

- 1) J. Andriessen, P. Dorenbos and C.W.E. van Eijk, *Mat. Res. Soc. Symp. Proc.*, **348** 355 (1994)
- 2) C. Pedrini, D. Bouttet and C. Dujardin, in *Proceedings of the International Conference on Inorganic Scintillators and their Applications*, eds. P. Dorenbos and C.W.E. van Eijk, p103, Delft University Press, Delft, 1996
- 3) J. Sauer, *Chem. Rev.*, **89** 199 (1989)
- 4) J. Almlöf and U. Wahlgren, *Theoret. Chim. Acta*, **28** 161 (1973)

- 5) Relativistic Quantum Chemistry: The MOLFDIR program package, L. Visscher, O. Visser, P.J.C. Aerts, H. Merenga and W.C. Nieuwpoort, *Computer Physics Communications* **81** 120 (1994)
- 6) Relativistic Quantum Chemistry: The MOLFDIR program package, L. Visscher, W.A. de Jong, O. Visser, P.J.C. Aerts, H. Merenga and W.C. Nieuwpoort, in *METECC-95*, E. Clementi and G. Corongiu, (STEF, Cagliari, 1995)
- 7) L. Fox, *An Introduction to Numerical Linear Algebra*, Clarendon Press, Oxford, 1979
- 8) T. P. Hamilton and P. Pulay, *J. Chem. Phys.* **84**(10) 5728 (1986)
- 9) G. B. Bacskay, *Chem. Phys.* **65** 383 (1982)
- 10) Thomas R. Cundari and Walter J. Stevens, *J. Chem. Phys.* **98** 5555 (1993)
- 11) B. Henderson and G.F. Imbusch, *Optical Spectroscopy of Inorganic Solids*, Clarendon Press, Oxford, 1989
- 12) A.H. Harker, *HADES II/PC: The Harwell Automatic Defect Evaluation System for Personal Computers*, (Harwell: Publication Office), (1989)
- 13) R. Pandey and J.M. Vail, *J. Phys.: Cond. Matter*, **1** 2801 (1989)
- 14) C. Pisani, R. Dovesi and P. Ugliengo, *Phys. Stat. Sol. (b)*, **116** 249 (1983)
- 15) C. Pisani, R. Dovesi and P. Ugliengo, *Phys. Stat. Sol. (b)*, **116** 547 (1983)
- 16) N.Yu. Kirikova, V.E. Klimenko and V.N. Makhov, in *Proceedings of the International Conference on Inorganic Scintillators and their Applications*, eds. P. Dorenbos and C.W.E. van Eijk, p196, Delft University Press, Delft, 1996
- 17) A.E. Nosenko, V.N. Shevchuk and A.S. Voloshinovskii, in *Proceedings of the International Conference on Inorganic Scintillators and their Applications*, eds. P. Dorenbos and C.W.E. van Eijk, p220, Delft University Press, Delft, 1996
- 18) B.C. Grabmaier, W. Rossner and T. Berthold, in *Proceedings of the International Conference on Inorganic Scintillators and their Applications*, eds. P. Dorenbos and C.W.E. van Eijk, p29, Delft University Press, Delft, 1996
- 19) R. Deych, J. Dobbs, S. Marcovici and B. Tuval, in *Proceedings of the International Conference on Inorganic Scintillators and their Applications*, eds. P. Dorenbos and C.W.E. van Eijk, p36, Delft University Press, Delft, 1996
- 20) D. Bouttet, C. Dujardin, C. Pedrini, W. Brunat, D. Tran Minh Duc and J.Y. Gesland, in *Proceedings of the International Conference on Inorganic Scintillators and their Applications*, eds. P. Dorenbos and C.W.E. van Eijk, p111, Delft University Press, Delft, 1996
- 21) J.W.M. Verweij, C. Madej, H.L. Lautesse, C. Pedrini, B. Moine, M.Th. Cohen-Adad and G. Boulon, in *Proceedings of the International Conference on Inorganic Scintillators and their Applications*, eds. P. Dorenbos and C.W.E. van Eijk, p332, Delft University Press, Delft, 1996
- 22) P. Dorenbos, J.T.M. de Haas, C.W.E. van Eijk, N.N. Ryskin, E.V. Zharikov and A.A. Kiryukhin, in *Proceedings of the International Conference on Inorganic Scintillators and their Applications*, eds. P. Dorenbos and C.W.E. van Eijk, p365, Delft University Press, Delft, 1996

- 23) A. Szabo and N.S. Ostlund, Modern Quantum Chemistry, McGraw-Hill Publishing Company, New York (1982)
- 24) P.A. Rodnyi, P. Dorenbos and C.W.E. van Eijk, Phys. Stat. Sol. (b), **187** 15 (1995)
- 25) M. Marsman, P. Dorenbos and C.W.E. van Eijk, in Proceedings of the International Conference on Inorganic Scintillators and their Applications, eds. P. Dorenbos and C.W.E. van Eijk, p156, Delft University Press, Delft, 1996

Appendix A

Gaussian Basis Sets

Lithium

The lithium basis set used in chapter 5 for the LiBaF₄:Ce calculations is a segmented contracted basis. The contraction scheme is (6111). The exponents and coefficients are:

S	
583.677850000	0.002421600
87.465763000	0.018366000
19.979867000	0.086292500
5.628597600	0.265102600
1.766619500	0.478960200
0.585672430	0.308176600
0.736603380	-0.093630600
0.067051490	0.638230900
0.025710550	0.430382000

Cerium

The small basis set for Ce used in the non-relativistic calculations is a segmented contracted basis. The contraction scheme is (4322/4211/4211). The exponents and coefficients are:

s		p		d	
50563.078	0.0166001	2383.3398	0.0244934	297.66639	0.0380686
7624.1048	0.1166973	563.10164	0.1653555	87.399204	0.2197978
1734.6306	0.4306567	177.92475	0.4919077	31.380124	0.5264647
469.78702	0.5665720	62.635045	0.4769569	11.655706	0.4193660
700.94718	-0.1147211	27.047588	0.4739006	6.1047986	0.4958934
81.168677	0.6594528	10.797621	0.5867927	1.9558493	0.6259546
35.782997	0.4120855	4.4186707	0.5455808	0.35808	1.0000000
69.370368	0.2784065	1.8164039	0.5122086	0.14538	1.0000000
11.019743	-1.1323360	0.60472662	0.5634847		
13.119354	-0.3183287	0.22177225	0.5086430		
2.1795111	1.1521180				
2.5787978	-0.2682437				
0.33572966	1.1098845				
0.01149362	0.1584908				
0.03414466	0.8674480				

Appendix A.

The large basis set used for the non-relativistic calculations on CeF_3 is a generalised contracted basis (6/5/4). The segmented contracted version of this basis set has a contraction scheme (711111111111/41111111111/41111111). The exponents are:

s	p	d
7121549.6222689068	38721.5360558228	1881.4802231306
1066836.1110528151	9169.5926880411	567.9298975953
242815.0662528069	2975.8382621897	220.9456384930
68769.7728121559	1136.0392121282	96.9760903732
22430.1944243533	480.6783928634	45.6584543843
8095.3566097776	218.0917793407	22.2334898107
3156.6754216478	103.8749530994	11.0803429985
1309.7724035093	50.9471758500	5.4179508602
573.1901039615	24.4990532035	2.6010416880
262.2100204373	12.2351243729	1.2009713087
105.1504232151	5.8450607328	0.4455424946
48.3504035463	2.8737810094	0.1673383013
18.8411250551	1.3823894037	
9.8329036622	0.5900448634	
3.7822495042	0.2527148523	
1.9392878691		
0.5628688437		
0.2732791999		

The optimised Ce basis set used for the calculations on $\text{La}_2\text{Hf}_2\text{O}_7\text{:Ce}$ is a (18/15/12) primitive basis generalised contracted to (6/5/4). The exponents are:

s	p	d
7121549.6222689068	38721.5360558228	1881.4802231306
1066836.1110528151	9169.5926880411	567.9298975953
242815.0662528069	2975.8382621897	220.9456384930
68769.7728121559	1136.0392121282	96.9760903732
22430.1944243533	480.6783928634	45.6584543843
8095.3566097776	218.0917793407	22.2334898107
3156.6754216478	103.8749530994	11.0803429985
1309.7724035093	50.9471758500	5.4179508602
573.1901039615	24.4990532035	2.6010416880
262.2100204373	12.2351243729	1.2009713087
105.1504232151	5.8450607328	0.4455424946
48.3504035463	2.8737810094	0.1673383013
18.8411250551	1.3823894037	
9.8329036622	0.5900448634	
3.7822495042	0.2527148523	
1.9392878691		
0.5628688437		
0.2732791999		

For the relativistic calculations on Ce complexes we have two generalised contracted basis sets: One for the 4f states of Ce and one for the 5d states of Ce.

The basis set for the Ce 4f state is a (6/9/6/2//10/15/14/9/3) basis:

The large component:

s	p	d	f
7122983.0136677921	36650.1839543551	1264.9795101488	97.5207000582
1067016.0452476069	8681.8700585044	534.6226345412	47.4547875705
242845.4536522813	2817.9811327393	232.0759812242	22.7512931226
68769.1073868605	1075.5062283196	100.2148787853	11.2932647708
22416.9110784454	454.6457571109	45.7843185941	5.3962322067
8067.5148966666	205.7345225768	21.5187619008	2.5798454384
3115.7246632465	97.5207000582	10.3177504293	1.2105858409
1264.9795101488	47.4547875705	4.7560161167	0.5009954029
534.6226345412	22.7512931226	2.1478653846	
232.0759812242	11.2932647708	0.8951611900	
100.2148787853	5.3962322067	0.3580800000	
45.7843185941	2.5798454384	0.1453800000	
21.5187619008	1.2105858409		
10.3177504293	0.5009954029		
4.7560161167	0.2175075105		
2.1478653846			
0.8951611900			
0.3331657429			

The small component:

s	p	d	f
36650.1839543551	7122983.0136677921	36650.1839543551	1264.9795101488
8681.8700585044	1067016.0452476069	8681.8700585044	534.6226345412
2817.9811327393	242845.4536522813	2817.9811327393	232.0759812242
1075.5062283196	68769.1073868605	1075.5062283196	100.2148787853
454.6457571109	22416.9110784454	454.6457571109	45.7843185941
205.7345225768	8067.5148966666	205.7345225768	21.5187619008
97.5207000582	3115.7246632465	97.5207000582	10.3177504293
47.4547875705	1264.9795101488	47.4547875705	4.7560161167
22.7512931226	534.6226345412	22.7512931226	2.1478653846
11.2932647708	232.0759812242	11.2932647708	0.8951611900
5.3962322067	100.2148787853	5.3962322067	0.3580800000
2.5798454384	45.7843185941	2.5798454384	0.1453800000
1.2105858409	21.5187619008	1.2105858409	
0.5009954029	10.3177504293	0.5009954029	
0.2175075105	4.7560161167	0.2175075105	
	2.1478653846		
	0.8951611900		
	0.3331657429		
	4.7560161167		
	0.3580800000		
	0.1453800000		
g			
97.5207000582			
47.4547875705			
22.7512931226			
11.2932647708			
5.3962322067			
2.5798454384			
1.2105858409			
0.5009954029			

Appendix A.

The basis set for the Ce 5d state is a (6/9/7//10/17/12/11) basis:

The large component:

s	p	d
7122983.0136677921	36650.1839543551	1264.9795101488
1067016.0452476069	8681.8700585044	534.6226345412
242845.4536522813	2817.9811327393	232.0759812242
68769.1073868605	1075.5062283196	100.2148787853
22416.9110784454	454.6457571109	45.7843185941
8067.5148966666	205.7345225768	21.5187619008
3115.7246632465	97.5207000582	10.3177504293
1264.9795101488	47.4547875705	4.7560161167
534.6226345412	22.7512931226	2.1478653846
232.0759812242	11.2932647708	0.8951611900
100.2148787853	5.3962322067	0.3580800000
45.7843185941	2.5798454384	0.1453800000
21.5187619008	1.2105858409	
10.3177504293	0.5009954029	
4.7560161167	0.2175075105	
2.1478653846		
0.8951611900		
0.3331657429		

The small component:

s	p	d	f
36650.1839543551	7122983.0136677921	36650.1839543551	1264.9795101488
8681.8700585044	1067016.0452476069	8681.8700585044	534.6226345412
2817.9811327393	242845.4536522813	2817.9811327393	232.0759812242
1075.5062283196	68769.1073868605	1075.5062283196	100.2148787853
454.6457571109	22416.9110784454	454.6457571109	45.7843185941
205.7345225768	8067.5148966666	205.7345225768	21.5187619008
97.5207000582	3115.7246632465	97.5207000582	10.3177504293
47.4547875705	1264.9795101488	47.4547875705	4.7560161167
22.7512931226	534.6226345412	22.7512931226	2.1478653846
11.2932647708	232.0759812242	11.2932647708	0.8951611900
5.3962322067	100.2148787853	5.3962322067	0.3580800000
2.5798454384	45.7843185941	2.5798454384	0.1453800000
1.2105858409	21.5187619008	1.2105858409	
0.5009954029	10.3177504293	0.5009954029	
0.2175075105	4.3177504293	0.2175075105	
	2.1478653846		
	0.8951611900		
	0.3331657429		
	4.7560161167		
	0.3580800000		
	0.1453800000		

Cobalt

The basis set used for the Co^{4+} calculations of chapter 3 was an uncontracted basis set with exponents:

The large component:

s	p	d
62215.5696176057	2353.5348831193	73.0866923680
9345.2500769493	557.7055230741	15.2920582492
2129.2831188329	179.5246950185	4.0752719620
604.5224630384	67.3635830398	1.0963960884
199.2452332807	27.4529129592	
4.4780198649	11.7137001716	
73.0866923680	4.7992484093	
15.2920582492	2.0131290829	
4.0752719620	0.8103996276	
1.0963960884		

The small component:

s	p	d	f
2353.5348831193	62215.5696176057	2353.5348831193	73.0866923680
557.7055230741	9345.2500769493	557.7055230741	15.2920582492
179.5246950185	2129.2831188329	179.5246950185	4.0752719620
67.3635830398	604.5224630384	67.3635830398	1.0963960884
27.4529129592	199.2452332807	27.4529129592	
11.7137001716	4.4780198649	11.7137001716	
4.7992484093	73.0866923680	4.7992484093	
2.0131290829	15.2920582492	2.0131290829	
0.8103996276	4.0752719620	0.8103996276	
	1.0963960884		

The Co basis used for the CoF_6^{2-} calculations was a generalised contracted basis (5/5/3//6/9/8/5):

The large component:

s	p	d
1084972.4046765571	2344.7803037885	84.1211960383
162536.2440878314	555.6471279394	25.1128634902
36991.6657512951	178.8630683156	9.1834004938
10477.4164326834	67.1082326484	3.7092623217
3418.4052294473	27.3476842044	1.4923545649
1234.4886328448	11.6614995468	0.5677846809
481.3642010999	4.7724007891	
198.7287460788	1.9906731303	
20.7965155176	0.7986484906	
0.3605114786		
84.1211960383		
25.1128634902		
9.1834004938		
3.7092623217		
1.4923545649		
0.5677846809		

Appendix A.

The small component:

s	p	d	f
2344.7803037885	1084972.4046765571	2344.7803037885	84.1211960383
555.6471279394	162536.2440878314	555.6471279394	25.1128634902
178.8630683156	36991.6657512951	178.8630683156	9.1834004938
67.1082326484	10477.4164326834	67.1082326484	3.7092623217
27.3476842044	3418.4052294473	27.3476842044	1.4923545649
11.6614995468	1234.4886328448	11.6614995468	0.5677846809
4.7724007891	481.3642010999	4.7724007891	
1.9906731303	198.7287460788	1.9906731303	
0.7986484906	20.7965155176	0.7986484906	
	0.3605114786		
	84.1211960383		
	25.1128634902		
	9.1834004938		
	3.7092623217		
	1.4923545649		
	0.5677846809		

Fluorine

The small basis used for the non-relativistic CeF_3 calculations is a segmented contracted basis. The contraction scheme is (43/6)::

s		p	
1040.6625	0.0192338	51.500717	0.013513
156.68433	0.1333205	10.482701	0.093476
35.119879	0.4609976	3.01404	0.283429
9.2932511	0.5266653	0.96196	0.423782
13.989198	-0.0797469	0.30107	0.360588
1.1622875	0.5838995	0.08567	0.148650
0.32317710	0.5075939		

The large basis set used in the non-relativistic calculations on CeF_3 is a generalised contracted basis set: contraction (3/3). The segmented contracted version of this basis has a contraction scheme (41111111/3111). The exponents are:

s	p
39243.7115248981	70.2683391067
5882.4388067934	16.2059373641
1338.8040554062	4.9233191247
379.0446309700	1.6536950565
123.4595333588	0.5344070759
44.2793910224	0.1702177393
16.9803544817	
6.7201653343	
1.8657300048	
0.7051905664	
0.2490032869	

The basis set for F used in the CoF_6^{2-} calculations is a generalised contracted basis set (3/2//3/4/4):

The large component:

s	p
18648.5000000000	63.1253000000
2790.7700000000	14.5012000000
633.2580000000	4.3823300000
178.5990000000	1.4535500000
57.7896000000	0.4632370000
20.4555000000	0.1265780000
7.5879600000	
1.9921300000	
0.7498540000	
0.2418450000	

The small component:

s	p	d
63.1253000000	18648.5000000000	63.1253000000
14.5012000000	2790.7700000000	14.5012000000
4.3823300000	633.2580000000	4.3823300000
1.4535500000	178.5990000000	1.4535500000
0.4632370000	57.7896000000	0.4632370000
0.1265780000	20.4555000000	0.1265780000
	7.5879600000	
	1.9921300000	
	0.7498540000	
	0.2418450000	

Hydrogen

The hydrogen basis set used for the SiH_4 calculations of chapter 3 is given by:

Large component (only s). Contraction scheme (411):

79.99016053	0.00625958
11.96435285	0.04808010
2.72256964	0.23531523
0.77282765	0.78728941
0.25176829	1.00000000
0.08842324	1.00000000

Small component (only p). Contraction scheme (11111):

79.99016053	0.00625958
11.96435285	0.04808010
2.72256964	0.23531523
0.77282765	0.78728941
0.25176829	1.00000000
0.08842324	1.00000000

The hydrogen basis used for LSO geometry optimisation in chapter 6 is a segmented contracted basis. The contraction scheme is (31). The s exponents and coefficients are:

13.0077	0.0334946
1.96208	0.234727
0.444529	0.813757
0.121949	1.00000

Appendix A.

Lanthanum

The small basis for the non-relativistic calculations is a segmented contracted basis. The contraction scheme is (4322211/42211/411):

s		p		d	
48846.811	0.0165911	2295.9512	0.0245181	284.32638	0.0383258
7365.8806	0.1166332	542.48305	0.1655263	83.404867	0.2205760
1675.5336	0.4306097	171.19443	0.4924502	29.88067	0.526605
453.55232	0.5667209	60.188384	0.4765061	11.067873	0.4192390
677.09644	-0.1144920	25.926240	0.4733901	5.7627901	0.4944886
78.087338	0.6617722	10.320874	0.5876312	1.8441223	0.6274833
34.316216	0.4097463	4.1960854	0.5434560		
66.862944	-0.2765479	1.7284006	0.5141018		
10.54276	1.1308920	0.578104959	0.5750222		
12.493048	-0.3177556	0.21024956	0.4963662		
2.0741487	1.1518320				
2.4094278	-0.2825104				
0.32338676	1.1171017				
0.03249189	0.8897142				
0.01110070	0.1319676				

Oxygen

The oxygen basis used in the $\text{La}_2\text{Hf}_2\text{O}_7$ calculations was a generalised contracted basis (3/3):

s	p
30981.0743119833	58.9814848490
4643.8494004933	13.6047228266
1056.8887521234	4.1423308854
299.2076357282	1.4319091422
97.4257362706	0.4508167866
34.9007528983	0.1258026030
13.3443281743	
5.2577055221	
1.4794939557	
0.4997855928	
0.1874811510	

The small basis set used for the non-relativistic calculations is a segmented contracted basis. The contraction scheme is (721/511):

s		p	
10334.736	0.0008449	117.21023	0.0022198
1500.3950	0.0067550	26.967137	0.0172064
337.95497	0.0343071	8.3338649	0.0750846
96.051304	0.1250896	2.9811654	0.2122762
31.613952	0.3167742	1.1284031	0.3725583
11.423798	0.4533328	0.42167369	0.3985842
4.3012501	0.2144500	0.15059051	0.1832060
10.195221	-0.0837570		
0.93361357	0.5751097		
0.2853772	0.5103155		

The exponents of the oxygen basis for the relativistic calculations are given by:

The large component:

s	p
14362.1300000000	47.5925000000
2154.8458000000	10.8657000000
490.3337000000	3.2595000000
138.5686000000	1.0756000000
44.8513000000	0.3412000000
15.8495000000	0.0927000000
5.8637000000	
1.4900000000	
0.5612000000	
0.1813000000	

The small component:

s	p	d
47.5925000000	14362.1300000000	47.5925000000
10.8657000000	2154.8458000000	10.8657000000
3.2595000000	490.3337000000	3.2595000000
1.0756000000	138.5686000000	1.0756000000
0.3412000000	44.8513000000	0.3412000000
0.0927000000	15.8495000000	0.0927000000
	5.8637000000	
	1.4900000000	
	0.5612000000	
	0.1813000000	

Silicon

The basis set used for the calculations on SiH₄:

The large component (411111111/311111):

s		p	
79939.68000000	0.00026600	312.67640000	0.00399403
11984.04000000	0.00206200	73.63921000	0.03038483
2727.77100000	0.01068300	23.21085000	0.12913868
772.52970000	0.04313300	8.38255100	1.00000000
251.92260000	1.00000000	3.17439900	1.00000000
90.79819000	1.00000000	1.21318400	1.00000000
35.38782000	1.00000000	0.29112340	1.00000000
14.51901000	1.00000000	0.08185835	1.00000000
4.05572300	1.00000000		
1.48263400	1.00000000		
0.25209220	1.00000000		
0.09239991	1.00000000		

Appendix A.

The small component (uncontracted):

s	p	d
312.67640000	79939.68000000	312.67640000
73.63921000	11984.04000000	73.63921000
23.21085000	2727.77100000	23.21085000
8.38255100	772.52970000	8.38255100
3.17439900	251.92260000	3.17439900
1.21318400	90.79819000	1.21318400
0.29112340	35.38782000	0.29112340
0.08185835	14.51901000	0.08185835
	4.05572300	
	1.48263400	
	0.25209220	
	0.09239991	

The small silicon basis set used for the LSO calculations has a contraction scheme (5321/5111). The exponents and coefficients are:

s		p	
6786.309800000	0.005756800	164.197020000	0.011682300
1016.116600000	0.043234100	38.016534000	0.081133000
231.120870000	0.190615800	11.643929000	0.283100800
64.952409000	0.481376800	3.918351900	0.501019700
19.979195000	0.422399400	1.331111500	0.335466100
34.660741000	-0.094264800	0.059495550	0.315862000
3.578301500	0.581338500	0.450291010	0.259818300
1.313344100	0.493979600	0.163855210	0.555270400
1.747735700	-0.163132800		
0.231076670	0.664368500		
0.084704400	0.440739600		

Strontium

The small basis set used for the calculations on SrCl_2 is a segmented contracted basis set. The contraction scheme is (4332111/4321/31). The basis is given by:

s		p		d	
21296.967	0.0168869	932.62089	0.0263411	82.058787	0.0540576
3209.8256	0.1186841	219.09499	0.1740745	23.102868	0.2701788
727.91698	0.4354442	68.182401	0.5004686	7.6585784	0.5355593
196.09818	0.5610052	23.397862	0.4654344	2.4975601	0.3939006
293.22238	-0.1113119	10.702446	0.3339042		
33.290922	0.6447398	4.3530597	0.5649084		
14.124638	0.4276644	1.8377163	0.1984297		
25.870075	-0.2475516	0.94147585	0.4359256		
4.4541813	0.7651154	0.38674626	0.5360821		
1.9740548	0.3740287	0.16315313	0.1154534		
3.1023461	-0.2780315				
0.61550194	0.7270601				
0.27245235	0.4354796				
0.03	1.0000000				
0.01	1.0000000				

Appendix B

Expressions for the Second Derivative of the Total Energy

In section 3.3 expressions were derived for the second derivative of the total energy with respect to the quantity \mathbf{X} . In that section only the real components of the derivative were given. For the sake of completeness we give here also the imaginary components of the second derivative:

$$E''_{ai,bj} = -2 \operatorname{Re}(F_{ab}^C) \delta_{ij} + 2 \operatorname{Re}(F_{ij}^C) \delta_{ab} + 2 \left\{ 2 (\operatorname{Im}(ai) \parallel \operatorname{Im}(bj)) - \operatorname{Re}((ib \parallel ja) - (ij \parallel ba)) \right\} \quad 1$$

$$E''_{ai,bp} = \left\{ (1-f) \cdot \operatorname{Re}(F_{ip}^W) + 2f \cdot \operatorname{Re}(F_{ip}^O) \right\} \delta_{ab} + 2f \cdot \left\{ 2 (\operatorname{Im}(ai) \parallel \operatorname{Im}(bp)) - \operatorname{Re}((ib \parallel pa) - (ip \parallel ba)) \right\} \quad 2$$

$$E''_{ai,pj} = - \left\{ 2(1-f) \cdot \operatorname{Re}(F_{ap}^W) + f \cdot \operatorname{Re}(F_{ap}^O) \right\} \delta_{ij} + 2(1-f) \cdot \left\{ 2 (\operatorname{Im}(ai) \parallel \operatorname{Im}(pj)) - \operatorname{Re}((ip \parallel ja) - (ij \parallel pa)) \right\} \quad 3$$

$$E''_{ap,bq} = -2f \cdot \operatorname{Re}(F_{ab}^O) \delta_{pq} + 2f \cdot \operatorname{Re}(F_{pq}^O) \delta_{ab} + 2af^2 \cdot \left\{ 2 (\operatorname{Im}(ap) \parallel \operatorname{Im}(bq)) - \operatorname{Re}((pb \parallel qa) - (qp \parallel ab)) \right\} \quad 4$$

$$E''_{ap,qi} = \left\{ (1-f) \cdot \operatorname{Re}(F_{ai}^W) - f \cdot \operatorname{Re}(F_{ai}^O) \right\} \delta_{pq} + 2f(1-af) \cdot \left\{ 2 (\operatorname{Im}(ap) \parallel \operatorname{Im}(qi)) - \operatorname{Re}((pq \parallel ia) - (ip \parallel aq)) \right\} \quad 5$$

$$E_{pi,qj}^{I,I} = -2(1-f) \cdot \text{Re}(F_{pq}^W) \delta_{ij} + 2(1-f) \cdot \text{Re}(F_{ij}^W) \delta_{pq} + 2(1-2f+af^2) \cdot \{2(\text{Im}(pi)\|\text{Im}(qj)) - \text{Re}((qi\|pj) - (ji\|pq))\} \quad 6$$

$$E_{ai,bj}^{R,I} = 2 \text{Im}(F_{ab}^C) \delta_{ij} + 2 \text{Im}(F_{ij}^C) \delta_{ab} + 2\{2(\text{Re}(ai)\|\text{Im}(jb)) - \text{Im}((ib\|ja) + (ji\|ab))\} \quad 7$$

$$E_{ai,bp}^{R,I} = \{(1-f) \cdot \text{Im}(F_{ip}^W) + 2f \cdot \text{Im}(F_{ip}^O)\} \delta_{ab} + 2f \cdot \{2(\text{Re}(ai)\|\text{Im}(pb)) - \text{Im}((ib\|pa) + (pi\|ab))\} \quad 8$$

$$E_{ai,pj}^{R,I} = \{2(1-f) \cdot \text{Im}(F_{ap}^W) + f \cdot \text{Im}(F_{ap}^O)\} \delta_{ij} + 2(1-f) \cdot \{2(\text{Re}(ai)\|\text{Im}(jp)) - \text{Im}((ip\|ja) + (ji\|ap))\} \quad 9$$

$$E_{ap,bq}^{R,I} = 2f \cdot \text{Im}(F_{ab}^O) \delta_{pq} + 2f \cdot \text{Im}(F_{pq}^O) \delta_{ab} + 2af^2 \cdot \{2(\text{Re}(ap)\|\text{Im}(qb)) - \text{Im}((pb\|qa) + (qp\|ab))\} \quad 10$$

$$E_{ap,qi}^{R,I} = -\{(1-f) \cdot \text{Im}(F_{ai}^W) - f \cdot \text{Im}(F_{ai}^O)\} \delta_{pq} + 2f(1-af) \cdot \{2(\text{Re}(ap)\|\text{Im}(iq)) - \text{Im}((qp\|ai) + (pi\|qa))\} \quad 11$$

$$E_{pi,qj}^{R,I} = 2(1-f) \cdot \text{Im}(F_{pq}^W) \delta_{ij} + 2(1-f) \cdot \text{Im}(F_{ij}^W) \delta_{pq} + 2(1-2f+af^2) \cdot \{2(\text{Re}(pi)\|\text{Im}(jq)) - \text{Im}((iq\|jp) + (ji\|pq))\} \quad 12$$

$$E_{bj,ai}^{I,R} = E_{ai,bj}^{R,I} \text{ etc.} \quad 13$$

Samenvatting

Elektronische Structuurberekeningen aan Cerium-Houdende Kristallen

Detectoren voor straling worden in onze samenleving steeds meer gebruikt. In het dagelijkse leven worden detectoren voor infrarood licht gebruikt in inbraak-alarmen, afstandsbedieningen en diverse draadloze apparaten. Detectoren voor zichtbaar licht worden gebruikt in videocameras en elektronische afbeeldings-systemen. In de industrie worden detectoren voor gamma-straling en röntgenstraling gebruikt voor proces-controle en voor de analyse van produkten en monsters. In de medische wereld worden detectoren voor gamma-straling en röntgenstraling gebruikt voor zogenaamde tracing technieken en voor afbeeldings-systemen. In de hoge-energie fysica worden detectoren voor alle mogelijke soorten straling gebruikt voor de analyse van de produkten van botsingsexperimenten met behulp van elementaire deeltjes.

Er zijn verschillende manieren om straling te detecteren, enigszins afhankelijk van de soort straling die gedetecteerd dient te worden. De detectie van zogenaamde harde gamma- en röntgenstraling wordt voornamelijk gedaan met behulp van scintillatoren.

Scintillatoren zijn materialen die licht uitzenden als ze worden geraakt door ioniserende straling. Het uitgezonden licht kan vervolgens worden gedetecteerd met behulp van een photomultiplicatorbuis of een fotodiode.

De eisen die worden gesteld aan een detector kunnen per toepassing sterk verschillen. Als gevolg daarvan zullen de eisen die worden gesteld aan de scintillator ook sterk per toepassing verschillen. Mede hierdoor wordt er steeds gezocht naar nieuwe scintillatoren, in de hoop dat voor iedere mogelijke toepassing steeds betere scintillatoren beschikbaar komen. Een grondig theoretisch begrip van de werking van scintillatoren zou deze zoektocht enorm helpen.

De werking van een scintillator is nogal ingewikkeld. We kunnen echter drie verschillende stadia onderscheiden in het scintillatieproces:

- i) Het ontstaan van elektron-gat paren door de interactie van de ioniserende straling met het kristal.

- ii) De migratie van deze vrije elektronen en gaten door het kristal.
- iii) De recombinatie van een elektron en een gat op een luminocentrie centrum in het kristal, onder uitzending van licht.

In dit proefschrift bestuderen wij het derde stadium van het scintillatieproces. Wij kijken verder uitsluitend naar ionogene materialen die cerium bevatten. In deze materialen treedt cerium doorgaans op als luminocentrie centrum. Het cerium ion vangt een elektron en een gat in en wordt daardoor in een aangeslagen toestand gebracht. Het vervalt vervolgens via een elektrische dipool overgang, onder uitzending van een foton.

Het cerium ion vervalt van een $Ce^{3+} 5d)^1$ toestand naar een $Ce^{3+} 4f)^1$ toestand. Verder wordt aangenomen dat de positie van het Ce 4f niveau ten opzichte van de valentieband en de positie van de Ce 5d niveaus ten opzichte van de geleidingsband bepalen hoe efficiënt cerium in staat is een gat of een elektron in te vangen.

Het werk beschreven in dit proefschrift is erop gericht de posities van de Ce 4f en 5d niveaus ten opzichte van de valentieband uit te rekenen.

We beschrijven het systeem met een cluster van ionen, ingebed in een verzameling puntladingen, die de Madelung-potentiaal emuleren.

Omdat cerium een tamelijk zwaar atoom is, verwachten wij dat relativistische effecten belangrijk zijn. De berekeningen zouden dan ook bij voorkeur dienen te worden uitgevoerd binnen een relativistisch rekenmodel. In de vakgroep Theoretische Chemie van de Rijksuniversiteit Groningen is een programmapakket ontwikkeld met de naam MOLFDIR. Dit pakket is in staat relativistisch correcte Hartree-Fock-Dirac berekeningen te doen aan willekeurige moleculen. Omdat onze clusters vrij groot zijn en een vrij lage puntgroep symmetrie hebben, was het beslag dat het MOLFDIR pakket legde op de beschikbare computerfaciliteiten dermate groot dat de berekeningen vaak onmogelijk waren. We hebben toen besloten om het MOLFDIR pakket efficiënter te maken.

Optimalisatie van het MOLFDIR Pakket

We hebben een aantal convergentieversnellers geïmplementeerd in het SCF gedeelte van het MOLFDIR pakket: Dempnen op de dichtheid, Aitken extrapolatie, Pople's extrapolatie, DIIS en een gedeeltelijke implementatie van de QCSCF methode. De testen die uitgevoerd werden met deze methodes laten zien dat 'dempnen op de dichtheid' om een initiële convergentie van ten minste 10^{-2} op de dichtheid te bereiken, gevolgd door de DIIS methode bijna altijd superieure resultaten geeft. De convergentie was in alle gevallen minimaal drie maal zo snel als die van het oorspronkelijke programma, terwijl de overhead van de DIIS procedure

minimaal was. De andere convergentieversnellers hadden allemaal wel systemen waarvoor ze het goed deden, maar ze waren minder betrouwbaar en deden het gemiddeld aanzienlijk minder goed dan de DIIS procedure.

Het tweede dat we hebben gedaan om het MOLFDIR pakket efficiënter te maken, is onderzoeken of we een nog beter gebruik konden maken van symmetrie. Dit blijkt inderdaad te kunnen, maar levert niet zoveel besparingen op als we hadden gehoopt. Dit wordt veroorzaakt door het feit dat bij de dubbelgroepen met een oneven hoofdas de matrix-representaties voor de irreduceerbare representaties niet zo kunnen worden gedefinieerd dat alle integralen reëel blijven. De implementatie van het nieuwe integralen schema is nog niet af.

Resultaten van de Berekeningen

Na deze optimalisaties hebben we aantal fluorides, oxides en chlorides onderzocht. Voor deze onderzoeken hebben we een combinatie gebruikt van niet-relativistische berekeningen, waarbij, in een aantal gevallen, de binnen-elektronen van de ionen werd beschreven door effectieve potentialen, waarin relativistische effecten zijn verwerkt, en relativistische berekeningen.

De resultaten van deze berekeningen laten duidelijk zien dat de volledig relativistische Hartree-Fock-Dirac berekeningen het beste zijn wat we op dit moment kunnen doen. Dit is vooral zichtbaar in de berekende positie van het Ce 4f niveau, en dus ook in de berekende Ce 4f - 5d overgangsenergie. De opsplitsing van de Ce 5d niveaus blijkt slechts marginaal te worden beïnvloed door relativistische effecten en wordt dus al goed beschreven door de niet-relativistische Hartree-Fock methode.

Hartree-Fock-Dirac berekeningen zijn echter niet altijd mogelijk, vanwege het enorme beslag dat ze leggen op de computerfaciliteiten. Het enige realistische alternatief dat we dan tot onze beschikking hebben is het doen van een niet-relativistische Hartree-Fock berekening, waarbij we de binnen-elektronen van de ionen beschrijven met een effectieve potentiaal, waarin de relativistische effecten voor de binnen-elektronen zijn verwerkt. Deze berekeningen geven veel betere resultaten dan "pure" niet-relativistische Hartree-Fock berekeningen, maar schieten toch nog te kort ten opzichte van de Hartree-Fock-Dirac berekeningen. Voor het vrije Ce³⁺ ion maken we met de effectieve potentialen een fout van 0,9 eV in de positie van het 4f niveau.

De Fluorides

De berekeningen aan de fluorides laten goede resultaten zien.

Voor CeF_3 kunnen we de Ce 5d opsplitsing goed uitrekenen. De resultaten voor de VB - Ce 4f afstand en de Ce 4f - 5d afstand zijn iets minder nauwkeurig, vanwege de fout die we maken door het gebruik van de effectieve potentialen. Toch is voor alle resultaten de fout ten opzichte van het experiment kleiner dan 0,4 eV.

In $\text{LiBaF}_3\text{:Ce}$ verwachten we grote roosterrelaxaties na het dopen met cerium. Door een geschikte clusterkeuze kunnen we deze relaxatie uitrekenen. De daaruit voortkomende Ce 5d opsplitsing stemt goed overeen met de experimentele resultaten. Daaruit kunnen we de conclusie trekken dat onze voorspelling voor de roosterrelaxatie ook correct is.

De resultaten voor $\text{LiLuF}_4\text{:Ce}$ zijn redelijk. Ook in dit materiaal verwachten wij grote roosterrelaxaties na het dopen met cerium. Afgaande op de experimentele resultaten wordt de originele S_4 puntgroep symmetrie van de cerium positie door de roosterrelaxatie (of door een Jahn-Teller vervorming) verbroken. Een betrouwbare geometrie-optimalisatie, zonder symmetriestructies is op dit moment niet haalbaar, dus we waren niet in staat om een correct Ce 5d spectrum uit te rekenen. We konden echter wel de totale opsplitsing correct uitrekenen door gebruik te maken van een geometrie-optimalisatie die de S_4 symmetrie intact liet.

De Chlorides

De resultaten voor de chlorides zijn wat minder goed dan die voor de fluorides. Dit wordt veroorzaakt door de grote ionradius en de grote polariseerbaarheid van chloor. De resultaten zijn echter nog steeds redelijk.

Voor $\text{SrCl}_2\text{:Ce}$ zijn we in staat om een redelijke schatting te geven van de roosterrelaxatie ten gevolge van het dopen met cerium. De schatting werd gemaakt met behulp van het programma HADES. Gegeven de onzekerheden die aan deze HADES-berekeningen kleven, is de overeenstemming van de berekende Ce 5d opsplitsing met het experiment vrij goed. Voor de andere berekende observabelen, zoals de posities van de ceriumniveaus ten opzichte van de valentieband, zijn geen experimentele gegevens beschikbaar.

Voor CeCl_3 is er een goede overeenkomst tussen theorie en experiment voor de bandgap, de VB - Ce 4f afstand en voor de Ce 4f - 5d afstand. De fout in de berekende waarden is in alle gevallen kleiner dan 0,4 eV. Dit is een goed resultaat als bedacht wordt dat de berekeningen slechts semi-relativistisch waren. De Ce 5d opsplitsing in CeCl_3 blijft een probleem. De

berekende waarde is meer dan twee maal zo klein als de experimentele. Aangezien er wat twijfel bestaat ten aanzien van de correctheid van het experimentele absorptie-spectrum van CeCl_3 is het wenselijk dat er een tweede onafhankelijk absorptie of luminicentie-excitatie experiment voor CeCl_3 , of nog beter $\text{LaCl}_3:\text{Ce}$ wordt gedaan.

De Oxides

De berekeningen aan de oxides gaven serieuze problemen en de resultaten waren niet altijd bruikbaar. Door een goede doordachte keuze van de clusters en de basissets kunnen echter ook in dit geval redelijke resultaten worden verkregen. De problemen met de oxides worden voor een deel veroorzaakt door de noodzaak erg diffuse basissets te gebruiken om de O^{2-} ionen mee te kunnen beschrijven. Deze diffuse zuurstoffuncties reiken tot ver over de clusterrand in het gebied waar de puntladingen liggen, die de Madelung-potentiaal genereren. Hierdoor voelen deze diffuse functies een potentiaal en een veld, die sterk afwijken van de kristalpotentiaal en het kristalveld. Hierdoor ontstaan kunstmatig laag liggende zuurstofniveaus in de bandgap van het kristal. Deze laag liggende zuurstofniveaus hinderen het vinden van de Ce 5d niveaus en de bodem van de geleidingsband. Een andere oorzaak voor de problemen is gelegen in de, in het algemeen, lage symmetrie van de oxides en het feit dat cerium doorgaans een ion vervangt met een veel kleinere ionstraal.

Ondanks deze problemen waren we in staat om redelijk lijkende resultaten te vinden voor $\text{La}_2\text{Hf}_2\text{O}_7:\text{Ce}$. Het is nog niet mogelijk deze resultaten te vergelijken met het experiment.

$\text{LSO}:\text{Ce}$ is een zeer ingewikkeld materiaal vanwege zijn lage symmetrie. De lutetium posities hebben slechts C_1 puntgroep symmetrie. De observabelen van het zuivere gastmateriaal kunnen met een redelijke nauwkeurigheid worden berekend. De bandgap en de breedtes van de valentieband en de Lu 4f band komen redelijk overeen met de experimentele resultaten.

De berekeningen aan het systeem met de cerium onzuiverheid zijn minder nauwkeurig. Dit ligt voor een groot deel aan het feit dat we niet in staat waren een betrouwbare schatting te maken voor de roosterrelaxatie. Ondanks dat is de vergelijking tussen het berekende en het experimentele absorptiespectrum niet al te slecht. De fout in de berekende laagste Ce 4f \rightarrow 5d overgang is kleiner dan 0,4 eV (10%).

Onze volledig relativistische berekening aan kubisch CeAlO_3 laat zien dat de resultaten van berekeningen aan oxides net zo nauwkeurig kunnen zijn als die van berekeningen aan fluorides. Alle berekende waarden komen goed overeen met de experimentele waarden. De cerium positie in kubisch CeAlO_3 heeft een hoge puntgroep symmetrie (O_h) en de Ce - O

afstand is groot (2,65 Å). Als aan deze voorwaarden is voldaan kunnen we blijkbaar goede nauwkeurige resultaten behalen voor oxides.

De Hoofdconclusie

Concluderend kunnen we zeggen dat onze procedure om de posities van lokale ceriumniveaus ten opzichte van de valentieband uit te rekenen redelijk goede resultaten geeft. In veel gevallen waren we in staat om de niveaus te voorspellen met een fout kleiner dan 0,5 eV.

Onze clusters zijn vrij klein en slecht ingebed in het rooster. Dit kan tot problemen leiden. Voor clusters met een lage puntgroep symmetrie en zeer diffuse functies op de liganden zijn de problemen het grootst.

List of Publications

H. Merenga and J. Andriessen, Report on the applicability of traditional convergence accelerators in the MOLFDIR program package, NCF progress report, Stratech 92-02, May 1992.

H. Merenga and J. Andriessen, Progress Report on the Implementation of Convergence Enhancers in the MOLFDIR Program Package, NCF progress report, Stratech 92-06, Oct. 1992.

H. Merenga and J. Andriessen, Report on the Implementation of the Quadratic Convergent SCF Procedure in the MOLFDIR Package, NCF progress report, Stratech 93-10, May 1993.

H. Merenga and J. Andriessen, A New SCF Integral Program for the MOLFDIR Program Package, NCF progress report, Stratech 93-12, Aug. 1993.

H. Merenga and J. Andriessen, Optimisation of the one-electron integral program Relonel, Stratech 93-13, Oct. 1993.

H. Merenga and J. Andriessen, Report on the implementation of a new SCF integral program for the MOLFDIR package, NCF progress report, Stratech TUD-THER-94-01, May 1994.

J. Andriessen, H. Merenga, P. Dorenbos and C.W.E. van Eijk, Energy Levels of Cerium in YAP, YAG and LSO, in New Challenges in Computational Quantum Chemistry, R. Broer, P.J.C. Aerts and P.S. Bagus eds., p199, University of Groningen, 1994.

H. Merenga and J. Andriessen, Four-Component Hartree-Fock-Dirac Calculations with the MOLFDIR Program Package: The Challenge to Improve Efficiency, in New Challenges in Computational Quantum Chemistry, R. Broer, P.J.C. Aerts and P.S. Bagus eds., p249, University of Groningen, 1994.

L. Visscher, O. Visser, P.J.C. Aerts, H. Merenga and W.C. Nieuwpoort, Relativistic Quantum Chemistry: The MOLFDIR program package, Computer Physics Communications, **81**, 120, 1994.

H. Merenga, J. Andriessen and C.W.E. van Eijk, Positions of 4f and 5d Energy Levels of Ce^{3+} in the Band Gap of CeF_3 , YAG and LSO, in Record of the International Workshop Physical Processes in Fast Scintillators, PHYSCI 94, P.A. Rodnyi and C.W.E. van Eijk eds., p50, Stratech TUD-SCIR-94-04, Delft University of Technology, 1994.

H. Merenga, J. Andriessen and C.W.E. van Eijk, Positions of 4f and 5d Energy Levels of Ce^{3+} in the Band Gap of CeF_3 , YAG and LSO, Radiation Measurements, **24**, 343, 1995.

L. Visscher, W.A. de Jong, O. Visser, P.J.C. Aerts, H. Merenga and W.C. Nieuwpoort, Relativistic Quantum Chemistry: The MOLFDIR program package, in METECC-95, E. Clementi and G. Corongiu eds., STEF, Cagliari, 1995

J. Andriessen, A. Sobolev, A. Kuznetsov, H. Merenga, P. Dorenbos and C.W.E. van Eijk, Theoretical Investigation of the 4f and 5d Levels of Cerium in LSO, Studied with HF-LCAO and the Embedded Cluster Scattered Wave Method, in Proceedings of the International Conference on Inorganic Scintillators and Their Applications, P. Dorenbos and C.W.E. van Eijk eds., p130, Delft University of Technology, 1996.

H. Merenga, J. Andriessen and C.W.E. van Eijk, 4f and 5d Level Splitting of Ce^{3+} in $SrCl_2:Ce$, $CeCl_3$ and CeF_3 , in Proceedings of the International Conference on Inorganic Scintillators and Their Applications, P. Dorenbos and C.W.E. van Eijk eds., p138, Delft University of Technology, 1996.

J. Andriessen, H. Merenga, C.M. Combes, P. Dorenbos and C.W.E. van Eijk, Calculation of 4f and 5d Energy Levels of Cerium in $LiYF_4$ and $LiLuF_4$ and $LiBaF_3$, An Estimate of Local Distortion, in Proceedings of the International Conference on Inorganic Scintillators and Their Applications, P. Dorenbos and C.W.E. van Eijk eds., p142, Delft University of Technology, 1996.

Curriculum Vitae

De auteur werd geboren op vrijdag 6 april 1962 te Groningen. Van 1966 tot 1968 bezocht hij de kleuterschool. Van 1968 tot 1974 bezocht hij de basisschool. Van 1974 tot 1980 doorliep hij het OVWO op het Gereformeerd Lyceum/Havo te Groningen.

In 1980 begon de auteur zijn studie scheikunde aan de RUG. Op 19 mei 1983 haalde hij met voldoende het kandidaatsexamen in de wiskunde en de natuurwetenschappen. Op 27 november 1986 haalde de auteur met voldoende het doctoraal examen in de wiskunde en natuurwetenschappen, hoofdvak: structuurchemie.

Van 16 december 1986 tot 16 december 1990 was de auteur als wetenschappelijk medewerker verbonden aan de vakgroep Theoretische Chemie van de RUG.

Van 1 maart 1992 tot 1 maart 1996 was de auteur als toegevoegd onderzoeker verbonden aan de sectie Instrumentatie Stralings Onderzoek van de TUD. Het onderzoek dat in dit proefschrift staat beschreven is in deze periode gedaan.

